# Mechanisms of Germinal Center and Non-canonical B cell Responses

by

**Nikita Trivedi**

BSc, M.G. Science Institute, 2008

MSc, Gujarat University, 2010

MS, University of Texas at San Antonio, 2013

Submitted to the Graduate Faculty of

School of Medicine in partial fulfillment

of the requirements for the degree of

Doctor of Philosophy

University of Pittsburgh

2019

UNIVERSITY OF PITTSBURGH

SCHOOL OF MEDICINE

This dissertation was presented

by

**Nikita Trivedi**

It was defended on

November 6, 2019

and approved by

Greg Delgoffe, Assistant Professor, Department of Immunology

Lawrence Kane, Professor, Department of Immunology

Jay Kolls, Professor, Department of Microbiology and Molecular Genetics

David Rothstein, Professor, Department of Immunology

Dissertation Director: Mark Shlomchik, Professor, Department of Immunology

**Mechanisms of Germinal Center and Non-canonical B cell Responses**

Nikita Trivedi, PhD

University of Pittsburgh, 2019

B cell responses to pathogens and vaccines can be mediated by Germinal center (GC) and non-GC processes. Using *Ehrlichia muris* as a model pathogen for non-canonical B cell responses, we found that antibody forming cells (AFC) and memory B cells (MBC) can be generated in the absence of a GC reaction. In addition, non-lymphoid sites of infection such as the liver can support B cell proliferation, somatic hypermutation (SHM) and MBC generation and localization. *Ehrlichia* induced B cell responses are marked by diverse surface phenotypes and T-bet expression and a subset of T-bet$^{+}$ MBC colonize the marginal zone (MZ) compartment of spleen. These data provide insights into non-canonical B cell responses, tissue resident B cell responses and T-bet$^{+}$ B cell biology.

B cell differentiation into a GC B cell (GCBC) phenotype is marked by distinct B cell receptor (BCR) signaling in comparison to naïve B cells (NBC). This has been attributed to regulatory mechanisms involving protein and lipid phosphatases that function exclusively in GCBC. We extend these findings by uncovering the role of actin as a negative regulator of BCR signaling in NBC and GCBC. In addition, we discover the unique dynamics of BCR endocytosis and antigen (Ag) presentation in GCBC. These data reveal a previously unappreciated role for the lipid phosphatase Phosphatase and tensin homolog (PTEN) in BCR dynamics and Ag presentation. Another lipid phosphatase Src homology 2 domain containing inositol polyphosphate 5-

phosphatase 1 (SHIP-1) is crucial for proliferation and survival of GCBC. Taken together, these data highlight the distinct ways GCBCs are rewired for efficient GC function.

## Table of Contents

## List of Tables

## List of Figures

## 1.0 Germinal Center and Non-Canonical B Cell Responses

Humoral immunity is critical for clearance of pathogens and in mounting rapid memory response upon re-infection. Typically, these immune responses are generated in secondary lymphoid tissues (SLT). These SLTs include the regional lymph nodes, tonsils, Peyer's patches, spleen etc. tissues that are strategically located at the site of potential pathogen encounter. The spleen is a major secondary lymphoid organ which plays a vital role in the clearance of blood-borne pathogens. Classical B cell response to infections initiate as a T cell-dependent antibody response marked by the formation of a germinal center (GC) reaction. In these GCBCs undergo clonal expansion, somatic hypermutation (SHM) and antigen-specific B cells get selected. This process generates high affinity AFCs and MBCs. However, certain pathogens such as *Salmonella, Borrelia, E. muris* do not induce the GC pathway and instead antibody forming cells (AFCs) and memory B cells (MBCs) are generated through a non-canonical extra-follicular (EF) pathway (1-4). These two different pathways of generating B cell responses are discussed in the following sections.

### 1.1 GC Reaction

Within secondary lymphoid organs, antigen (Ag) encounter leads to B-T interaction at the border of T cell and B cell zones. This interaction leads to the differentiation of naïve B cells (NBCs) into GCBCs. Ag-activated B cells migrate into the center of the B cell follicle and undergo rapid proliferation. As the GC matures, two different zones start emerging. These compartments

are termed as the light zone (LZ), and dark zone (DZ). The LZ contains GCBCs, follicular helper T cells (Tfh), and follicular dendritic cells (FDCs) (5, 6). The DZ consists of densely packed and proliferating GCBCs and stromal cells. The chemokine receptor C-X-C chemokine receptor type 4 (CXCR4) is expressed on the surface of DZ GCBCs, and CD83 and CD86 proteins are expressed on the surface of LZ GCBCs (5, 6). DZ stromal cells express stromal cell derived factor 1 (SDF1), which is the ligand CXCR4 and this interaction retains GCBCs in the DZ. LZ FDCs, express the chemokine C-X-C motif ligand 13 (CXCL13) and its receptor C-X-C chemokine receptor type 5 (CXCR5) is abundantly expressed on the surface of LZ GCBCs (5, 6).

Classically, DZ GCBCs are referred to as centroblasts, and LZ GCBCs are referred to as centrocytes (5-8). In the DZ, centroblasts undergo proliferation and SHM in the Ab variable region genes (5-8). Upon entry into the LZ, the centroblasts cease proliferation and become centrocytes (5-8). In the LZ, centrocytes encounter FDCs that express complement receptors and Fc gamma receptor 2B (FcϒR2B) (5). FDCs hold Ag in the form of immune complexes and present it to the B cells (5). These centrocytes acquire Ag from FDCs and present it to T cells in the context of MHC II (5-8). The interaction with T cells provides survival signals to GCBCs. Contrary to this classical model, imaging studies and cell cycle analyses have found that both LZ and DZ GCBCs have B cells in different phases of the cell cycle, suggesting that GCBCs can proliferate in either of these compartments (5-8). In the context of interactions with Tfh, GCBCs have to compete with each other to receive the required T cell help (5-8). The number of B cells can be 5 to 20 times higher than the number of Tfh cells within any given GC reaction. GCBCs that have higher affinity for an Ag will take up Ag efficiently and present it to T cells and get positively selected (5-8).

Upon differentiation into a GC phenotype, B cells undergo several phenotypic changes and rewiring at the signaling level that allows efficient GC function. These modifications in GCBCs are discussed in Chapters 3-5.

## 1.2 Non-canonical B cell Responses

After encounter with a cognate T cell, activated B cells either enter a follicle or migrate into EF areas and continue to proliferate. In the spleen EF responses can occur in periarteriolar lymphocytic sheaths, red pulp and in bridging areas between follicles and in the lymph nodes this can occur in medullary cords (9). These EF sites are capable of SHM, isotype switching and B cell differentiation into long-lived phenotypes (9). During ongoing GC reactions, B cells continue responding from EF sites, so these sites are a contributor to humoral immunity. In autoimmune conditions such as lupus, both pathways contribute in the production of autoantibodies (10). The majority of our understanding of B cell immune responses is based on GC responses but there are many pathogens that do not induce a GC reaction and the humoral immunity to these pathogens is dependent on EF sites.

In the case of *Borrelia burgdoreferi*, GC responses are short-lived and have a deformed structure and the B cell responses occur at EF sites (2-4). In *Salmonella typhimurium* infection, GC responses are delayed and instead a massive EF B cell response is observed (1). Typically, these responses are thought to be non-specific in nature. However, *Salmonella* infection of BCR restricted mice has shown that these responses in fact require antigen (Ag) sensing through the BCR (11). Moreover, *Salmonella* infection-induced EF B cell patches have been shown to undergo SHM and clonal expansion (11). Also, there is substantial isotype switching to IgG in the absence

of a GC reaction to *Salmonella* (11). These data have revised the view on B cell responses to pathogens and highlighted the role of EF or non-canonical B cell responses. Another pathogen that does not induce a GC response is *Ehrlichia muris* (12*).* Recently it has been shown that TNF-α production upon *E. muris* infection disrupts the splenic architecture, leading to a dampened GC response and instead induction of a massive EF AFC response (13). Further details regarding *E. muris* and the non-canonical B cell responses are discussed in the next chapter.

# 2.0 Liver is a generative site for the B cell response to *Ehrlichia muris*

## 2.1 Introduction

### 2.1.1 *Ehrlichia muris*

Ehrlichia muris is a gram-negative, obligate, intracellular pathogen that causes human monocyte ehrlichiosis (HME) (14, 15). There are many strains of Ehrlichia that are known to cause infections such as *Ehrlichia chaffeensis*, Ixodeus ovatus (IOE), *Ehrlichia muris*, *Ehrlichia ewingii*, *Ehrlichia canis* and *Ehrlichia ruminantium* (14, 15). The strains most commonly causing human infection are *E. chaffeensis* and *E. ewingii* (16). Ehrlichia uses dogs and deers as animal reservoirs and human infection can occur incidentally in a tick-borne manner (16). The infection is generally self-limiting in immunocompetent hosts (17). However, in immunocompromised hosts it can cause severe complications and can affect multiple systems, with symptoms resembling toxic shock (17). HME is generally characterized by nausea, vomiting, fever, headache, myalgia, arthralgia, liver inflammation and liver dysfunction (17). The infection responds well to doxycycline treatment and clinical improvement is observed within 24 to 48 hours post-treatment (17). In our study, we have used *E. muris* which closely resembles *E. chaffeensis* and induces a systemic infection but does not cause pathology (14, 15). This model gives us the advantage of studying the immune response without complications from immunopathology.

### 2.1.2 *Ehrlichia* Infection

Generally, *Ehrlichia* infection occurs within macrophages, hepatocytes, and endothelial cells (18). Within these cells, the infection can form morulae, which are cytosolic vacuoles that help to contain the *Ehrlichia* (18). Upon infection, *Ehrlichia* can spread from one cell to another via filopodia. Filopodia formation requires actin polymerization and re-organization of filamentous actin (F-actin) (19, 20). Agents such as Cytochalasin D reduce actin polymerization and in turn filopodia formation. Inhibiting filopodia formation by treatment of cells with Cytochalasin D reduces bacterial burden, highlighting the importance of membrane extensions in the spread of *Ehrlichia* infection (19, 20). Data from electron microscopy experiments have also shown the transmission of *Ehrlichia* via filopodia extensions (19, 20). During infection, *Ehrlichia* can also spread by host cell lysis and infection of neighboring cells (19, 20).

*Ehrlichia* species have several pathogen-associated molecular patterns (PAMPs) on their outer membrane. Several outer membrane proteins (Omps) of the Omp28 family such as Omp12, Omp19, and Omp29 have been described previously and are known to be immunodominant (21). These Omps also facilitate adhesion of *Ehrlichia* onto host cells (21). The outer membrane of Ehrlichia is also rich in tandem repeat units (TRPs) that are secreted via a type 1 secretion system (22). These TRPs are known to play many roles that disrupt host functions. Some of these functions include: 1) regulate the cytoskeleton by interactions with actin and myosin filaments, 2) re-program the transcription factors that are associated with host survival (18). *Ehrlichia* species also express a protein called outer membrane entry triggering protein (EtPE-C). EtPE-C facilitates the entry of *Ehrlichia* into the host cell by binding to DNase X (23). Typically, upon entry, *Ehrlichia* enters endocytic compartments that fuse with transferrin receptor (TfR) positive endosomes to acquire iron from the host cytosol (18). *Ehrlichia* also escapes degradation by the lysosomal

pathway (18). Through its Type 4 secretion system, *Ehrlichia* secretes ECH_0825, which leads to inhibition of ROS production and cell death (18).

### 2.1.3 Immune responses to *Ehrlichia*

*Ehrlichia* is an obligate intracellular pathogen and therefore cell mediated immunity has a major role in protection against pathogen. Several different species of *Ehrlichia* have been used to study the immune response to the infection. *E. chaffeensis,* and *E. muris* are mildly virulent strains for murine infection, whereas, IOE is a highly virulent strain that leads to pathogenesis and liver disease in mice (14). There are many different immune cells that play a key role in control of *Ehrlichia* infection.

Neutrophils are innate immune cells that play a crucial role in clearance of extracellular and intracellular pathogens by phagocytosis, generation of reactive oxygen species (ROS), and anti-microbial peptides. However, contrary to the usual protective roles of neutrophils, in the case of *Ehrlichia* infection, neutrophils play a pathogenic role (24). Depletion of neutrophils during an ongoing infection with IOE increased bacterial clearance and reduced pathology (24). Neutrophil depletion also led to a reduction in the number of tumor necrosis factor alpha (TNF-α) producing CD8 T cells, which is known to be a major contributor to fatal ehrlichiosis (24).

Macrophages are one of the main cells that get infected by *Ehrlichia*. Macrophage heterogeneity has recently been dissected in context of *Ehrlichia* infection. In case of protective *E. muris* infection, M2 polarized macrophages dominate in the liver (25). However, infection with the virulent *IOE* strain leads to accumulation of iNOS producing M1 macrophages and induction IL-17 production by T, NK and NKT cells (25). These data highlight the role for macrophage polarization in shaping the immune response to *Ehrlichia*.

Typically, cytotoxic CD8 T cells provide protection against intracellular infections by producing perforin and granzyme B and eliminating infected cells, and by producing cytokines such as TNF-α and interferon gamma (IFN-γ) that activate phagocytic cells. Infections with mildly virulent species of *Ehrlichia* such as *E. muris*, triggers protective CD8 T cell response (26). In fact, adoptive transfer of CD8 and CD4 T cells from *E. muris* infected mice leads to protection against IOE infection (26). However, a direct infection with virulent IOE leads to over-production of TNF-α by CD8 T cells that contributes to pathology (26). Mice lacking the TNFR were protected from liver injury and pathology and had prolonged survival (26). However, mice lacking TNFR also had greater bacterial burden, suggesting a role for TNF-a in the control of intracellular infection (26).

Like CD8 T cells, depletion of NK cells also leads to reduced pathology and prolonged survival in case of IOE infection (27). However, in case of *E. muris* infection, depletion of NK cells leads to reduced memory CD4 T cells and AFCs, suggesting a role for NK cells in promoting long-term adaptive immunity to *Ehrlichia* (26). During *Ehrlichia* infection, IFN-γ produced by CD4 Th1 cells, and NKT cells enhances the phagocytic functions of macrophages and aids in bacterial clearance (28). Despite being an intracellular pathogen, *Ehrlichia* infection leads to a robust B cell response that is known to be protective.

### 2.1.4 Humoral Immunity to *Ehrlichia* infection

It is generally believed that cellular, but not humoral, immunity is crucial for the clearance of intracellular pathogens. In *Ehrlichia chaffeensis* infection, SCID mice develop fatal infection (29, 30). However, transfer of immune sera or antibodies from immunocompetent mice reduced

bacterial burden and prolonged survival of SCID mice (29). These data demonstrate that humoral immunity can play a significant role in the clearance of intracellular pathogens.

Generally, B cell responses are elicited via a germinal center response. However, in the case of certain pathogens such as *Borrelia*, *Salmonella* and *Ehrlichia*, GCs are not formed or their induction is delayed and instead a non-canonical B cell response leads to AFC formation (2-4). The responding B cells during *Ehrlichia* infection are known to express CD11c, B220, CD19, CD1d and high expression of CD11b and CD43 (31). IgM-secreting B cells persist in the bone marrow of antibiotic treated mice and provide long-term protection against challenge infection (32, 33). Generation of IgM memory B cells during *Ehrlichia* infection is CD4 T cell-dependent and requires IL-21R signaling (31, 33, 34). IgM memory B cells are required for IgG immune responses to a challenge infection and thus IgM memory B cells confer long term protection to *Ehrlichia* infection (31, 33, 34). The gastric omentum is also known to be a site of generation for protective IgM responses in case of *Ehrlichia* infection (35). Mice that lack spleen, lymph node, and Peyer's patches have IgM B cells responding to acute *Ehrlichia* infection in the gastric omentum (35). Moreover, these mice also have long-lasting humoral immunity that can protect against a challenge with IOE (33). Thus, even in the absence of GCs, *Ehrlichia* infection induces a potent non-GC AFC response that is generated in SLT and non-lymphoid locations such as the gastric omentum.

### 2.1.5 Age-associated B cells or T-bet expressing B cells

In the past several years, B cell subsets that express the transcription factor T-bet have been discovered in many different models. T-bet expression in B cells was originally documented as a regulator of isotype switch induced in response to TLR9 signals (36, 37). T-bet expression has

been closely associated with so-called age-associated B cells (ABC) (38, 39). ABC are found especially in older female mice and in autoimmune-prone mice (38, 39). These T-Bet$^{+}$ ABC are typically CD11b+ and CD11c+, but lack expression of CD21 and CD23 (38, 39). A similar population has been identified in humans and is associated with lupus. T-bet+ B cells can also be induced by various infections and T-bet can also be expressed in PB (40-42). A subset of MBC formed during certain conditions, including *Ehrlichia* infection, can express T-bet as well (43, 44). The role of T-bet in B cells and its relationship to ABC, MBC and PB development and function is an active area of research, and the relationships among these cells and processes is not fully clear.

### 2.1.6 Tissue resident immunity

During infection or autoimmunity, immune responses occur in lymphoid organs such as the regional lymph nodes or spleen, but sometimes immune responses are also observed in the infected non-lymphoid tissue. In case of influenza, tuberculosis infections, localized immune is observed in the lungs (45, 46). There are several infections such as hepatitis B and C, Schistosoma, Plasmodium, that lead to liver infection and interfere with liver function. In case of chronic HCV infection in humans, lymphoid follicles form in the liver parenchyma (47-49). Moreover, these lymphoid follicles were found to contain clonally expanded B cells within intraportal lymphoid follicle-like structures (47-49). HCV-infected patients also have high levels of AID mRNA in blood and in liver biopsies in comparison to healthy controls (48, 50). In the case of primary biliary cirrhosis (PBC), the intrahepatic portal tracts express high levels of CXCL13 (51). This leads to B cell aggregation that proliferate locally and secrete anti-mitochondrial antibodies (CXCR5-CXCL13) (51). In mice and humans, liver is a site for IgA production by B cells. These IgA Abs

are specific to oral and gut associated Ags (52, 53). Moreover, in the case of alcohol-associated liver injury, there is an increase in the numbers of IgA secreting cells (52, 53). Schistosoma infection leads to the presence of IgG1 secreting plasma cells in the liver parenchyma and the hepatic lymph node (54, 55). There are several instances where non-lymphoid organs can adapt to support the functions of B cells and other immune cells. Liver is a prominent site of infection for *Ehrlichia*; however, the role of liver in generating immune responses to this infection is not known.

### 2.1.7 Study Goals

The conventional B cell response to pathogens such as the influenza virus and the malarial parasite is dependent on a GC pathway that results in the production of antibody-forming cells (AFC) and MBC (56, 57). However, certain pathogens such as Borrelia burgdorferi, Salmonella typhimurium and *Ehrlichia muris* suppress or delay the onset of a GC response and B cell responses instead follow a non-canonical pathway (1, 3, 11, 12) *E. muris* is a gram-negative, obligate, intracellular bacterium, that induces an alternative B cell differentiation pathway (12). Ehrlichia infection induces large numbers of IgM AFC and considerable, yet comparatively lower, numbers of IgG AFC (12, 29, 31). Recently, it was found that *Ehrlichia* infection induces the expression of the transcription factor T-bet in a subset of splenic B cells (43). Moreover, after Ag clearance, T-bet+ splenic B cells persist as MBC and are capable of differentiating into multi-lineage effector B cells upon challenge (43, 44). Despite the fact that liver is a primary site for infection in humans and mice that undergo pathology (14) during the course of infection, there is only very limited information on hepatic B cell responses to *Ehrlichia* (27, 58). In particular, the extent to which this response can occur locally in the liver and if so, what are the consequent outputs, is unknown.

In this study, we corroborate and extend earlier findings that show that *Ehrlichia* infection induces a non-canonical B cell differentiation pathway that results in the production of AFC and MBC (12, 33). Most interestingly, we find that liver, as a primary site of infection, is also a major locus for B cell proliferation and SHM during the acute phase of the immune response. To assess whether there is crosstalk between local liver and splenic responses, we use high throughput sequencing (HTS), which reveals bi-directional trafficking of mutated B cell blasts and PBs between the spleen and liver. After pathogen clearance, we observe T-bet expressing MBC that persist in the spleen and which are localized in the liver. Moreover, we find that both splenic and hepatic B cells induced by *Ehrlichia* infection during the acute and memory phases possess T-bet protein signature. This study highlights the role of non-lymphoid organs such as the liver as a generative site for humoral immunity and provides new insights into T-bet expressing B cells.

## 2.2 Materials and Methods

**Mice:** The mice used in this study were bred under specific pathogen free conditions in the animal facility at the University of Pittsburgh. All mouse work was done according to the protocols approved by the University of Pittsburgh Institutional Animal Care and Use Committee. The following mice strains were used: C57BL/6 (Jackson Laboratories), B18+/+ and B18+/+ Vk8R+/+ (59), huCD20 TamCre (60), T-bet fl/fl (61), huCD20 TamCre T-bet fl/fl, and B18+/- Vk8R+/- CD45.1/2.

**Bacteria, Ags, Infection and Treatment Procedures:** *E. muris* was kindly provided by Dr. Nahed Ismail, Department of Pathology, University of Pittsburgh. E. coli strains containing recombinant plasmids for E. muris Ags Omp 12 and Omp 19 were provided by David Walker at University of Texas Medical Branch (62). The recombinant His tagged proteins were produced and purified using Ni-NTA spin kit from Qiagen as per standard protocols (62). *E. muris* infections were done according to procedures described previously (63). Briefly, *E. muris* inoculum was prepared by passage through wild-type C57BL/6 carrier mice. Single cell suspensions from spleens harvested from carrier mice were used for infection of experimental mice. Mice were infected intraperitoneally with $10^5$ *E. muris*/mouse. The bacterial burden was assessed by quantitative RTPCR as described previously (63). Tamoxifen treatments were done at day 3, 5 and 7 post infection at a concentration of 1 or 2 mg per dose orally in corn oil. For labeling B cells in the circulation, 1μg CD19 PE was injected intravenously. After 3 minutes, blood, spleen and liver were harvested and analyzed. For MBC homing experiments, CD45.2 MBC subsets were FACS sorted, CFSE labeled and transferred intravenously into B18+/- Vk8R+/- CD45.1/2 mice. 28

**ELISpot Assays and Flow Cytometry Analysis:** Single cell suspensions from spleen were obtained by mechanical disruption of the tissue, followed by treatment with ACK buffer for lysis of red blood cells. Single cell suspension of the liver was prepared by mechanical disruption using the MACS dissociator along with use of 50KU/mL DNase and collagenase 100U/mL, followed by treatment with ACK buffer for lysis of red blood cells. The single cell suspension from the liver was subjected to 80:20 Percoll gradient for isolation of lymphocytes. For ELISpot assay, Immulon 4-HBX plates were coated with the following Ags: anti-kappa at 5 mg/ml, Omp12 at 4mg/mL and Omp19 at 4mg/mL. Non-specific binding was blocked with 1% bovine serum

albumin (BSA) in PBS. Splenocytes were incubated overnight at 37$^{O}$C. AFC were detected by using alkaline phosphatase-conjugated secondary antibodies (to IgG or IgM, Southern Biotech) and 5-bromo4-chloro-3-indolyl-phosphate in agarose. For flow cytometry staining, non-specific binding was blocked using anti-FcR clone 2.4G2 and dead cells were excluded using cell viability dye (Tonbobio). The antibodies were either purified in our lab or purchased and are as follows. Anti-B220 (Biolegend RA3-6B2), anti-CD19 (BD ID3), anti-IgM (home-made B7-6), anti-CD21 (homemade 7G6), anti-CD23 (ebioscience B3B4) for B cells, anti-CD4 (Biolegend GK1.5), antiTCR-β (Biolegend H57-597) for T cells, anti-CD138 (Biolegend 281-2) and anti-CD44 (Biolegend IM7) for B cell blasts and PBs, anti-CD73 (Biolegend TY-11.8), anti-CD80 (ebioscience 16-1oA1), anti-PD-L2 (ebioscience TY25) for MBC, PNA (vector labs), anti-CD95 (BD Jo2) for GCBC, antiCD169 (Biolegend 3D6.112) for metalophillic macrophages, anti-CD11b (Santa Cruz MI-70), antiCD11c (ebioscience N418), anti-CD69 (ebioscience H1.2F3), anti-AID (ebioscience mAID-2) and anti-T-bet (Biolegend 4B10). The click IT Plus Edu kit was purchased from Invitrogen and the staining was done according to the recommended protocol.

**Immunofluorescence imaging:** 7 mm spleen sections were prepared from OCT-frozen tissues, fixed in acetone for 10 min, and stored at -80$^{O}$C. The slides were thawed and re-hydrated using PBS and blocked using PBS+1% BSA and 2.4G2 for 10 minutes. The slides were then stained with relevant Abs as described in the figure legends in a dark humid chamber for 30 minutes. The Abs were either purified in our lab or purchased and are as follows. Anti-B220 (Biolegend RA3-6B2), anti-CD19 (BD ID3), anti-IgM (home-made B7-6), for B cells, anti-CD4 (Biolegend GK1.5), anti-TCR-β (Biolegend H57-597) for T cells, anti-CD138 (Biolegend 281-2) for PB, anti-CD169 (Biolegend 3D6.112) for metalophillic macrophages, anti-CD11c (ebioscience

N418) and anti-T-bet (Biolegend 4B10). The slides were washed thrice using PBS and the same steps were followed for secondary Ab. For intracellular staining, the sections were permeabilized using 0.3% Triton X-100 reagent before staining. Sections were mounted using ProLong Anti-fade Gold (Life Technologies) and imaged using Olympus Fluorescence Microscope IX3-BSW and acquired using Cell Sens Dimension software.

**V region sequencing:** V region sequencing was done on FACS sorted PB or micro-dissected B cell patches. 7 mm spleen sections were prepared from OCT-frozen tissues on the membrane-coated PEN slides (Leica). PB patches were detected using anti-IgM Alexa488 staining. Microdissections were performed using Zeiss PALM MicroBeam Laser Capture Microdissection System. Dissected patches were collected in the cap of PCR microtubes in 12uL of digestion buffer (50 mM Tris-HCl, 50mM KCl, 0.63 mM EDTA, 0.22% Igepal, 0.22% Tween20, 0.8 mg/ml proteinase K). The patches or FACS sorted PB were digested at $37^{O}$C for 4 hours and at then at $90^{O}$C for 5 minutes. Primers, V region amplification and data analysis has been described previously (11). Briefly, a primary PCR was performed using the primers MsVHE-short: 5-GGGAATTCGAGGTGCAGCTGCAG-3 and a mix of 4 JH region anti-sense primers 3 SalI P-mJH01: 5-TGCGAAGTCGACGCTGAGGAGACGGTGACCGTGG-3 3SalIP-mJH02: 5-TGCGAAGTCGACGCTGAGGAGACTGTGAGAGTGG-3 3SalIP-mJH03: 5-TGCGAAGTCGACGCTGCAGAGACAGTGACCAGAG-3 3SalIP-mJH04: 5-TGCGAAGTCGACGCTGAGGAGACGGTGACTGAGG-3. A second nested PCR was performed using 1uL of the product from the 1st PCR using the primers MsVHE: 5-GGGAATCGAGGTGCAGCTGCAGGAGTCTGG-3 and a mix of JH antisense primers 5'-TGGTCCCTGTGCCCCAGACATCG -3', 5'- GTGGTGCCTTGGCCCCAGTAGTC -3', 5'-

AGAGTCCCTTGGCCCCAGTAAGC -3' and 5'- GAGGTTCCTTGACCCCAGTAGTC -3. High fidelity polymerase PfU Turbo (Agilent) was used for the PCR amplification to minimize the possibility of PCR error while generating the V region sequence. The resulting PCR products were cloned and sequenced using Zero Blunt PCR cloning kit (Thermofisher). Sequence analysis was done by using http://www.imgt.org/IMGT_vquest/analysis.

**Cell Sorting and RNA preparation:** PB were sorted as TCR-β negative, CD138 positive, CD44 positive, CD19 intermediate, B cell blasts were sorted as TCR-β negative, CD44 positive, CD138 negative, CD19 positive, naïve B cells were sorted as CD19 positive, CD138 negative and CD44 negative, CD73 negative. For HTS, B cells were sorted from naïve mice as CD45 positive, CD19 positive, CD73 negative, and MBC were sorted from memory mice as CD45 positive, CD19 positive and CD73 positive. For mRNA sequencing analysis, B220 positive, CD73 positive MBC were sorted as CD11b, CD11c double negative and CD11b, CD11c double positive from memory mice. The staining was done as described earlier for FC. After sorting, cells were spun down and washed with PB and re-suspended in RLT+1% beta-mercaptoethanol. RNA was prepared with RNAeasy microplus kits from Qiagen, according to recommended protocol.

**HTS library preparation and analysis:** For HTS, B cell blasts, PB, and MBC were FACS sorted and RNA was prepared as described above. The method for high-throughput sequencing of the B cell repertoire was performed as previously described (11, 64). Briefly, RNA was reverse-transcribed into cDNA using a biotinylated oligo dT primer. An adaptor sequence was added to the 3' end of all cDNA, which contains the Illumina P7 universal priming site and a 17-nucleotide unique molecular identifier (UMI). Products were purified using streptavidin-coated magnetic

beads followed by a primary PCR reaction using a pool of primers targeting the IGHA, IGHD, IGHE, IGHG, IGHM, IGKC and IGLC regions, as well as a sample-indexed Illumina P7C7 primer. The immunoglobulin-specific primers contained tails corresponding to the Illumina P5 sequence. PCR products were then purified using AMPure XP beads. A secondary PCR was then performed to add the Illumina C5 clustering sequence to the end of the molecule containing the constant region. The number of secondary PCR cycles was tailored to each sample to avoid entering plateau phase, as judged by a prior quantitative PCR analysis. Final products were purified, quantified with Agilent Tapestation and pooled in equimolar proportions, followed by high-throughput paired-end sequencing on the Illumina MiSeq platform. For sequencing, the Illumina 600 cycle kit was used with the modifications that 325 cycles were used for read 1, 6 cycles for the index reads, 300 cycles for read 2 and a 20% PhiX spike-in to increase sequence diversity.

FASTA files provided by Juno were analyzed with ImmuneDB v0.24.0 using default parameters for all stages (65).The GL reference sequences were acquired from IMGT's GENE-DB https://www.imgt.org/genedb/. After clonal assignment, lineages were generated with clearcut (66) using neighbor-joining, excluding mutations that occurred in only one sequence. Data were then exported from ImmuneDB for downstream analysis. Clones were included in this analysis only if they had between 1 and 4 non-templated CDR3 residues (as measured from the first non-GL-encoded nucleotide) or at least 4 common V-gene mutations across all sequences. ETE3 v3.1.1 (67) was used to calculate tree metrics and numpy v1.15.0 was used for all statistical testing.

**RNA seq analysis:** Samples were sequenced using Illumina NextSeq 500 with 75 bp paired-end reads and aligned to the mm10 genome using the STAR aligner (68). The number of

uniquely aligned reads ranged from 22 to 32 million. Gene-level counts were determined using featureCounts (69), and raw counts were quantile normalized to each other for differential expression using the voom method (70) in the limma R package (71) The presence of certain liver-specific transcripts indicated unavoidable liver cell contamination in the liver sample; to prevent this from confounding our analysis, differential expression was performed only on genes, which were having at least 30 counts in the all liver and spleen samples. All RNA-seq data were deposited in the NCBI's Gene Expression Omnibus database (GEO) with accession ID GSE137154. All gene-set enrichments were preformed using the rankSumTestWithCorrelation function in limma, which explicitly corrects for correlation among genes in the gene set being interrogated. For differential analysis of splenic and liver memory subsets in figure S18, the naive B cell transcriptional profile was extracted from a previously published microarray study (41). For normalization of the datasets, the "NormalizeBetweenArrays " function was used.

**Statistics:** Statistical analysis was performed with Prism (GraphPad Software). P values were determined using Student's t tests (two-tailed). For multiple comparisons, Two-Way ANOVA or Mann Whitney tests or Chi square analysis were applied. Differences between groups were considered significant for P values $< 0.05$ (* $p < 0.05$; ** $p < 0.01$; *** $p < 0.001$; **** $p < 0.0001$).

## 2.3 Results

It has been reported previously that inoculation of mice with *E. muris* leads to systemic infection of spleen, and liver (63, 72). However, unlike classical infections, splenic B cells do not form GCs in response to *E. muris* and instead respond by rapid EF expansion (12). In agreement

with previous reports, we found that *E. muris* infection was marked by considerable bacterial burden in spleen and liver along with enlargement of these organs (figure 1A-B). In both spleen and liver, infection elicited large numbers of AFCs by day 10, which remained elevated until at least day 28 post-infection (figure 1 D-E). There was a substantial IgG response, but the number of IgG AFC was remarkably lower than IgM AFC (figure 1 D-E). The responding B cells were observed in patches at EF sites in spleen and in the liver parenchyma (figure 2 A-D).

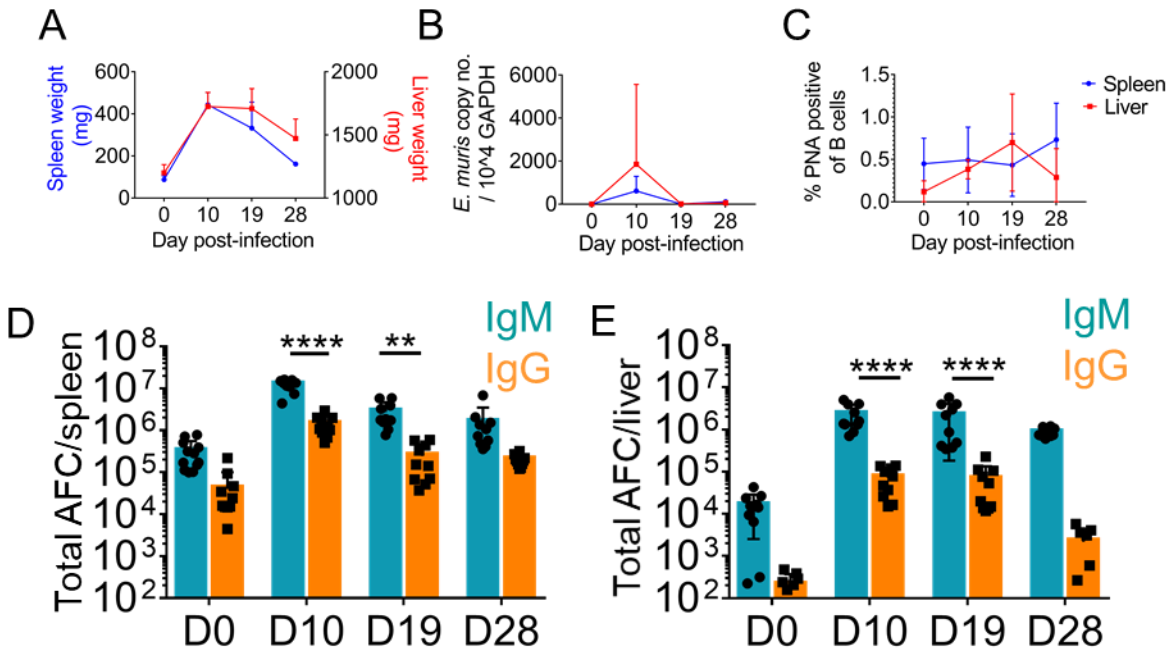


**Figure 1 *E. muris* infection does not induce a GC reaction**

**(A-C) Weight (A), Bacterial burden (B) and (C) Percentage of GCBCs of total B cells in spleen (blue) and liver (red) over the course of infection. (D,E) Total IgM and IgG AFC measured by ELISpot assay during *E. muris* infection in spleen (D) and liver (E). Data are representative of at least two independent experiments with and are represented as mean with SD of groups of at least two mice.**

Flow cytometric analysis of spleen and liver from infected mice revealed expanded populations of activated B cells that express CD44 (referred to as B cell blasts) and B cells that express CD44 and CD138 (referred to as PBs) (figure 3A-C). Consistent, with previous reports, we did not find induction of PNA-positive GC B cells by flow cytometry (figure 1C). *E. muris*-induced PBs express the transcription factor T-bet, as reported (43), as do the B cell blasts, some of which express even greater amounts of T-bet, a finding previously not appreciated (figure 3 D-E).

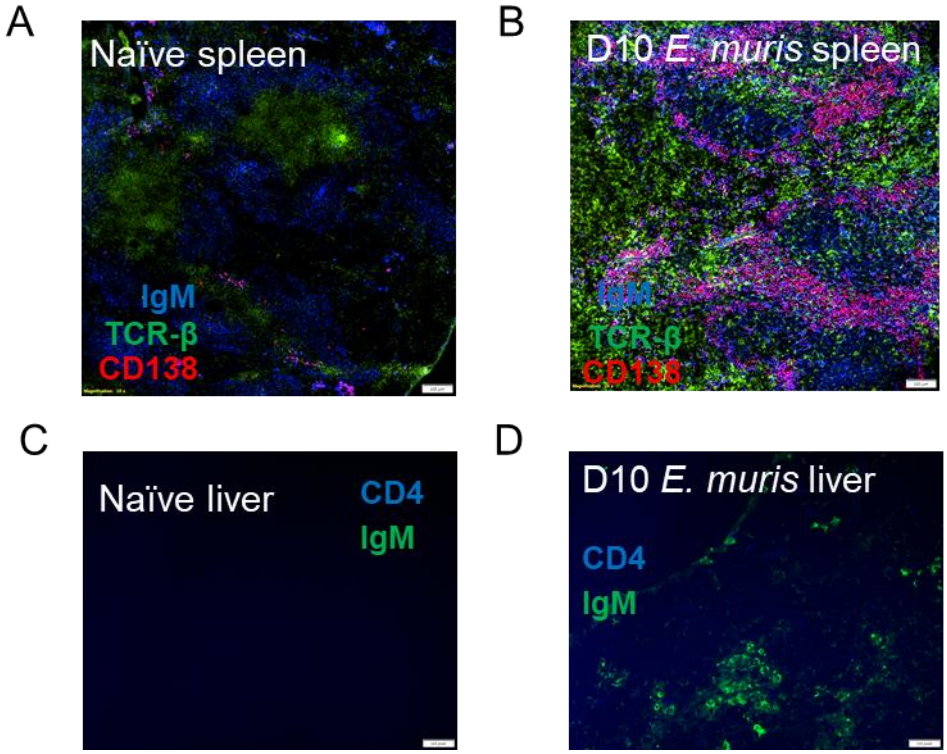


**Figure 2 *E. muris* infection induces a robust AFC response**

**(A-D) Immunofluorescence staining of cryo-sections from spleen (A-B) and liver (C-D) of naïve mice (A,C) and D10 *E. muris* infected mice (B,D) for B cells and T cells. Scale bars represent 100µm in A-B and 100 pixels in C-D. Data are representative of at least two independent experiments with and are represented as mean with SD of groups of at least two mice.**

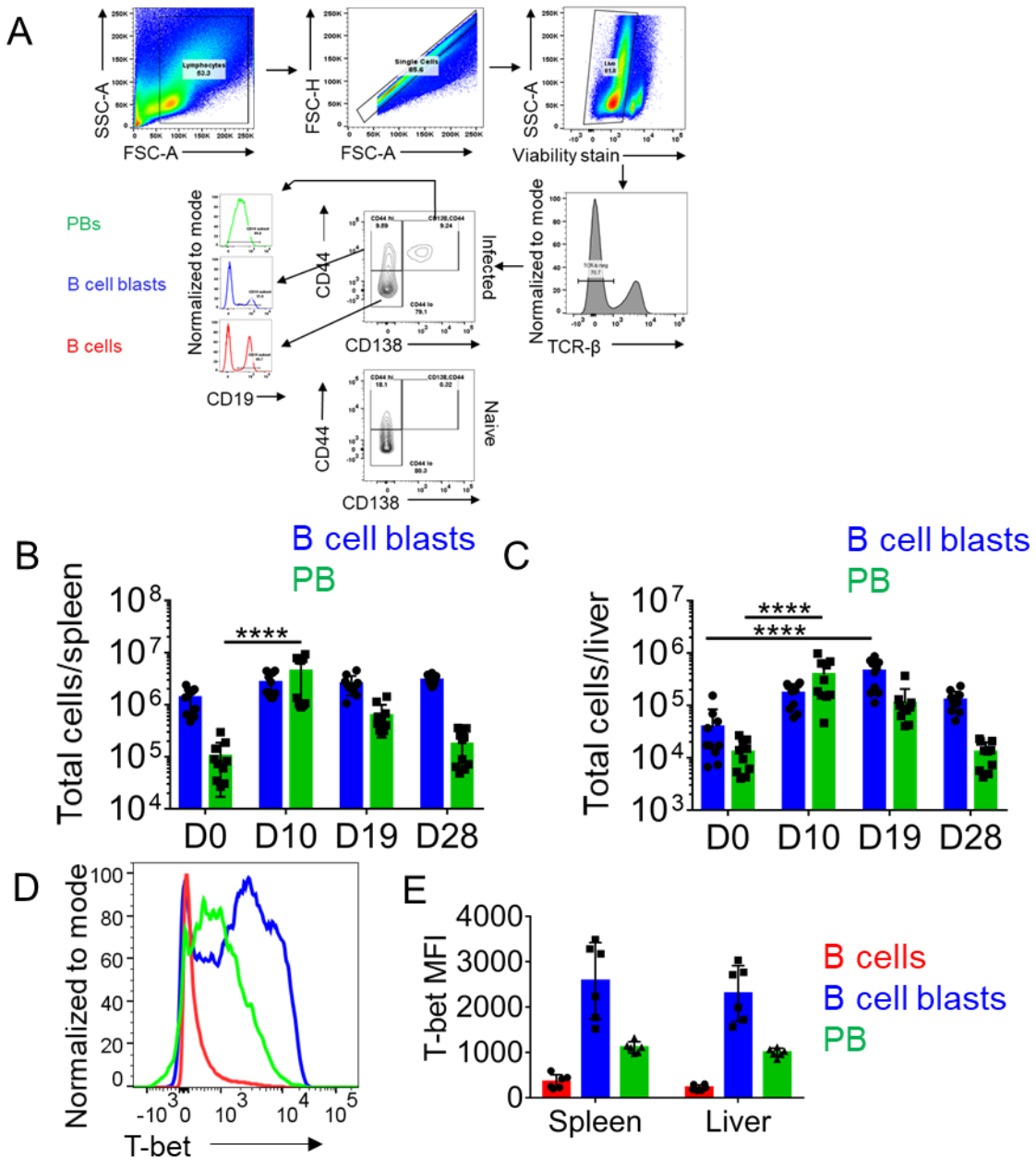


**Figure 3 *E. muris* infection induces a robust PB response**

**(A) Gating strategy for B cell blasts and PBs. (B-C) Total B cell blasts (blue) and PB (green) measured by FC over the course of *E. muris* infection in spleen (B) and liver (C), (D-E) Histogram (D) and Mean Fluorescence Intensity (E) of T-bet expression in B cells during acute *E. muris* infection. Data are representative of at least two independent experiments with and are represented as mean with SD of groups of at least two mice.**

To decipher the role of T-bet in the acute B cell response, we used tamoxifen (Tam)-inducible Cre mediated deletion of T-bet during an ongoing *E. muris* infection (figure 4A). The control mice - huCD20 TamCre and T-bet fl/fl - are combined into one group labeled as T-bet sufficient and huCD20 TamCre T-bet fl/fl mice are referred to as T-bet deficient. The mice were infected with *E. muris* and treated with 1-2 mg of tamoxifen 3, 5 and 7 days after infection. Assessment of T-bet expression on day 11 post-infection revealed that treatment with tamoxifen significantly reduced T-bet expression on splenic B cell blasts and PBs and showed a similar trend in hepatic B cell populations (figure 4B-E). Since liver is a metabolically active site, we suspect that tamoxifen 6 gets metabolized rapidly by liver cells and is not available for B cells. We assessed the total number of responding B cells and found that splenic plasmablasts were significantly higher in T-bet deficient mice compared to the T-bet sufficient group (figure 5A-D). There was no significant difference in the total numbers of splenic B cell blasts, hepatic B cell blasts, and hepatic PBs upon T-bet deletion (figure 5A-D). ELISpot assay showed a trend of increased IgM AFC in the spleen and liver but there was no significant difference in total and Ag-specific splenic and hepatic AFC upon T-bet deletion (figure 5E-J). These data are consistent with previously published data that shows that T-bet does not play a role in the regulation of AFC-associated transcription factors such as Blimp1 (73). Also, T-bet is dispensable for IgG1 AFC responses to the parasite *Heligmosomoides polygyrus* (73). However, unlike influenza infection and mouse models of lupus disease, we do not observe a dampened AFC response in the absence of T-bet (73, 74). This was an unexpected finding and, based on our data, we conclude that T-bet controls the differentiation of B cells into PBs but may not play a major role in shaping acute humoral immunity to *Ehrlichia*. Alternatively, it is possible that even though we did observe lower T-bet expression in responding populations, that deletion during development and beyond as performed in the influenza and lupus

models differed from inducible deletion we performed here or there was selection for escaped cells that masked a phenotype.

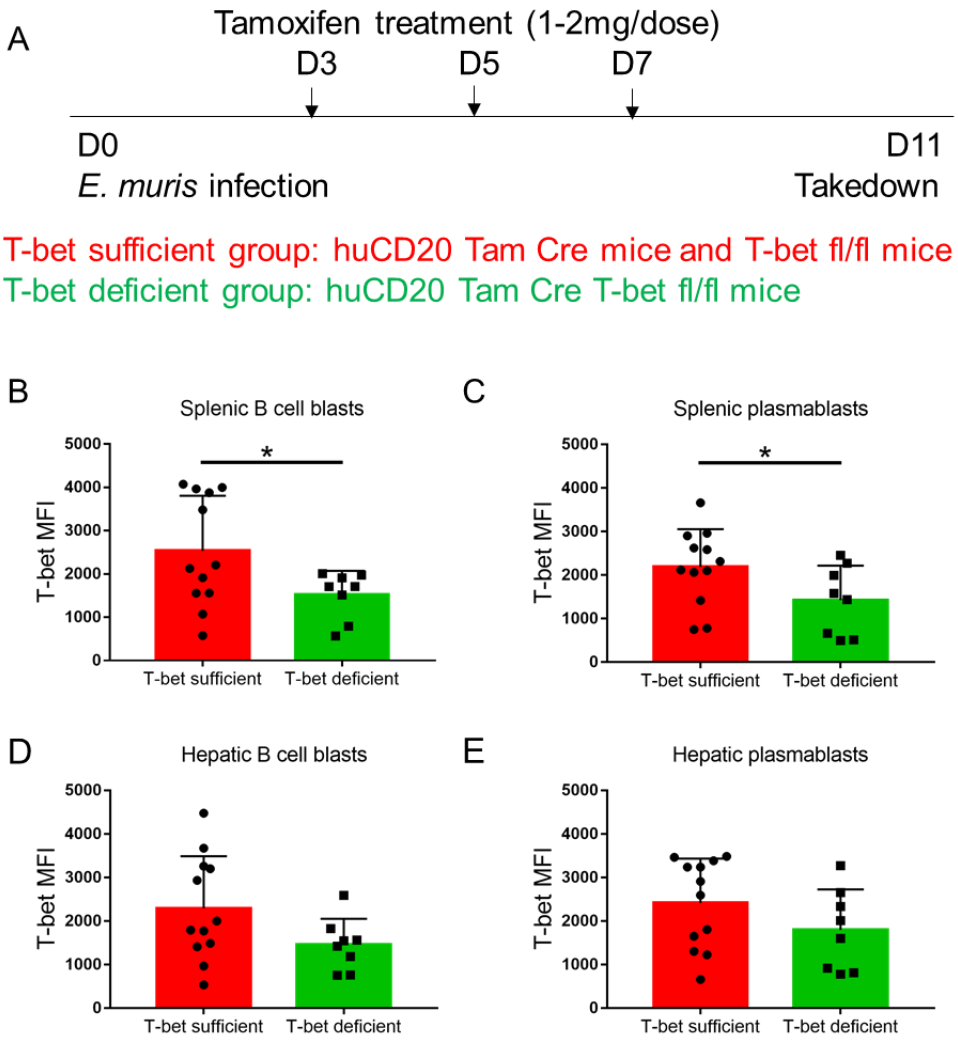


**Figure 4 Tamoxifen inducible B cell specific T-bet deletion**

**(A) Schematic diagram for T-bet deletion. (B-E) MFI of T-bet in B cell blasts and plasmablasts of T-bet sufficient (huCD20 TamCre and T-bet fl/fl) and T-bet deficient mice (huCD20 TamCre T-bet fl/fl). Data are representative of at least two independent experiments with and are represented as mean with SD of groups of at least two mice.**

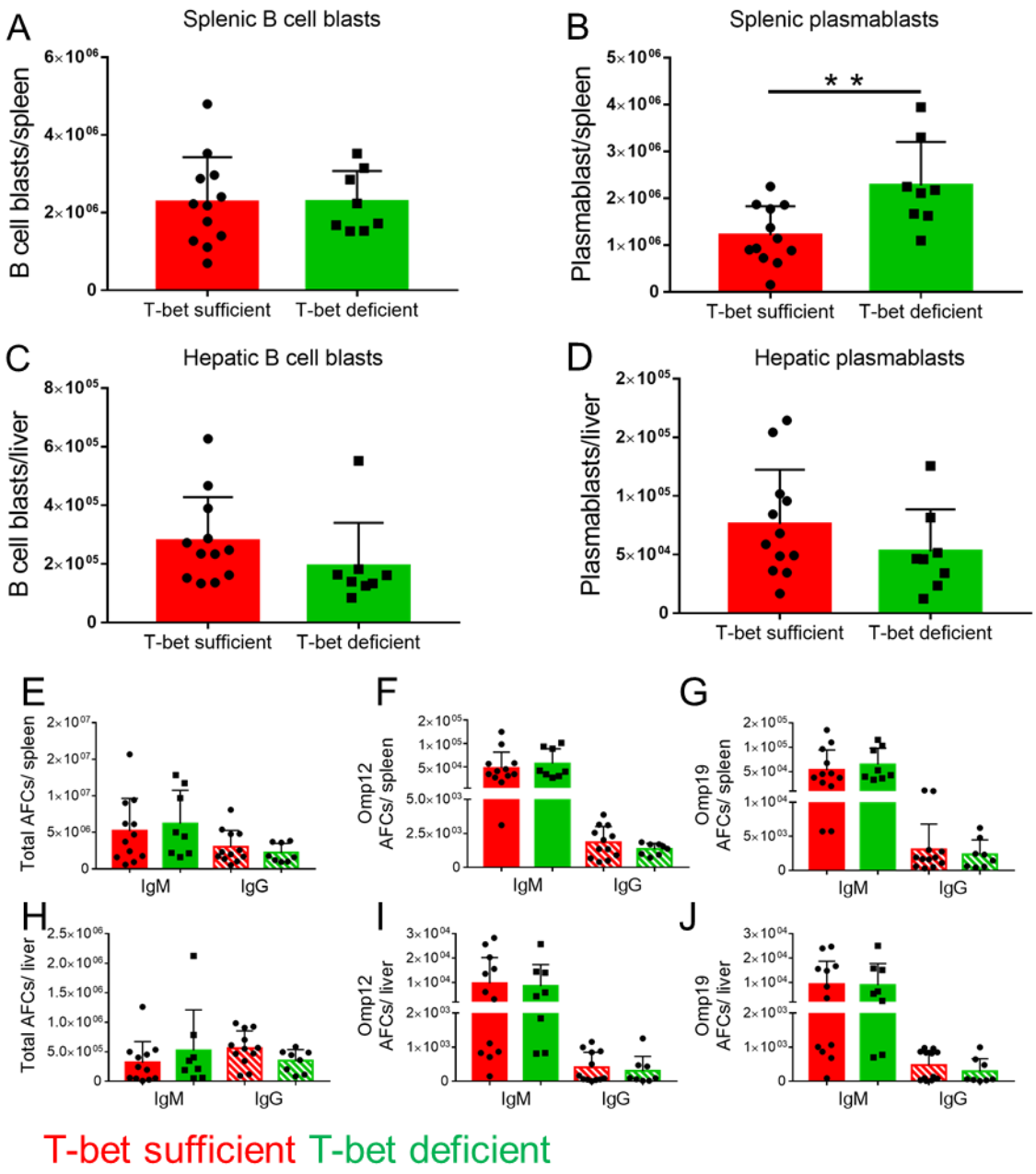


**Figure 5 B cell specific T-bet deletion increases PBs in the spleen**

**(A-D) Total number of plasmablasts (B,D) and B cell blasts (A,C) measured by flow cytometry in the spleen and liver of T-bet sufficient and T-bet deficient mice. (E-J) Total AFCs (E,H), Omp12 specific AFCs (F,I) and Omp19 specific AFCs (G,J) measured by ELISPOT assays in the spleen and liver of T-bet sufficient and T-bet deficient mice. Data are representative of at least two independent experiments with and are represented as mean with SD of groups of at least two mice.**

Given the atypical nature of the B cell response, we wanted to examine the specificity of the response to *Ehrlichia*. We used *E. muris* outer membrane proteins Omp 12 and Omp19 as coating Ags in ELISpot assays (62). Strikingly, though these Ags (Ags) were reported to be immunodominant *E. muris* Ags (31, 33), we found that less than 1% of IgM and IgG AFC were specific to these Ags in both spleen and liver (figure 6 A-D). This result is consistent with non-specific expansion of B cells mediated by signals through different pathogen recognition receptors (PRRs) without relying on BCR recognition or stimulation. However, if the B cell response were indeed specific, then restricting the BCR repertoire would negatively impact the AFC response. To examine this, we used heavy chain-restricted B18+/- mice that utilize B18 heavy chain gene paired with diverse light chains as well as heavy and light chain restricted B18+/- Vκ8R +/- mice that utilize B18 heavy chain and Vκ8R light chain genes. We observed a trend of reduced total and Ag specific AFC response in the spleens and livers of the BCR-restricted mice when compared to WT counterparts (figure 6). In spleen, we observed that heavy and light chain restriction led to significantly reduced total and Omp12 and Omp19 AFCs at day 12 post infection (figure 6A-B). The splenic total and Ag specific IgM AFCs were also significantly reduced merely by heavy chain restriction at day 12 post infection (figure 6A). The hepatic total IgM and IgG AFCs, Omp12 specific IgM and IgG AFCs and Omp19 specific IgM AFCs were significantly reduced in B18+/- Vκ8R +/- mice compared to WT mice at day 12 post infection (figure 6C-D). In all scenarios, BCR restricted mice mounted an increased response in comparison to baseline, however, failed to mount an AFC response that matched the magnitude of the WT repertoire (figure 6). No significant differences were observed in the AFC response between WT and BCR restricted mice at D22 post-infection as the acute response subsided (figure 6). These data demonstrate that the *Ehrlichia*-induced B cell response is a product of BCR specific and non-specific stimulations. However, Ag

sensing through the BCR is required for the massive AFC response that is seen upon *E. muris* infection and suggest that while it may be of low affinity, the majority of it depends on specific BCR recognition.

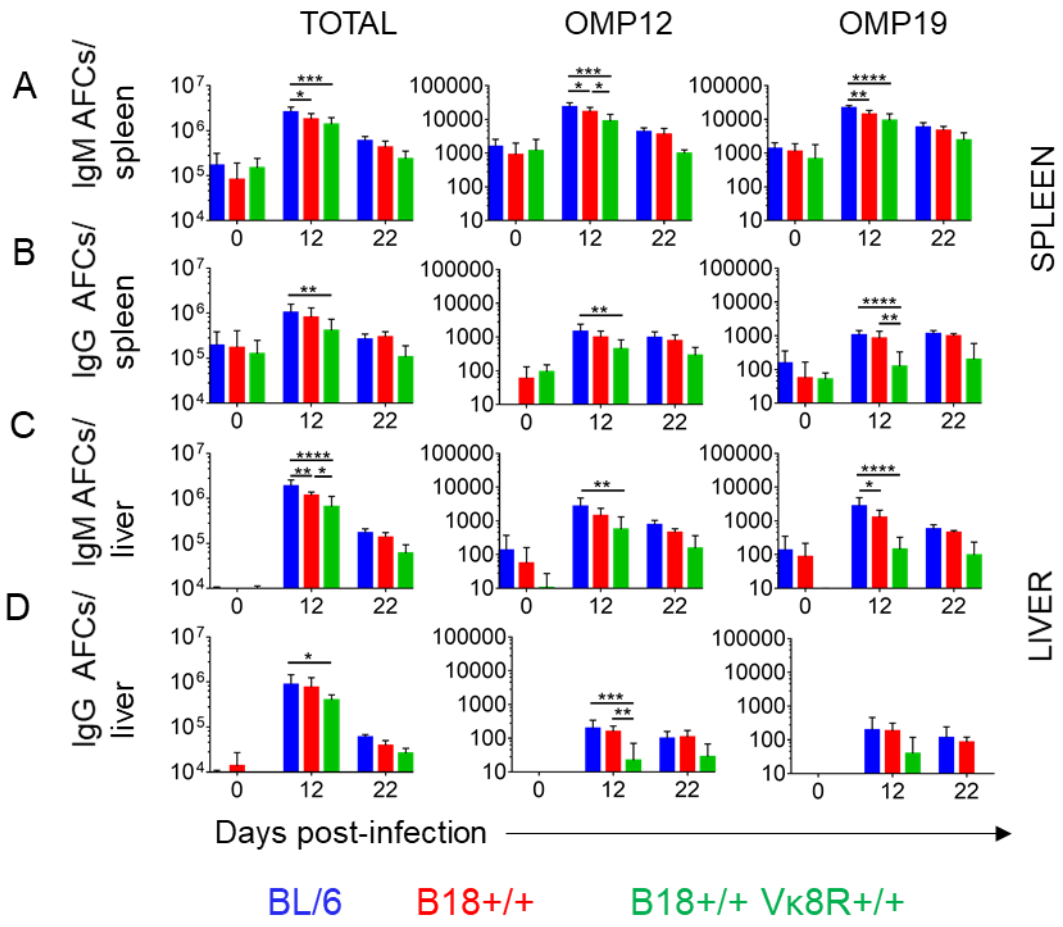


**Figure 6 BCR restriction reduces the magnitude of B cell response to *E. muris***

**(A-D panel 1) Total IgM and IgG response to *E.muris* in spleen (A-B) and liver (C-D) measured by ELISPOT assay, (A-D panel 2,3) Ag specific IgM and IgG response to *E.muris* in spleen (A-B) and liver (C-D) measured by ELISPOT assay. Data are representative of at least two independent experiments with and are represented as mean with SD of groups of at least two mice.**

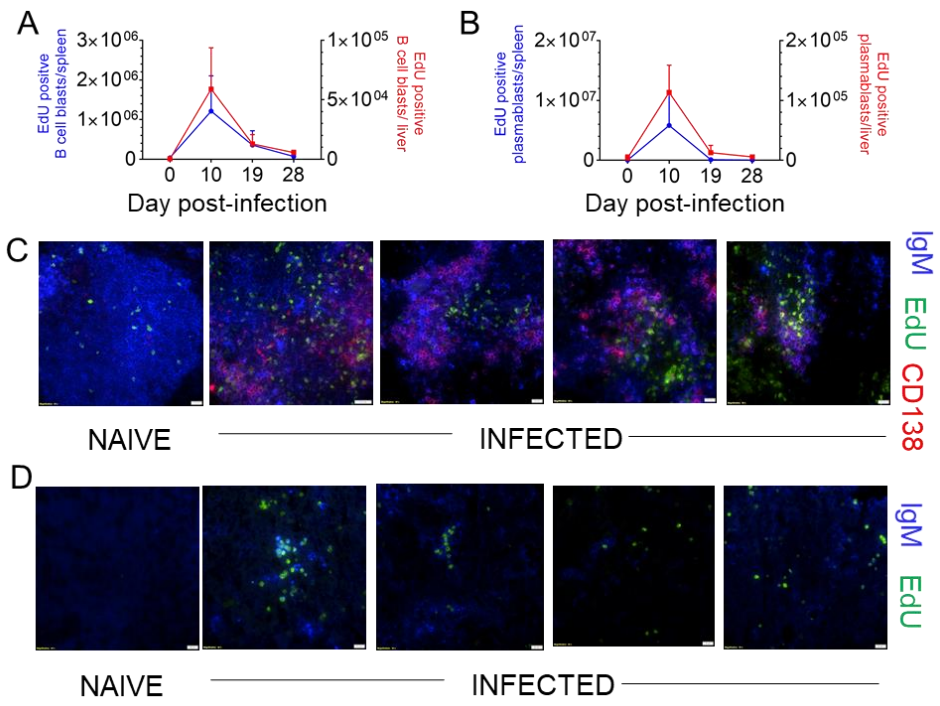


**Figure 7 Localized proliferation of B cells in the spleen and liver**

**EdU positive B cell blasts (A) and PB (B) of spleen (blue) and liver (red) over the course of infection measured by FC. (C-D) 40X image of proliferating B cells spleen (C) and liver (D). In C and D, scale bars represent 20µm. Data are representative of at least two independent experiments with and are represented as mean with SD of groups of at least two mice.**

While increased numbers of B cell blasts and PBs were found in the livers of *E. muris*-infected mice, it was not clear whether the hepatic B cell response is a product of infiltrating B cells derived from lymphoid organs or from local proliferation and differentiation of B cells in the liver. To investigate this, we injected the mice with EdU 30 minutes prior to the harvest of organs to label cells that were actively undergoing DNA synthesis during that period. As expected, there was a substantial increase in EdU positive splenic B cell blasts and PBs compared to the naïve control at 10 days post-infection (figure 7 A-B). Interestingly, hepatic B cell blasts and PBs were proliferating to an extent comparable to the splenic responders (figure 7 A-B). Histologic analysis

showed that proliferation of IgM and CD138 positive B cells in the spleen occurred within and outside of B cell follicles (figure 7C). Proliferation of IgM positive B cells in the liver was seen in the liver parenchyma and around the portal triads (figure 7D). These data indicate that liver is a generative site for the B cell response to *E. muris*.

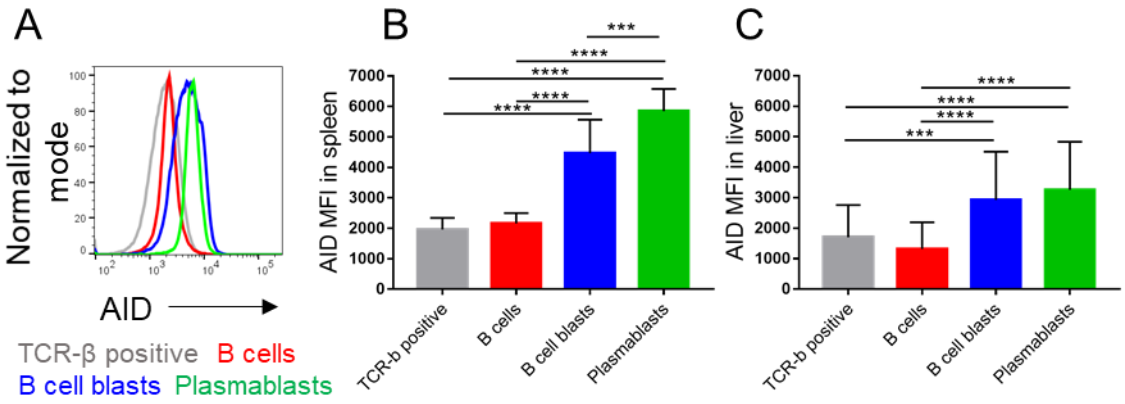


**Figure 8 *E. muris* infection induces AID expression in B cells**

**(A-C) Histogram (A) and quantification of AID in T cells, B cells, B cell blasts and plasmablasts in spleen (B) and liver (C). Data are representative of at least two independent experiments with and are represented as mean with SD of groups of at least two mice.**

To investigate the presence of SHM in PB responses that lacked GCs, we assessed the expression of the enzyme activation-induced cytidine deaminase (AID). We observed that both splenic and hepatic B cell blasts and PBs expressed significantly higher amounts of AID than naïve B cells and T cells (figure 8A-C). To further asses SHM, we amplified and sequenced V region genes from DNA of splenic and hepatic FACS sorted PBs. The mutation rate was 1% for PBs from spleen and 1.5% from liver (figure 9A-B). However, approximately 50% of V genes sequences were unmutated at both sites (figure 9A-B); this indicates that a significant percentage of cells did not induce the SHM program. Mutated PBs could either be generated during local proliferation or

undergo mutation at a separate site and then migrate. Since liver is a generative site, we hypothesized that mutation could occur within locally responding foci. To address where mutations were actually occurring, we used laser microdissection of IgM patches from the liver and spleen parenchyma. These microdissections typically captured ~20 cells, of which the full nucleus would be present in about ½ of them. The finding of intraclonal diversity among small groups of isolated cells demonstrates ongoing mutation at that site (11, 75, 76). Of 11 microdissections from spleen, 6 had clones with sequences 9 that were mutated from the closest GL (GL) Vh gene (Table 1). Of 10 microdissections from the liver, 7 had sequences with mutations when compared to the closest GL Vh gene (Table 1). These clonally related sequences could be assembled into 4 clonal lineage trees from the spleen (figure 10 A-D) and 4 clonal lineage trees from the liver (figure 10 E-H). The finding in multiple cases at each site that there were cells that shared mutations (i.e. the clones had trunks) and that also differed by other mutations (i.e. the clones had branches) provides evidence that SHM occurs locally in both the spleen and the liver parenchyma.

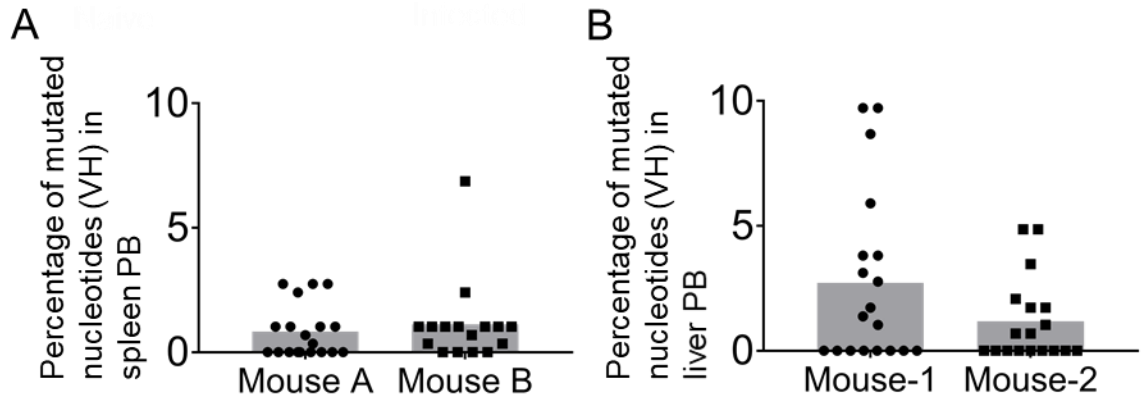


**Figure 9 Vh region mutations in splenic and hepatic PBs**

**(A-B) Percentage of mutated nucleotides in PB from spleen (A) and liver (B). Data are from one experiment with 2 mice in each experiment.**

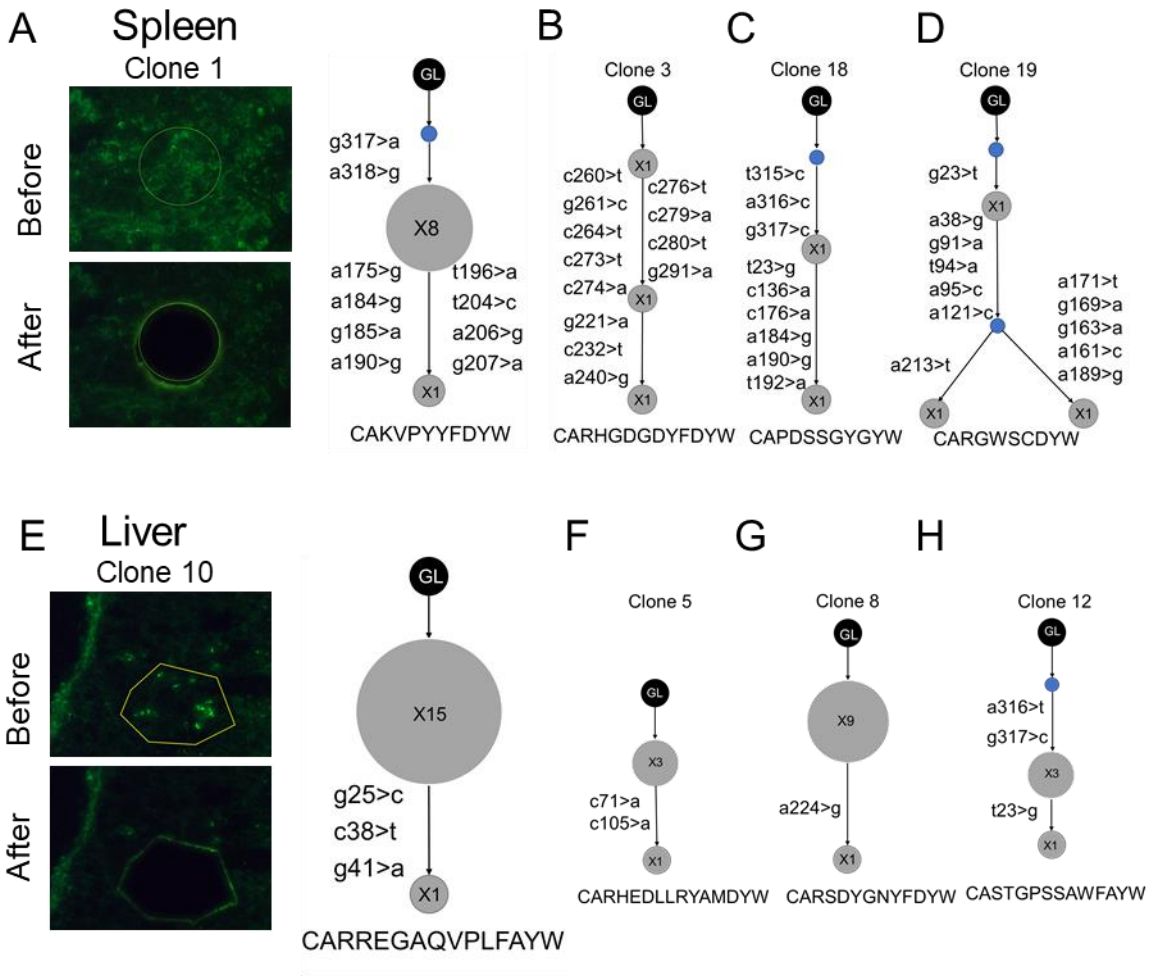


**Figure 10 Localized SHM in splenic and hepatic B cells**

**(A-H) Laser microdissections of IgM-positive PB patches (green) and corresponding clonal trees from Ig region sequencing from the spleen (A-D) and the liver (E-H). Inferred nodes are blue. Node size is proportional to the number of sequences. The CDR3 amino acid sequence of each clone shown at the bottom. Data are representative of at least two independent experiments.**

| Micro-dissection | Clone # | Organ | CDR3 AA | Vh usage | Number of unique sequences | Total sequences |
|---|---|---|---|---|---|---|
| 1 | 1 | Spleen | CAKVPYYFDYW | IGHV1-81*01 F | 2 | 9 |
| 1 | 2 | Spleen | CARRSGGAYW | IGHV1-67*01 P | 1 | 4 |
| 2 | 3 | Spleen | CARHGDGDYFDYW | IGHV1-81*01 F | 3 | 3 |
| 2 | 4 | Spleen | CARGDYDPYWYFDVW | IGHV1-81*01 F | 1 | 7 |
| 3 | 5 | Liver | CARHEDLLRYAMDYW | IGHV1-62-2*01 F | 2 | 4 |
| 4 | 6 | Liver | CAREGGFAYW | IGHV1-37*01 F | 1 | 14 |
| 5 | 7 | Liver | CARGYDGYFDYW | IGHV14-3*01 F | 1 | 9 |
| 6 | 8 | Liver | CARSDYGNYFDYW | IGHV1-56*01 F | 2 | 18 |
| 7 | 9 | Liver | CARSNWDDRGFDYW | IGHV1-80*01 F | 1 | 16 |
| 8 | 10 | Liver | CARREGAQVPLFAYW | IGHV1-81*01 F | 3 | 17 |
| 8 | 11 | Liver | CARYYYGRDYFDYW | IGHV1-82*01 F | 1 | 2 |
| 9 | 12 | Liver | CASTGPSSAWFAYW | IGHV14-3*01 F | 2 | 4 |
| 10 | 13 | Liver | CARYYSNYYAMDYW | IGHV1-9*01 F | 1 | 8 |
| 11 | 14 | Liver | CARSGGWLLQAMDYW | IGHV1-42*01 F | 1 | 14 |
| 12 | 15 | Spleen | CARGGPYGYHDASYAMDYW | IGHV1-7*01 F | 1 | 4 |
| 12 | 16 | Spleen | CARTGTGYYAMDYW | IGHV14-3*01 F | 1 | 3 |
| 13 | 17 | Spleen | CARPRAIYYGNSGFAYW | IGHV1-80*01 F | 1 | 2 |
| 14 | 18 | Spleen | CAPDSSGYGYW | IGHV14-3*01 F | 2 | 2 |
| 14 | 19 | Spleen | CARGWSCDYW | IGHV14-3*01 F | 3 | 3 |
| 15 | 20 | Spleen | CARAPSYYGSSHWYFDVW | IGHV1-4*01 F | 1 | 3 |
| 16 | 21 | Spleen | CARRGITTVFDYW | IGHV1-47*01 F | 1 | 3 |

**Table 1 LCM clone characteristics**

**CDR3 sequence, Vh gene, total number of sequences and number of unique sequences from microdissections of spleen or liver sections from which sequences were obtained.**

To more deeply investigate the extent of SHM and the magnitude of overlap of the responding B cell repertoire in different B cell populations at both sites, we performed high throughput sequencing (HTS) of the heavy chain VDJ mRNA, as described previously (11). We sorted splenic and hepatic B cell blasts and PBs at D13 post-infection and created libraries with V region sequences of these 4 populations. HTS analysis was done as previously described (65, 66). Clones were included in this analysis only if they had between 1 and 4 non-templated CDR3 residues (as measured from the first non-GL-encoded nucleotide) and/or at least 4 common V-gene mutations across all sequences. We found that about 75% of the clones within the 4 populations were unmutated (figure 11A), suggesting that *Ehrlichia* infection induced SHM in only a subset of B cells, which is consistent with our microdissection results (figure 10). Overall, 10-15% of the clones had an average mutation of >0 and <=1 and 5-10% of the clones had an average mutation between 1-5 (figure 11A). To gain insight into how clones grew and migrated, we categorized the clones according to their clonal lineage characteristics into 3 groups that might reflect different origins or patterns of clonal expansion: unmutated, GL branched (mutated clones that do not have a common shared mutation) and trunk (clones that have a common shared mutation and bifurcate further). Although the total number of unmutated clones was the greatest (at ~75%, Fig. 11A), GL branched clones were substantially larger in terms of both clone size and "instances" (defined as total number of unique sequences), while trunk clones were intermediate (figure 12). Hence, while there is a greater number of unmutated clones, those that do mutate have expanded considerably in terms of numbers of sequences and thus, presumably, numbers of cells.

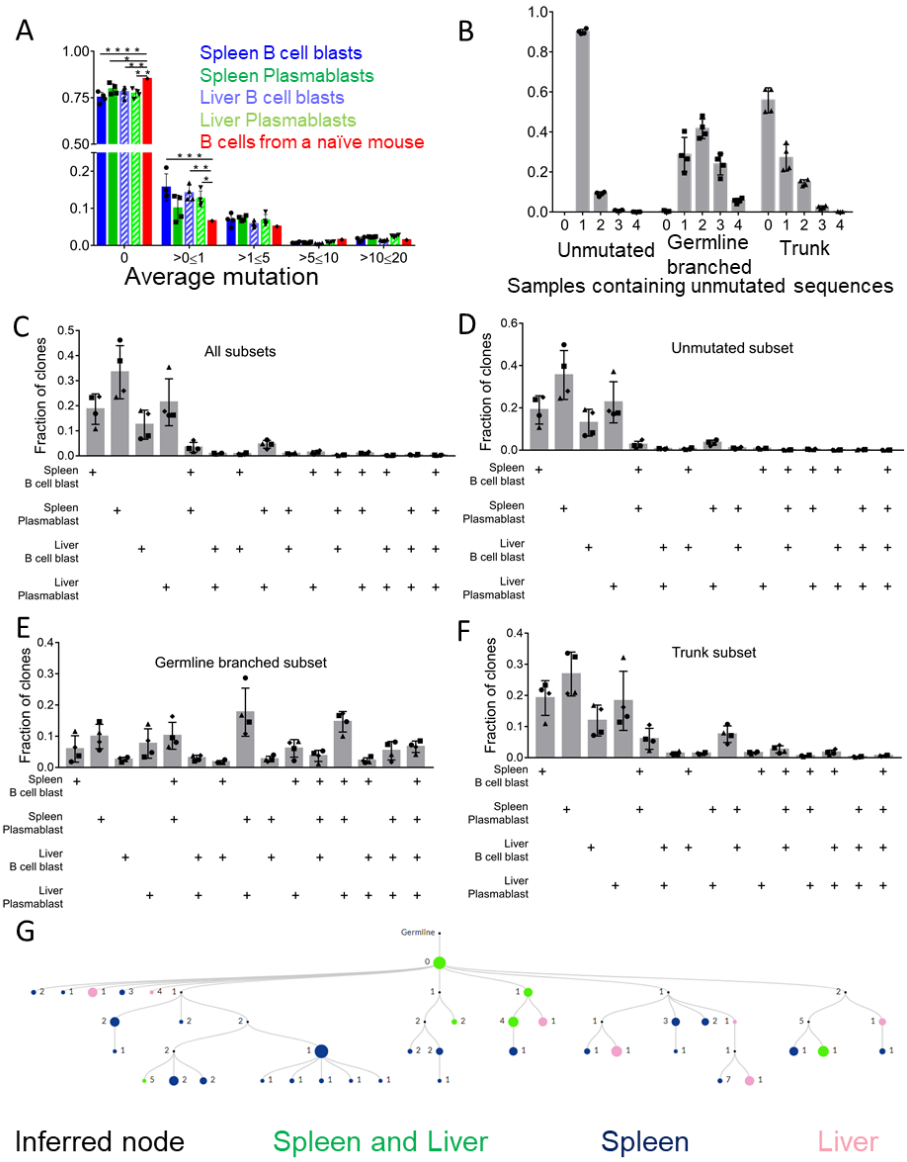


**Figure 11 SHM in spleen and liver B cell blast and PB population**

**(A) Mutation distribution in splenic and hepatic B cell blasts and PBs populations. (B) Fraction of unmutated, GL branched and trunk clones found in any of the 4 populations of hepatic and splenic B cell blasts and PBs. (C-F) Fraction of clones shared within splenic and hepatic B cell blasts and PBs populations of all clones (C), unmutated clones (D), GL branched clones (E), and trunk clones (F), (G) An example of a multi-tiered clonal lineage that was found in both spleen and liver. Nodes are color coded, the ones found in both organs are green, the ones found in spleen only are blue, the ones found in liver only are pink, inferred nodes are shown in black.**

**The size of the node is proportional to the number of sequences that make that node. Data are from one HTS experiment with 4 mice in the infected group and 1 uninfected control mouse.**

Within each category we then assessed the extent of sharing of clones between the 4 populations that were sequenced. Among unmutated clones, the vast majority (~90%) were found in only one population and only 10% were found in as many as 2 populations (figure 11B). However, the GL branched clones demonstrated extensive spread among the different populations, with 40% of clones found in 2 populations, ~25% clones found in 3 populations and ~5% shared among all 4 populations (figure 11B). In the case of the trunk clones, we found that about 20% of the clones were shared between 2 populations (figure 11B). These data suggested that the more mutations the responding B cells gathered, the more likely they were to differentiate and to spread between liver and spleen and to populate both B cell blasts and PBs.

To determine patterns of migration and differentiation we assessed the fraction of clones that overlapped among all the populations. Overall, splenic and hepatic PBs demonstrated the most overlap (~5%) (figure 11C). Upon breaking down the clones based on their unique clonal lineage categories defined above, we found that splenic and hepatic PB populations exhibited the most overlap that amounted to ~20% of the GL branched subset and 5% of the trunk subset (figure 11D-F). The GL branched category demonstrated the most overlap, wherein, 15% of the clones were shared amongst splenic B cell blast and PB along with hepatic PB and 5% of the clones were shared by all 4 populations (figure 11E). Analysis of the selection pressure on the B cell clones revealed that the responding GL branched clones exhibited a greater degree of selection pressure in comparison to trunk clones (figure 13). Because we only sampled a small fraction of the total clones in both spleen and liver, it should be recognized that the extent of sharing is a minimal estimate. Overall, these data demonstrated that *Ehrlichia* infection induced SHM in a subset of

responding B cells and that within the mutated clones, there was a great degree of differentiation and spreading.

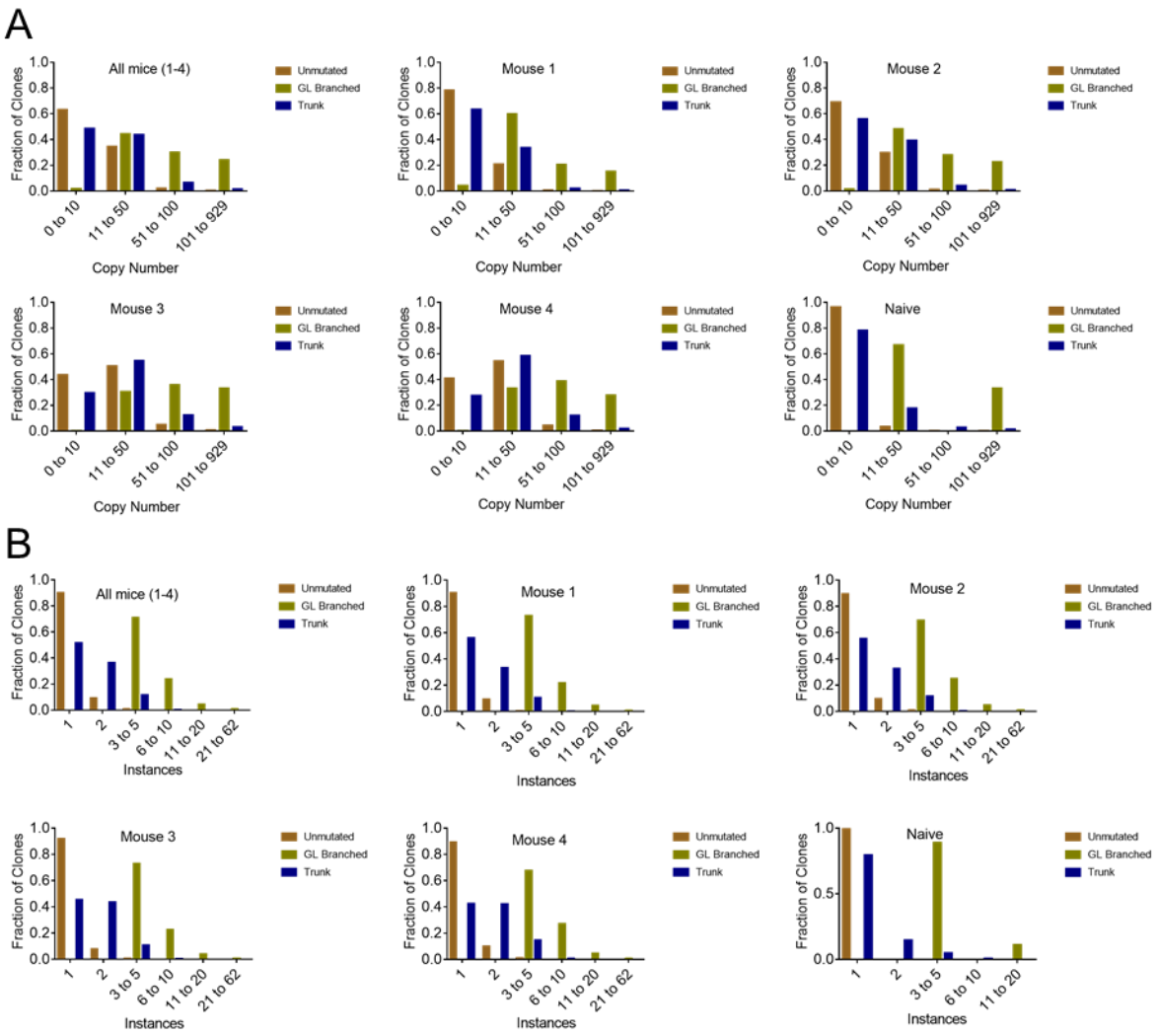


**Figure 12 Clone size analysis in the BCR repertoire after *Ehrlichia* infection**

**Analysis of clone size of unmutated, GL branched and trunk populations in *E. muris* infected mice (1-4) and naïve mice by copy number (A) and instances (B). Data are from one HTS experiment with 4 mice in the infected group and 1 uninfected control mouse.**

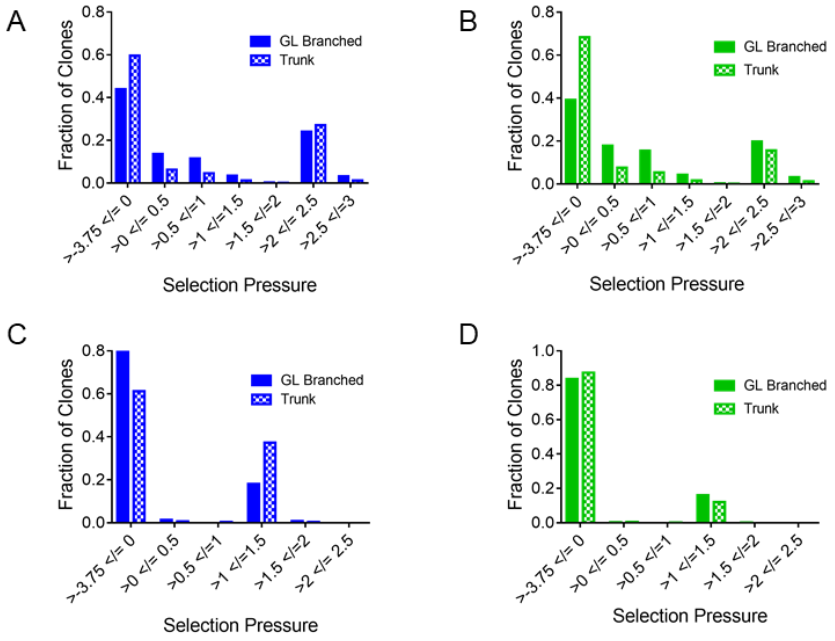


**Figure 13 Selection pressure analysis in the BCR repertoire after *Ehrlichia* infection**

**Distribution of clones with different degrees of selection pressure in CDRs (A, B) and FRs (C, D) of B cell blasts (A, C) and PB (B, D). In each scenario, selection pressure in GL branched was significantly different than that in the Trunk clones ($p<0.05$). Data are from one HTS experiment with 4 mice in the infected group and 1 uninfected control mouse.**

These conclusions were further supported by examination of detailed genealogies of representative larger expanded clones that were found in both spleen and liver (figures 11G and 14). In figures 11G and 14A the clones depicted had a GL sequence that was found in both organs; however, the clone further diversified, accumulating additional mutations that demarcated nodes and branches that were found only in spleen or liver. In figure 14B, the GL sequence was found only in the liver, but other nodes of the clone overlapped between the spleen and liver and a branch was found only in the spleen. The clone depicted in figure 14C demonstrates extensive additional mutation restricted to either spleen or liver (see left and center main branches). These data are most

consistent with bidirectional spreading of B cell clones along with continued local mutation and expansion after dissemination.

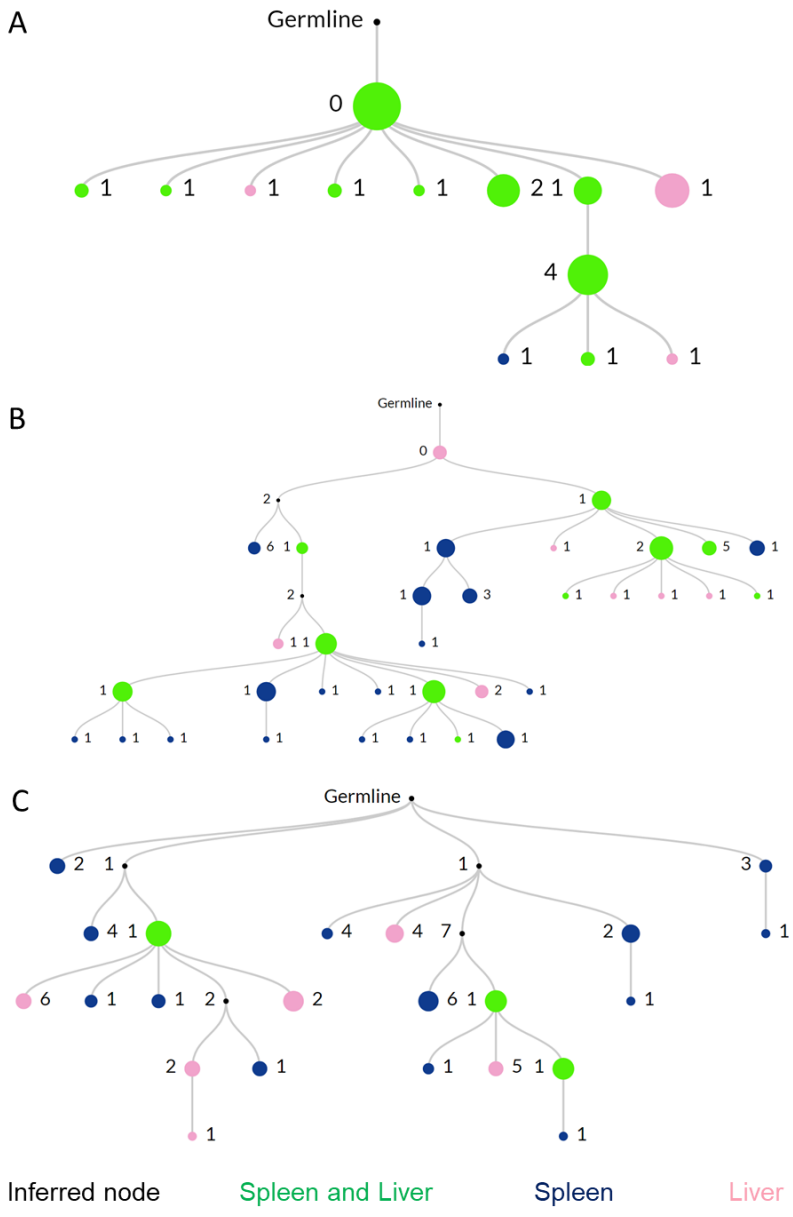


**Figure 14 Examples of B cell clonal lineages induced by acute *Ehrlichia* infection**

**(A-C) Examples of multi-tiered clonal lineage that were found in both spleen and liver. See legend of figure 11 for details on the organization of the clonal trees. Data are from one HTS experiment with 4 mice in the infected group and 1 uninfected control mouse.**

Previously, CD19, CD80, CD11c, and T-bet+ B cells have been shown to persist in spleen for substantial periods of time after initial *Ehrlichia* infection (33, 43, 77). These were interpreted to depend on inflammation or chronic low-level Ag stimulation, since *E. muris* causes persistent infection. We sought to determine whether generation and maintenance of both splenic and hepatic MBC populations depends on Ag persistence. To eliminate persistent Ehrlichia infection, we treated mice with doxycycline at 4 weeks post-infection, and then examined the MBC responses in the spleen and livers between weeks 6 and 12 post-infection. We refer to these mice as "memory mice." We gated on MBC by using a commonly used marker that includes classical MBC markers, CD73 (78), along with T-bet expression (figure 15). We found a significant number of MBC in both spleen and liver of the memory mice compared to their naïve counterparts (figure 16A-C). In both spleen and liver, these cells expressed the classical MBC markers CD80 and PD-L2 in a unimodal fashion (figure 16 D-E). By contrast, a distinct subpopulation of the $CD73^{+}T\text{-}bet^{+}$ cells expressed the ABC markers CD11b and CD11c (figure 16F-G). Moreover, these MBC were quiescent, with few expressing Ki67 (figure 16H).

IgM was expressed by most of the MBC, with a fraction lacking IgM being more predominant in the liver (figure 16I). These findings, though consistent with prior work (43), extend and modify previous findings in several ways. First, they reveal that the markers CD11b and CD11c, which up to now have been used to identify ABC-type MBC, only identify a fraction—in fact less than half—of all T-bet+ elicited MBC, indicating that many MBC have been overlooked in prior work and raising the question of whether there is additional functional heterogeneity among T-bet expressing MBC. As an approach to resolve this, we find that CD73 and CD80 both correlated well with T-bet expression and could be used as surrogates for T-bet

intracellular staining at least in this setting (figure 17). Second, they demonstrate a tissue-localized MBC population in the perfused liver that is phenotypically similar to that in the spleen.

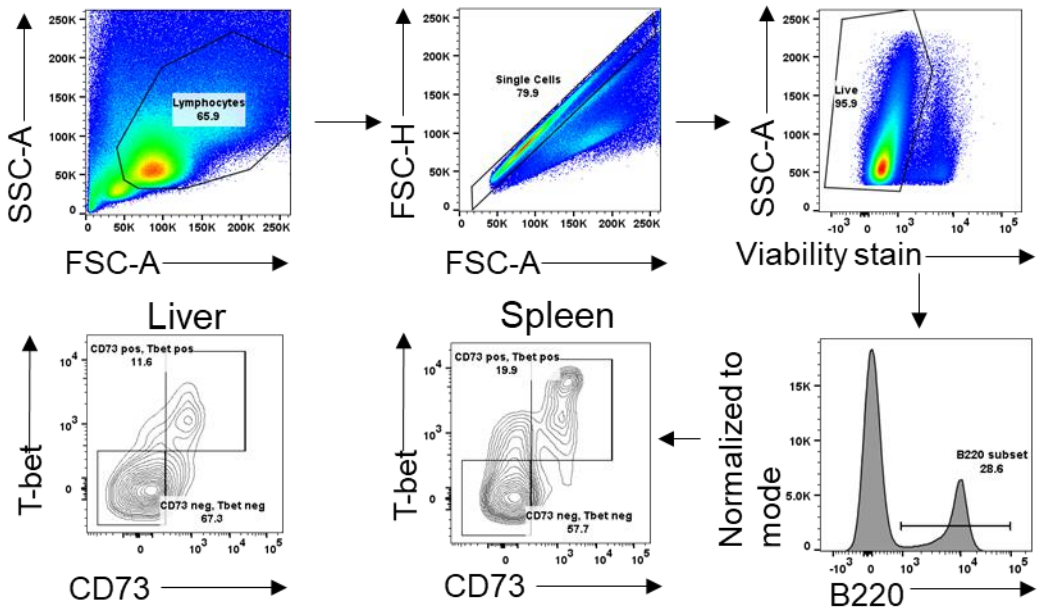


**Figure 15 Gating strategy for MBC subsets in spleen and liver.**

**Data are representative of at least two independent experiments.**

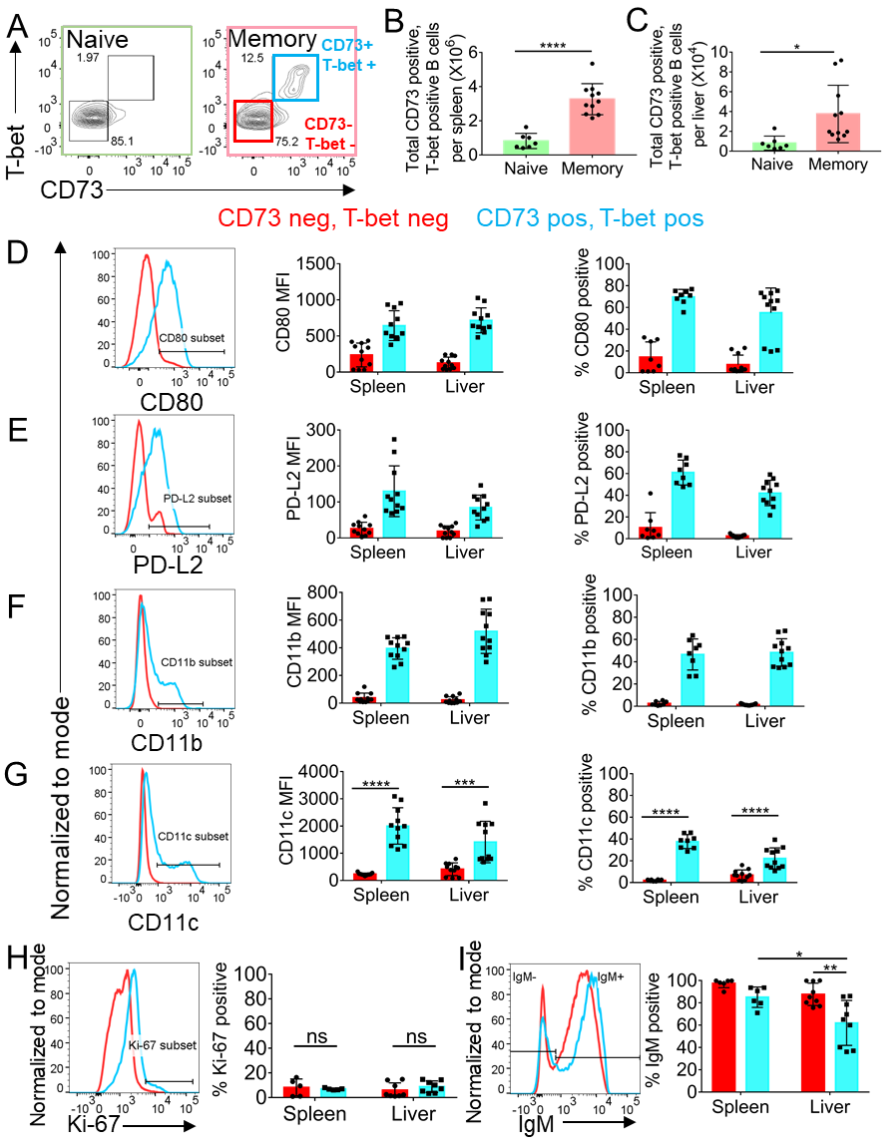


**Figure 16 Memory-like T-bet positive B cells persist in the spleen and liver after infection**

**(A) Gating strategy for CD73 positive and T-bet+ B cells present in spleen and liver of naive and memory mice. (B-C) CD73 positive and T-bet+ B cells in spleen (B) and liver (C) harvested after perfusion with PBS of naive and memory mice. (D-G) Histogram, MFI and percentage of cells positive for CD80 (D), PD-L2 (E), CD11b (F), CD11c (G) in CD73 and T-bet negative and CD73 and T-bet+ B cells in the spleen and liver of memory mice. (H-I) Histogram and percentage of Ki-67 positive cells (H) and histogram and percentage of IgM positive cells in CD73 and T-bet negative and CD73 and T-bet+ B cells in the spleen and liver of memory mice. Data are representative of at least two independent experiments with and are represented as mean with SD of groups of at least two mice.**

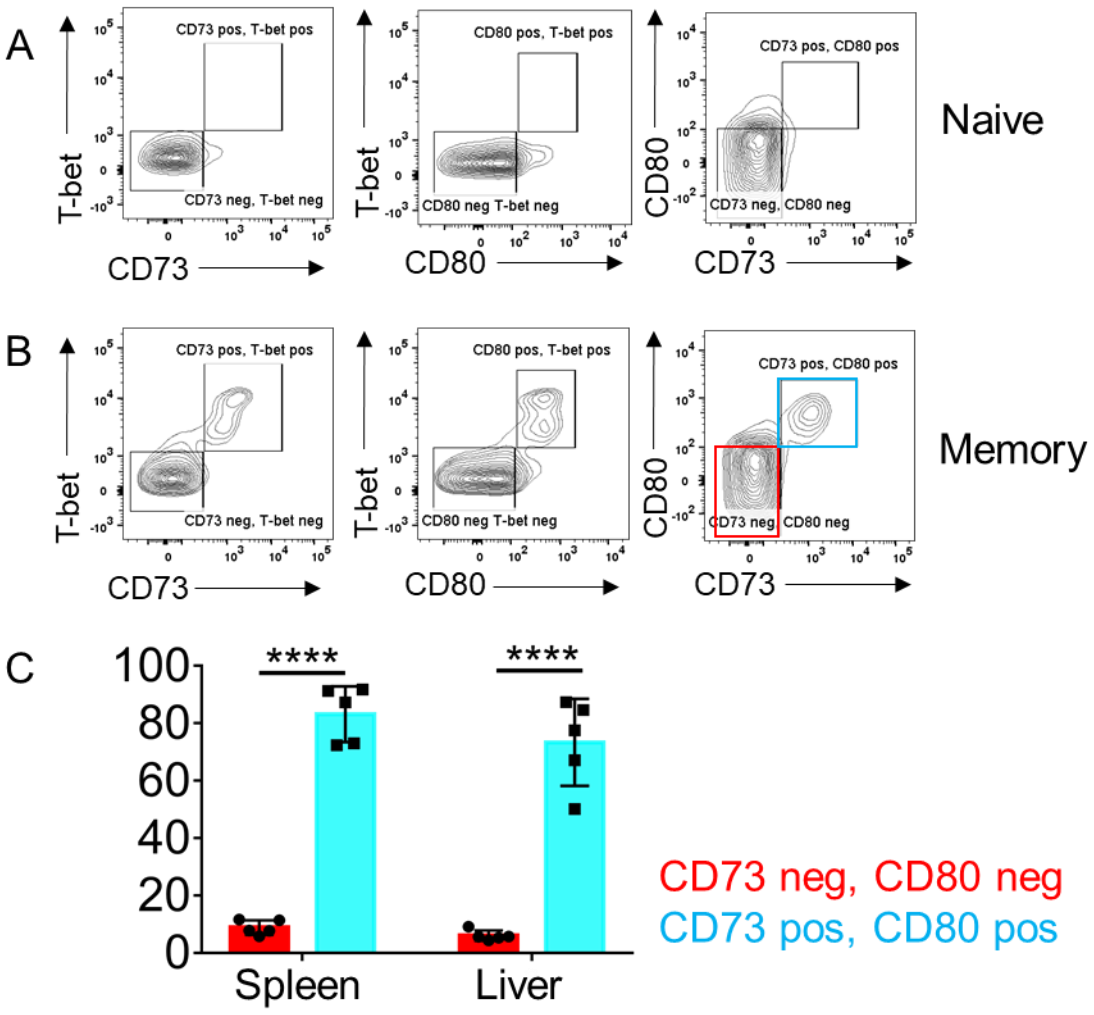


**Figure 17 CD73 and CD80 are surrogate markers for T-bet expression**

**Contour plots showing CD73 and T-bet double positive, CD80 and T-bet double positive and CD73 and CD80 double positive populations in B220 positive cells in naïve and memory mice. (C) Percentage of T-bet positive cells in CD73 and CD80 double negative and CD73 and CD80 double positive B cell populations in memory mice. Data are representative of at least two independent experiments with and are represented as mean with SD of groups of at least two mice.**

To rule out any contamination from circulating MBCs that were not removed from the liver by perfusion, we employed an approach that involved labeling all circulating B cells via intravenous injection of anti-CD19-PE. We harvested spleen, blood and liver 3 minutes after the injection. Though all the B cells in the blood become labeled, given the short window of time and because of the large size and molecular weight of the fluorophore PE, the antibody is not able to reach the liver parenchyma to a substantial extent. Thus, any liver localized MBC would be anti-CD19-PE low or negative. In practice, during tissue processing, tissue-localized cells encounter anti-CD19-PE released from the substantial vascular compartment of the liver (which is unperfused) and thereby become stained, albeit to a substantially lower level. Post-processing, we further stained the cells with anti-CD19 in a different color (BUV395). In the liver there was a clear population of cells that are much more dimly stained with anti-CD19-PE (~5x dimmer) but more brightly stained with anti-CD19-BUV395 (figure 18 A-B). No such population existed in the blood (figure 18 A-B). As expected, spleen had mostly CD19-PE-low cells as follicular B cells are not directly accessible to blood and are not quickly stained by an antibody (figure 18 A-B). There were about 10% of liver MBCs in unperfused liver that weakly stained with anti-CD19-PE and brightly stained with anti-CD19-BUV395. Moreover, the number of these cells is comparable to the number of MBCs that we observed in the liver after perfusion (figure 18C and figure 16C). These data provide support for the interpretation that there is a tissue-localized MBC population that persists after perfusion of livers. The other ~90% of cells in unperfused liver that stain brightly with anti-CD19-PE within 3 minutes are presumably in intravascular spaces, such as the sinuses, and these would very largely be washed away by perfusion. Moreover, by histology, we found CD19- and CD11c-expressing MBC in the liver parenchyma of immune mice (figure 19 A-B). Upon comparison to livers from naive mice, we observed significantly more CD19- and CD11c-

double positive cells per field in the immune mouse livers (figure 19 C-D). Taken together, these data suggest that there is a liver-localized MBC population induced by *E. muris* infection.

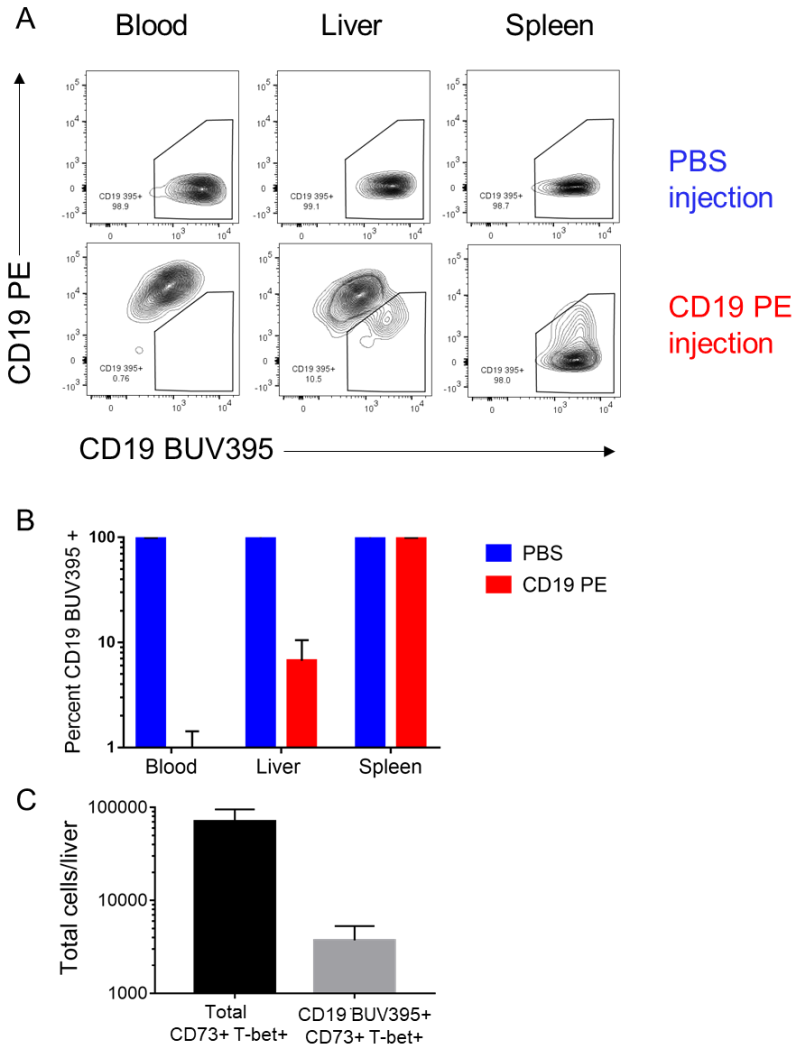


**Figure 18 Short term labeling of circulating MBC using CD19 PE**

**(A) Representative contour plots of CD73+ T-bet+ MBCs unlabeled (top panel) or CD19 PE labeled (bottom panel) in the blood, spleen liver and spleen. (B) Percentage of CD19 BUV395 positive cells in the blood, liver and spleen of mice i.v. injected with PBS or CD19 PE. (C) Number of total CD73+ T-bet+ MBC in the liver (black bar) and number of CD19 BUV395+ CD73+ T-bet+ MBC as per the gating shown in (A) in the liver (grey bar). Data are representative of at least two independent experiments with and are represented as mean with SD of groups of at least two mice.**

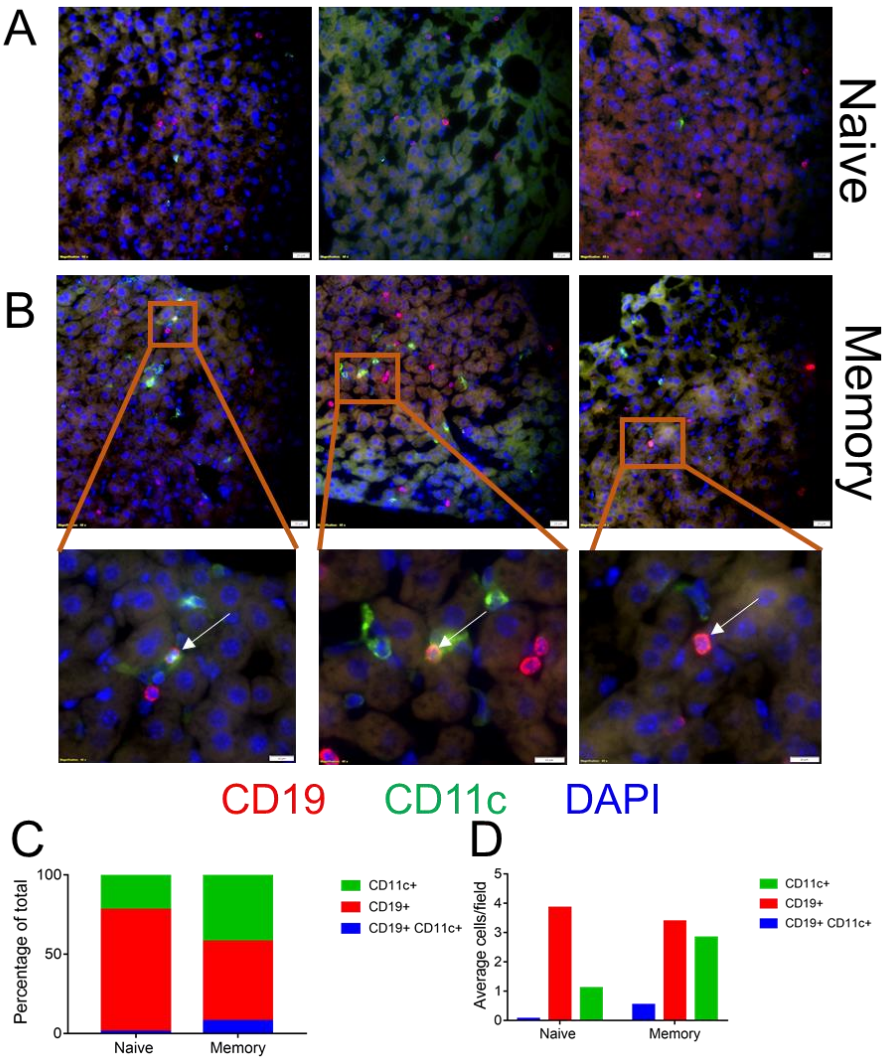


**Figure 19 *Ehrlichia* induced MBC localized in the liver parenchyma**

**(A-B) CD19 and CD11c staining in naïve livers (A) and memory livers (B) at 40X magnification, scale bars in the first and second row represent 20µm. Scale bars in the third row represent 10µm. CD19 and CD11c double positive cells are marked by white arrows. (B) 100 cells were counted from 20 fields from the liver parenchyma of 3 naïve mice and 371 cells were counted from 53 fields from the liver parenchyma of 4 memory mice. (C) Percentage of CD11c positive, CD19 positive and CD19 and CD11c double positive cells out of the total number of cells counted in the liver parenchyma of naïve and memory mice. (D) Average cells per each field in the liver parenchyma of naïve and memory mice. Chi-square analysis comparing the numbers of CD19+ and CD19+ CD11c+ B cells from naïve and memory groups had a p-value of 0.002318. Data are representative of at least two independent experiments.**

The validation of CD73 as a marker for T-bet+ MBC in this setting allowed us to sort CD73 positive hepatic and splenic MBC from memory mice and perform V region HTS to assess both SHM and clonal sharing among sites and subsets. As seen from the fraction of clones that are unmutated (figure 20A), 60% IgM MBC and 80% of IgG MBC clones were mutated in both organs. Overall, IgG clones harbored more mutations than IgM clones and 40% of splenic IgG clones and 20% of hepatic IgG clones had an average of between 5 and 20 mutations (figure 20A). A substantial fraction of clones had 1-5 mutations per sequence, which is comparable to levels seen in MBC after primary responses to model Ags that occurred in GCs (78, 79). Thus, the extra-GC pathway that generated these cells also induced an MBC compartment that was mutated to a similar extent as one generated by GC-dependent pathways. In addition, these data establish that the MBC compartment localized in the liver is similarly mutated to that in the spleen. Approximately 90% of the clones were found only in spleen, with about 5% found in only in liver and 5% shared between spleen and liver (figure 20C-D). The GL branched category had the most clones shared in spleen and liver, indicative of the fact that this category includes clones with more mutation and expansion, though a smaller category overall in terms of numbers of clones (figure 20C-D). A major reason for the relative lack of overlap of clones in spleen and liver could be the much larger size of the spleen MBC pool and differences in sampling depth. Alternatively, it is possible that only a few splenic MBCs engraft the liver and/or the majority of liver-derived MBCs engraft the splenic MBC compartment. It could also be that while B cell blasts and PB clones disseminate as they are generated, MBC form as local offshoots of dividing clones without much further disbursement after they differentiate. Due to an inability to sample all the cells in each organ these possibilities are difficult to distinguish. Analysis of clonal trees from large clones does reveal trees that are consistent with both migration after differentiation as well as extensive local

production of diversified MBC clonal populations (figure 21). However, these clones represent a small fraction of the overall MBC clonal distribution that was recovered.

Concurrent with this expansion was selection upon mutating clones, which occurred in both complementarity determining regions (CDRs) as positive selection and framework regions (FR) as negative selection; a large fraction (between ~1/3 and 2/3 of total, not shown) of both B cell blast and PB clones of both trunk and GL-branched showed more statistically significant selection compared to the underlying neutral mutation model. GL-branched clones also demonstrated more selection pressure than trunk clones in both B cell blast and PB populations (Fig. 13).

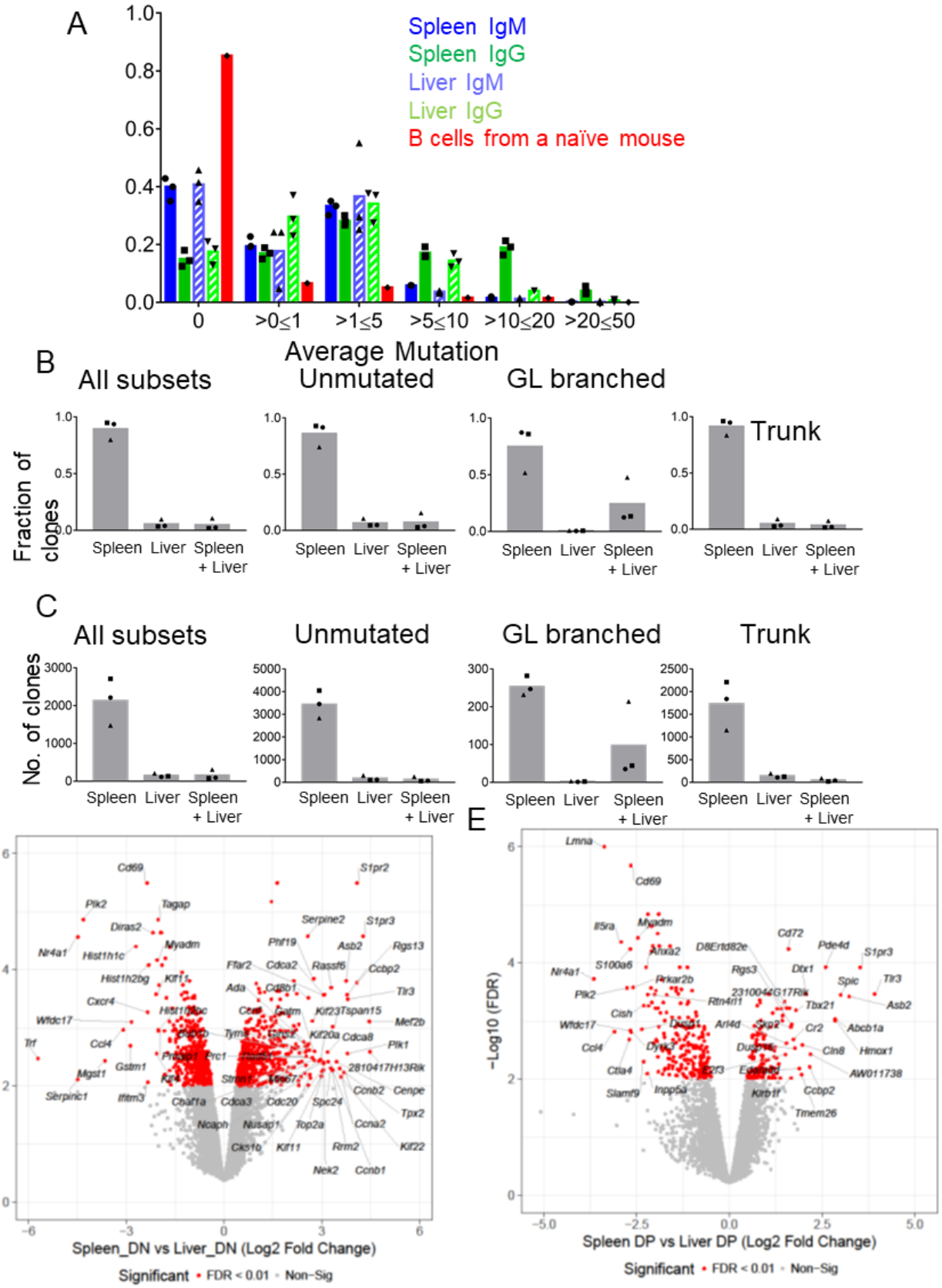
A
Spleen IgM
Spleen IgG
Liver IgM
Liver IgG
B cells from a naïve mouse
Average Mutation
0
>0≤1
>1≤5
>5≤10
>10≤20
>20≤50
B
All subsets
Unmutated
GL branched
Trunk
Fraction of clones
Spleen
Liver
Spleen + Liver
C
All subsets
Unmutated
GL branched
Trunk
No. of clones
D
Spleen_DN vs Liver_DN (Log2 Fold Change)
-Log10 (FDR)
Significant • FDR < 0.01 • Non-Sig
E
Spleen DP vs Liver DP (Log2 Fold Change)
-Log10 (FDR)
Significant • FDR < 0.01 • Non-Sig

**Figure 20 Repertoire and phenotypic characteristics of the MBC population of spleen and liver**

**Mutation distribution of MBC population in spleen and liver from memory mice and B cells from a naïve mouse. (B-C) Overlap within different subsets of MBC clones analyzed by fraction of clones (B), and number of clones (C). (D-E) Volcano plots demonstrating highly expressed genes in spleen and liver DN (D) and DP (E) MBC subsets. Data are from one RNA-seq experiment with DN and DP MBC FACS sorted from 3 different mice.**

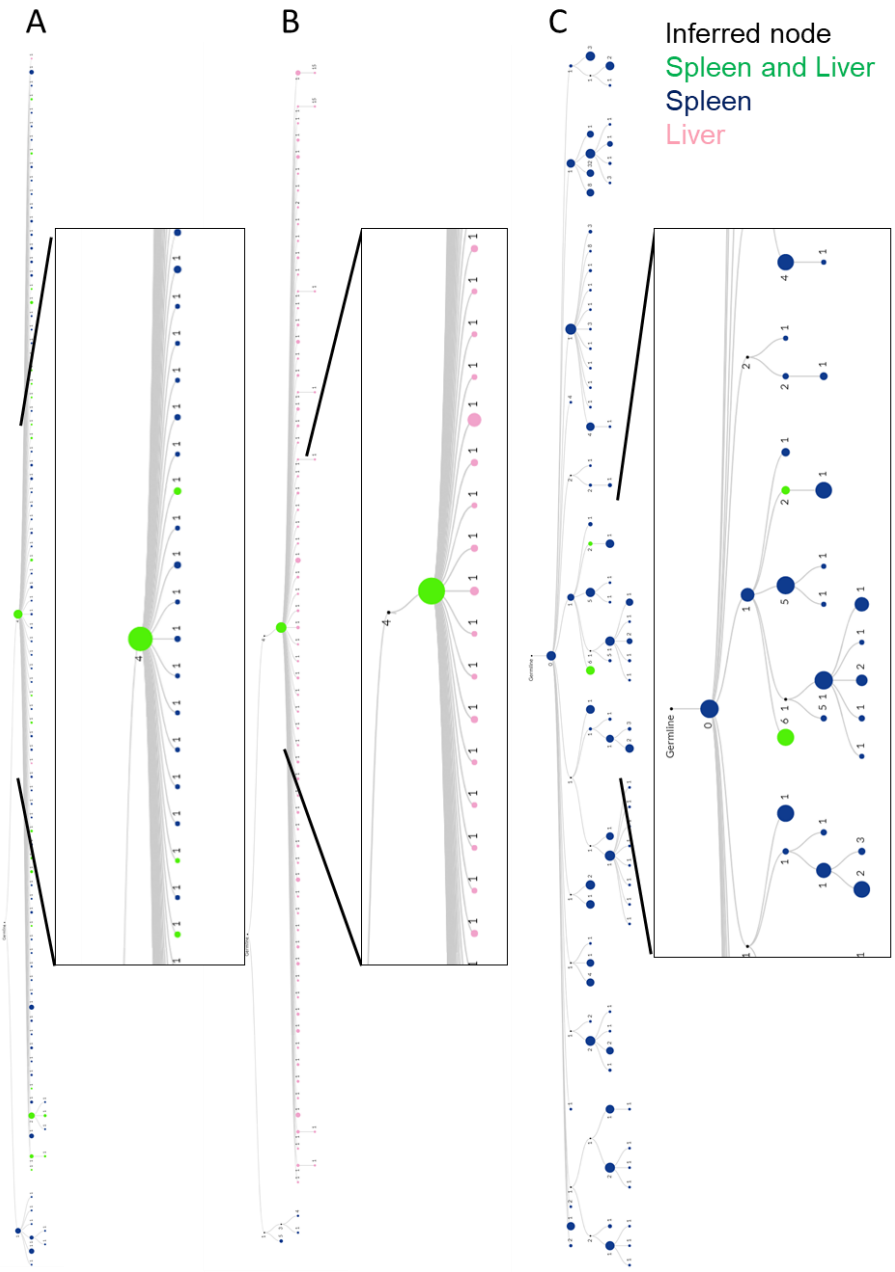


**Figure 21 Examples of MBC clonal lineages induced by *Ehrlichia* infection**

**(A-C) Example of a multi-tiered clonal lineage among MBC that was found in both spleen and liver (A), mostly liver (B) and mostly spleen (C). Nodes are color coded: ones found in both organs are green, the ones found in spleen only are blue, the ones found in liver only are pink, inferred nodes are shown in black. The size of the node is proportional to the number of sequences that comprise that node. Boxed areas show enlargement of representative parts of the clones. Data are from one RNA-seq experiment with DN and DP MBC FACS sorted from 3 different mice.**

To phenotypically characterize the splenic and hepatic MBC, we performed RNA-seq analysis of CD11b-CD11c- (double negative; DN) and double positive (DP) MBC on FACS sorted populations (figure 22A). We found 730 genes that were differentially expressed (FDR<0.01, 2-Fold change) in the splenic and hepatic MBC populations (figure 22B). Gene clusters marked with navy blue, red and dark red were significantly and differentially expressed in the DN subsets compared to the DP subsets regardless of the site of origin (figure 21B). Gene clusters marked with yellow, purple, pink, turquoise blue and light pink were differentially expressed in the liver MBC compared to the splenic counterparts (figure 22B). Amongst the genes that were differentially expressed between spleen and liver MBC subsets with an FDR<0.01 (figure 20 F,G), comparing liver and splenic DN subsets, we found genes related to cell cycle such as POLO like kinase 2 (Plk2) and genes related to signaling such as Nur77, GTPase activating protein Tagap, and Ras GTPase Diras2 to be upregulated in the liver (figure 20F). G-protein coupled receptors S1pr2 and S1pr3, and cell cycle associated gene cdca2 were upregulated in the spleen (figure 20F). Comparing the liver and splenic DP subsets, we found B cell development and maturation genes such as Lamin A (lmna) and interleukin 5 receptor alpha (IL5Ra) and genes related to signaling such as Mapk12 were upregulated in the liver (figure 20G). G protein coupled receptors S1pr3, inhibitory receptor CD72, and a protein involved in cAMP degradation - phosphodiesterase 4d (pde4d) - were upregulated in the spleen (figure 20G). A positive regulator of the Notch1 signaling pathway Dtx1 was also found to be differentially expressed in splenic DP MBCs (figure 20G). We found that liver MBC subsets both expressed CD69 when compared to splenic MBC subsets (figure 20F-G), consistent with expression patterns of bona fide tissue resident memory T cells. We verified CD69 expression on liver MBC subsets during the acute response by flow cytometry (figure 22 C-D). Together, these data demonstrate that while there are shared genes that are

expressed in MBC subsets regardless of their tissue localization, there are several genes unique to the subset and site of origin. This suggests that the local tissue microenvironment may be shaping the MBC differently in the spleen and liver, much as it does for T cells and macrophages (80, 81).

We performed gene set enrichment analysis (GSEA) compare it to a published dataset from CD11c-expressing splenic B cells isolated 30 days after *Ehrlichia* infection that were presumptive MBC (43). GSEA revealed that genes found in that database are significantly enriched in splenic and hepatic DP MBCs compared to DN MBC (figure 22E-F). These data are consistent with the previously published dataset with reference to *Ehrlichia* infection. Since we did not perform our own RNA-seq on naive B cells, we performed differential analysis of splenic and liver memory subsets with respect to naive B cells from a previously published study (41) (see Methods of inter-study normalization detail). Using a set of genes upregulated for nitrophenol (NP)-induced MBC (F. Weisel and M. Shlomchik, unpublished data and manuscript in preparation) we found that splenic DN, splenic DP, and hepatic DP MBC subsets had significant enrichment of memory genes, while hepatic DN MBC had a similar trend that did not reach statistical significance ($p>0.05$) (figure 23A-D). These data suggest that *Ehrlichia*-induced splenic DP and DN, along with hepatic DP MBC subsets, express genes that are characteristically expressed by classical GC-induced MBC.

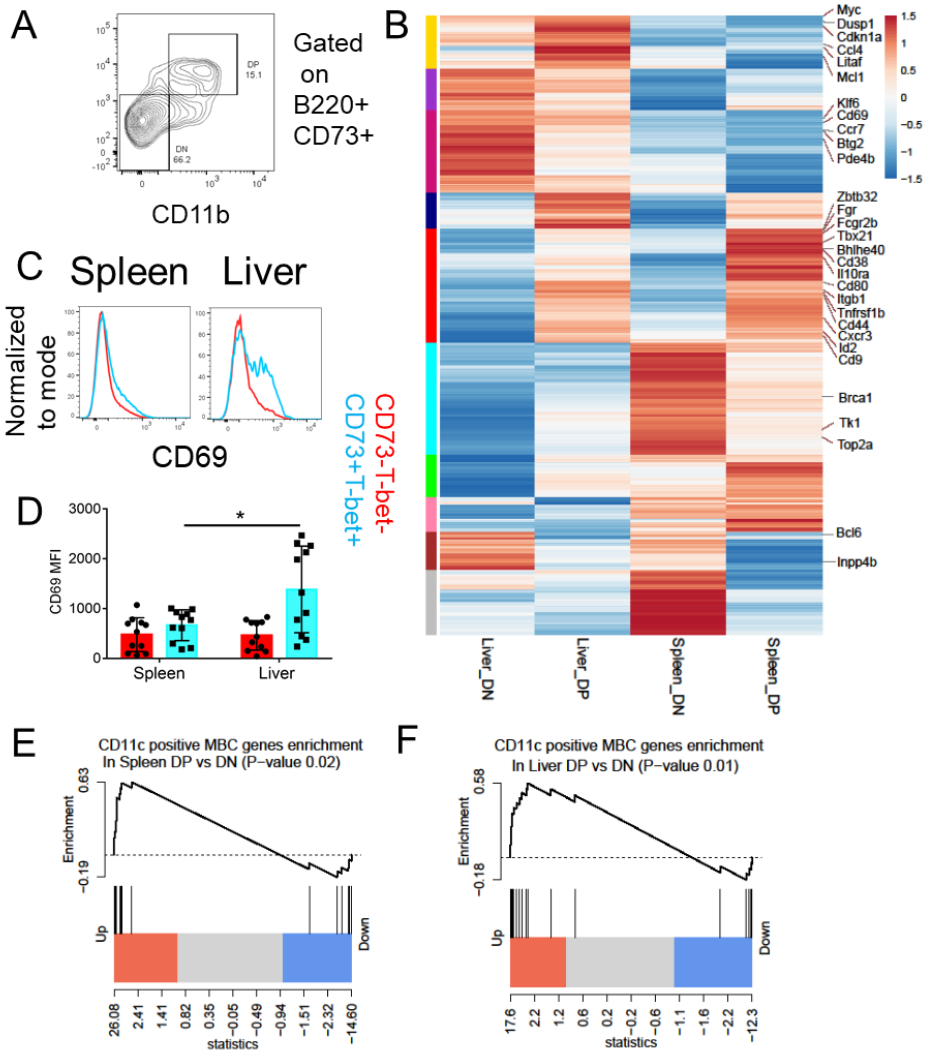


**Figure 22 Comparison of splenic and hepatic MBC subset gene expression**

**(A) DN and DP MBC subset gating based on CD11b and CD11c expression on CD73 positive MBCs from the spleen used for sorting of cells prior to RNA-seq analysis. (B) Heat map of 730 differentially expressed genes in splenic and hepatic MBC populations. (C-D) Histogram (C) and quantification (D) of CD69 MFI in splenic and hepatic MBCs during acute Ehrlichia infection. (E-F) RNA-seq data were used to construct gene set enrichment plots illustrating genes differentially expressed in the DP subset compared with the DN subset (*n* = 3 per group) for spleen (E) and liver (F) with respect to a known set of genes specific for CD11c positive MBC induced during Ehrlichia infection (Winslow et al., 2017). Data in B, E and F are from one RNA-seq experiment with DN and**

**DP MBC FACS sorted from 3 different mice. Data in A, C and D are representative of at least two independent experiments with and are represented as mean with SD of groups of at least two mice.**

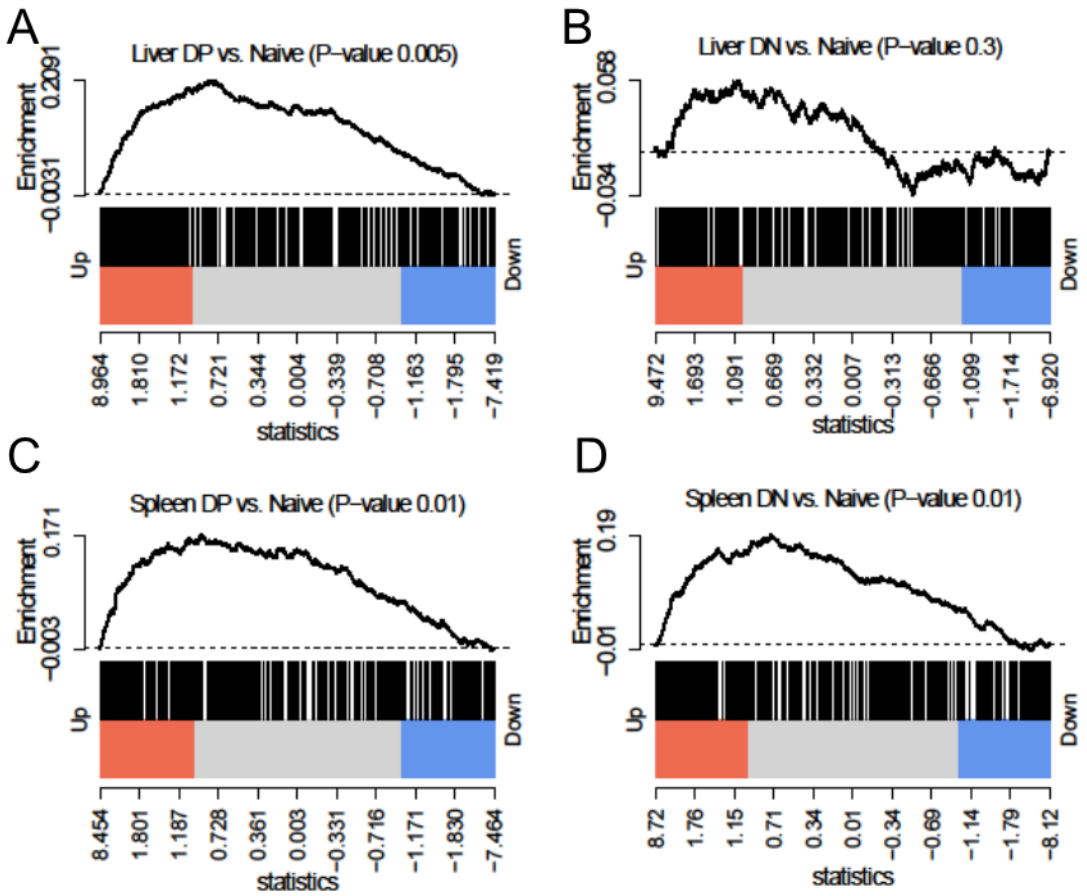


**Figure 23 Enrichment of "classical" memory genes in splenic and hepatic MBC subsets**

**(A-D) RNA-seq data were used to construct gene set enrichment plots illustrating genes differentially expressed in DP or DN subsets compared with naïve B cells from a previously published microarray dataset (Barnett et al., 2016) (n = 3 per group) for liver DP (A), liver DN (B), spleen DP (C) and spleen DN (D) with respect to a known set of genes specific for nitrophenol (NP) induced memory B cells (F. Weisel and M. Shlomchik, unpublished; manuscript in preparation). Data are from one RNA-seq experiment with DN and DP MBC FACS sorted from 3 different mice**

During the acute phase of *Ehrlichia* infection, the histologic MZ architecture is disrupted, with loss of CD169 positive metallophilic macrophages that demarcate the MZ. By flow cytometry, CD23lo CD21+ MZ phenotype B cells are also lost (figure 24A). At a memory time point the histologic MZ was largely regenerated with a border of CD169+ cells, albeit somewhat less organized than in a naïve animal (figure 24B-C). Remarkably, though, by flow cytometry at this time point, very few of the CD23lo CD21+ MZ phenotype cells that had repopulated this compartment were T-bet negative, unlike in the naïve mouse in which essentially all MZ phenotype B cells lacked T-bet expression (figure 24 B-E). In terms of cell number on average there were 2.3-fold more T-bet+ than T-bet- MZ B cells in the memory mice (figure 24 F-G). Histologically, in memory mice T-bet+ cells were found abundantly in the MZ region and were also scattered in the follicular (FO) region (figure 24B-C). A prior report had identified CD11c+ B cells in or near the MZ at day 63 post-infection (33), although as noted earlier, CD11c would only pick up <40% of total T-bet+ MBC. Generally, ABCs, which have been considered synonymous with T-bet+ B cells or even to be best defined as T-bet+ B cells , are thought to characteristically lack the expression of B cell subset markers CD21 (high on MZ B cells) and CD23 (high on FO B cells) (39). However, the T-bet+ B MBC formed in this setting post-*Ehrlichia* infection were mainly of a MZ phenotype, with strong expression of CD21, unlike classical ABC. Interestingly, the T-bet+ MBC that arose post-infection were diverse and included both ABC phenotype (CD21negCD23neg) as well as FO phenotype cells. From this we conclude that infection dramatically reprograms the MZ B cell compartment, largely replacing the initial T-bet population with T-bet+, and presumably *Ehrlichia*-responsive MZ phenotype B cells.

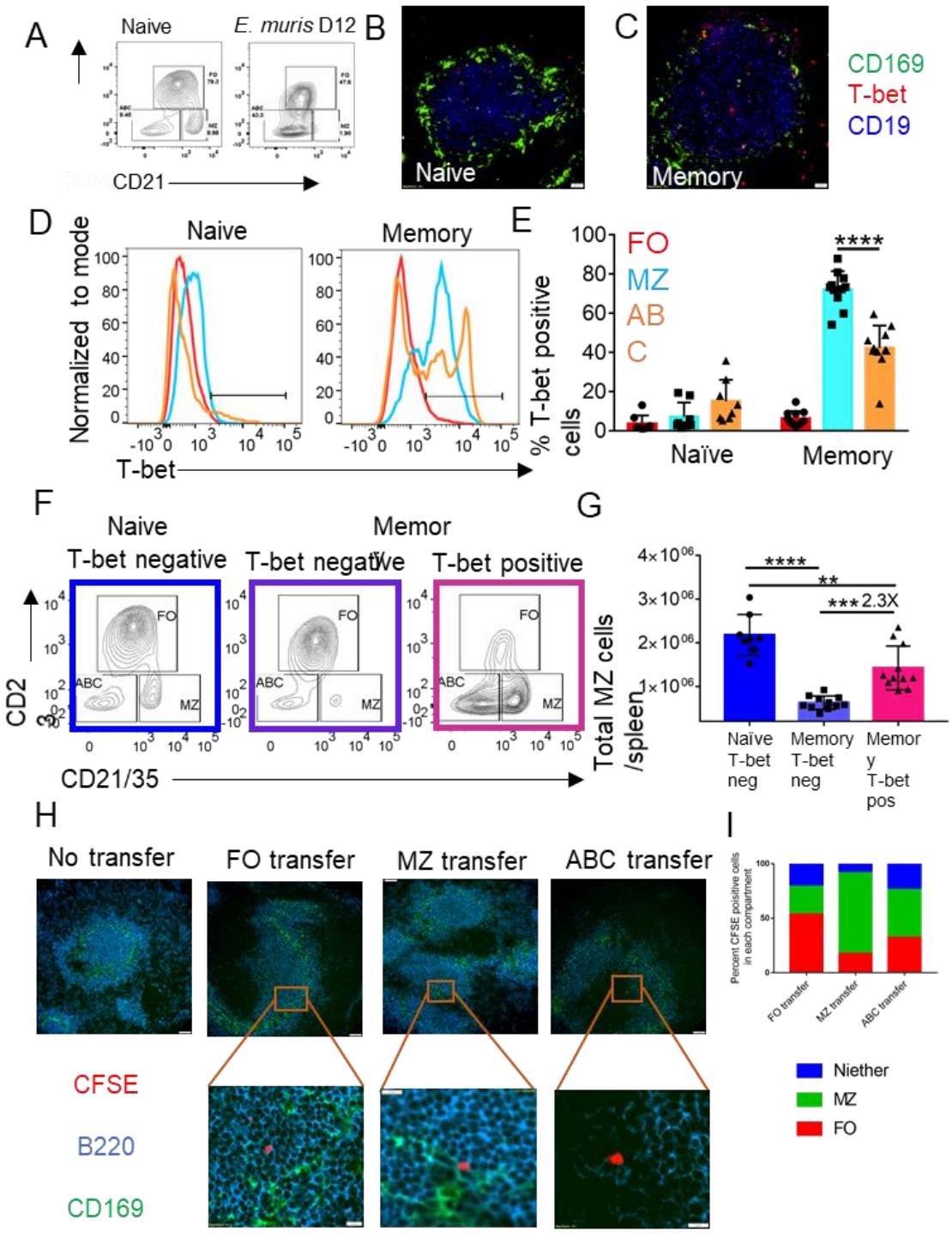


**Figure 24 After infection resolves, T-bet positive MBC dominate the MZ of the spleen.**

**(A) B cell subset gating on CD19 positive B cells in naïve or D12 post *E. muris* infection. (B-C) CD169 (green), T-bet (red) and CD19 (blue) staining in Naïve (B) and memory spleens at 40X magnification (C). In B-C scale bars represent 20µm. (D-E) Histogram (D) and percentage (E) of T-bet$^{+}$ B cells in naïve and memory mice (F)**

**B cell subset gating on naïve and memory T-bet$^+$ B cells. (G) Quantification of T-bet$^+$ MZ B cells in naïve and memory mice. (H) 20X images of CFSE-labeled CD19$^+$ CD73$^+$ CD45.2/2 splenic MBC populations sorted as CD23$^+$ CD21$^-$ (FO), CD21$^+$ CD23$^-$ (MZ) and CD21$^-$ CD23$^-$ (ABC) and transferred into *CD45.1/2* mice, shown at 42 hours post-transfer. Scale bars in the top and bottom panels represent 50μm and 10μm, respectively. (I) From the recipient mice as in (H), 67 CFSE labeled cells from the FO transfer group were counted over 42 images, 108 CFSE labeled cells from the MZ transfer group were counted over 21 images, and 105 CFSE labeled cells from the ABC transfer group were counted over 44 images. Percentages of the CFSE positive transferred MBC subsets found in FO or MZ or neither of those locations are presented in the bar graphs. Data are representative of at least two independent experiments with and are represented as mean with SD of groups of at least two mice.**

To assess whether the FO, MZ and ABC MBC subsets retain their phenotype and preferentially home to those sites upon transfer, we sorted FO, MZ and ABC CD45.2 MBCs based on the expression of CD21 and CD23. We CFSE-labeled the MBC subsets and transferred into a B18+/- Vκ8R+/- CD45.1/2 naïve mouse, then harvested the spleens of the hosts 42 hours after transfer to assess homing of the MBC subsets. Based on histologic analysis, >50% FO MBCs preferentially populated the follicle, >70% MZ MBCs populated the MZ area and the ABC populated all the zones (figure S43 H-I). These data suggest that the MBC subsets can re-home to the compartment that they originated in and that their localization is a relatively stable characteristic.

## 2.4 Discussion

Here we show that liver is a generative site for B cell responses to the gram-negative intracellular pathogen *E. muris*. This was established by showing the presence of B cells in the liver parenchyma and portal triads of infected mice, demonstrating that they are proliferating in situ via short-term EdU uptake, and most critically demonstrating clonal expansion and intra clonal V region mutation *in situ* via microdissection.

B cell responses in non-lymphoid organs have been reported in several other contexts. Influenza infection yields local responses in lung that involve generation of tertiary lymphoid tissue (82). In steady state in the small intestine there is local production of IgA AFC in the lamina propria (83); this response is likely largely driven by commensal flora (84). However, lung and gut are barrier mucosal sites that are constantly challenged with environmental pathogens and require protective Ab at their surfaces. On the other hand, liver has no direct mucosal interface with the environment.

Hepatitis infection in humans also can generate B cell infiltration, again involving tertiary lymphoid tissue (TLT) and even local GC formation (48, 49, 85). These responses are in the context of chronic infection and take weeks to months to evolve and may depend on TLT formation; in contrast, hepatic *E. muris* responses are detectable very early after infection and do not seem to involve organized TLT. Moreover, in the absence of TLT no GCs form in the liver (nor do they in the spleen), yet SHM and class switch are induced in a fraction of responding cells in the liver. Thus, under circumstances of infection, much more robust and mature local B cell responses can ensue directly within parenchymal tissue than had previously been considered.

Though antibodies (Abs) can spread throughout the body, there are several theoretical advantages of being able to mount local B cell responses: Some pathogens may not infect or spread

well to lymphoid tissue; intracellular bacteria such as *E. muris* would be in that category. Some pathogens such as *E. muris* and Plasmodium may be efficiently cleared systemically but persist in the liver as low-level infections (86, 87). Therefore, if local B cell responses were not possible, there might be little if any Ab produced against such pathogens. Intraparenchymal T cell responses and infiltration are more commonly seen; local B cell responses might optimize these, as they would allow for enhanced Ag presentation to T cells. In addition, B cells produce substantial amounts of inflammatory cytokines, such as IL-6 and TNF-α, which could stimulate other arms of the immune system and be directly protective in a local manner.

By tracking local responses at two different sites, we were able to use HTS of V regions to track the dissemination of expanded clones as the primary response evolves. Overall, there was remarkable clonal mixing, as exemplified by sample clonal trees in which liver and spleen were represented by multiple cells and branches. Limited sampling depth leads to a general underestimation of the extent of clonal size, diversification and cross-seeding of tissues. Nonetheless, it is reasonable to assume that not all clones disseminate. The response likely includes many small clones that neither induce SHM nor undergo isotype switch. Overall, mutations were only observed in about 25% of clones and it was these clones, which we termed "GL Branched", that tended to be found in multiple sites and in both PB and B cell blast compartments. More than half of all GL Branched clones were found in both spleen and liver. These clones are evidently much larger than those in either the Unmutated or Trunk subsets. It is not clear what controls whether clones initiate SHM and expand to a greater extent; it could be affinity-driven and/or depend on proximity to sites of proliferating bacteria and thereby the degree of persistent Ag-stimulation as well as T cell help.

Patterns of distribution of clone members were most consistent with bidirectional interchange of both PBs and B cell blasts in clones that were expanding and undergoing SHM. We found many examples of clonal relatives interspersed at different sites of extensive clonal trees, with no clear directionality towards either tissue as the clone evolved towards more distal branches. However, without direct lineage tracing it is not possible to prove any particular direction of evolution. Regardless of how such clones evolved, their disseminating nature illuminates a feature of the immune system that would anticipate pathogen dissemination by enabling actively responding B cell clones to populate sites distant from where they received their initial stimulus, thus creating a more comprehensive adaptive immune response.

At later "memory" time points, following elimination of persistent infection via administration of antibiotic, we found resting MBC in both spleen and liver. Compared to responding B cells at early time points post-infection, MBC clones had more V region mutations, with about 60% of IgM and 80% of IgG clones containing at least some mutations and about 1/3 of each containing between 1 and 5 average mutations per sequence. This suggests that either most MBC were formed at later time points in the response, after more mutations accumulated, or that the more expanded clones that had more mutations were more likely to spawn longer-lived MBC. As with the acute response, at least a minor fraction of GL Branched clones could be found in both spleen and liver. Again, this is likely an underestimate as we only sampled a small fraction of the spleen. At steady-state, expanded B cell clones are also disseminated in normal humans, as inferred from V region HTS of DNA obtained from unseparated cells isolated from gut, spleen, blood and lung samples from individual organ donors (88). Cerutti and colleagues identified an IgM MBC subset disseminated throughout human gut, which does not share clonal origin with most peripheral MBC but is the precursor of local IgM and IgA production (89). These MBC are likely

driven by gut commensals, but their precise site of origin remains unclear. In analogous elegant studies, Lindner et al. found dispersed clones of MBC in multiple Peyer's patches, though they did not examine lamina propria; these MBC were directly shown to migrate to spleen and they were clonally related to mammary gland IgA plasma cells (90). In these settings, the inductive phase was considered to occur in secondary lymphoid tissue, with subsequent spread of both MBC and plasma cells (PC).

We conclude that many of the B cells in the liver detected at memory time points are MBC; it is unlikely that they are passenger B cells from blood that remained despite our perfusion of the liver prior to harvest. Their memory characteristics, including isotype switch in a fraction, V region mutation, and particularly expression of T-bet, CD73 and CD80, are all unlike B cells found in blood. Intravenous injection of anti-CD19-PE also demonstrated the presence of a liver-localized MBC population that was resistant to rapid labeling. Using a distinct approach, we found by histology an elevated number of CD19+CD11c+ B cells localized in the parenchyma of livers of immune mice compared to naive mice. Because we have not directly studied their migration, we prefer to call these cells "tissue-localized" MBC to reflect that they are not in lymphoid structures or blood vessels, rather than referring to them as tissue-resident, which could imply long-term residence. While tissue MBC are relatively understudied compared to their T cell counterparts, prior work has identified such cells in gut at steady state in both mice and humans and they can be induced by influenza infection or oral immunization in mice (46, 52). In flu responses, these cells are mostly associated with TLT and may need such tissue to accumulate there. Notably, in neither of these two studies was parabiosis performed and thus they lack formal proof of long-term residence of the MBC that were observed in tissues.

As discussed for the primary response, the presence of MBC localized in the liver is distinctive, in that it is not a mucosal barrier site, unlike lung and gut. We could not find prior documentation of pathogen-induced MBC that persisted after infection in livers of either mice or humans. However, MBC populations have been clearly identified during chronic liver disease in humans, including chronic hepatitis and autoimmunity (49). In these cases, continuous immune stimulation is likely responsible for the development and maintenance of such populations. By analogy, MBC in liver after *E. muris* infection may have been formed during prior local acute responses and/or may have migrated from splenic populations, as exemplified by clones that are both liver-specific and found in both spleen and liver. The functional implications of liver-localized MBC for subsequent infection and protection are unclear, but it is tempting to speculate that they can provide protection for certain types of local reinfection, as is proposed for resident memory T cells (80) and certain types of tissue localized MBC (46, 52). This is an area that deserves further study in multiple different contexts.

Overall our analysis of the B cell response to *E. muris* reveals the capacity and complexity of GC independent B cell responses to infection. Though we had previously shown that *S. typhimurium* infection also induced non-GC responses in spleen that nonetheless underwent isotype switching, SHM and affinity maturation, these were nonetheless within secondary lymphoid tissue (SLT) (11). Intrahepatic responses to *E. muris* infection involve both portal triads and foci that are within the parenchyma itself. Analysis of HTS of V regions suggests that there are two pathways of extra-GC response, only one of which generates substantial clonal expansion, SHM and MBC formation. We further note that MBC that express CD73 and CD80 are effectively induced by the extra-GC response, further reinforcing the notion that neither is a specific marker for GC-derived MBC, as had been previously thought (91).

Based on the work of Winslow and colleagues (33), the responses that engender SHM and likely MBC are T cell-dependent, though this was not directly shown for responses within the liver. It is possible that in the absence of organized lymphoid structures in liver, or after infection-associated disruption of normal structure in the spleen, T cell help becomes limiting. This would allow only a portion of the responding B cells to achieve full developmental potential. In this view, the GC can be seen as a site that optimizes T-B interactions but that is not required for induction of AID and SHM (92-94). The EF response, in contrast to the GC response, generates abundant concurrent effector cells, i.e. PBs, almost from the onset of the reaction, and thus seems better adapted as a response to local infection.

Our findings also have implications for understanding T-bet+ MBC in terms of their origin, identity, location and function. First, in agreement with results of others, we confirm that these cells are indeed MBC. There are T-bet+ PB’s, but we could easily distinguish them by other surface markers, proliferation and higher expression of T-bet. Hence, T-bet expression itself cannot be used to define specific populations but needs to be put in biological context as well as combined with expression of surface markers in order to define specific B cell populations. Here we showed that T-bet+ MBC were present 8 weeks post-infection, after using antibiotics to eliminate residual bacteria. They were also largely not proliferating, as they were almost all Ki67 negative.

Our data also revealed more plasticity and context-dependent diversity among T-bet+ MBC than previously realized. While previous studies of responses to *E. muris* have relied on CD11c as a surrogate marker for MBC, we found that there are fully 50% of T-bet+ MBC that do not express CD11c or CD11b. Conversely, there are also many that *do* express CD21 and CD23, although the canonical ABCs − which have been considered synonymous with T-bet+ MBC − are

described as not expressing those markers (39). This basic immunophenotyping thus reveals considerable heterogeneity among the *E. muris*-induced T-bet+ MBC. Moreover, the RNA-seq analysis demonstrated certain shared genes that are expressed in MBC subsets, regardless of their tissue location, but also a substantial number of genes unique to the particular subset and site of origin. This suggests that the local tissue microenvironment may be shaping the MBC differently in the spleen and liver. Future work in this and other systems should explore the ontogeny of such diverse T-bet+ MBC subpopulations, including whether they represent static MBC subsets or transient states, and most importantly, evaluating their functional significance.

Finally, in the course of tracking the B cell response to *E. muris* over time, we made an unexpected and remarkable observation that infection caused a wholesale remodeling of the splenic MZ. After initial disruption and dissolution of the histologic MZ, accompanied by a loss of MZ marker expression, we observed that the MZ slowly reforms. MZ disruption, as part of more pervasive splenic architecture disruption, has been reported in the context of multiple infections, including LCMV, Salmonella, and malaria (95-97). However, it had not been previously documented that upon eventual reorganization of the MZ, that it is repopulated by MBC induced by infection, rather than by more typical primary MZ B cells. Hence, the repertoire and presumably the functional capacity of the MZ B cell compartment was markedly reprogrammed, with ~70% of MZ phenotype B cells expressing T-bet post-infection, compared to a negligible proportion prior to infection. This major alteration lasted for at least 8 weeks post-infection, and we assume for much longer. It is unclear why T-bet+ B cells, rather than naive MZ B cells, preferentially repopulate the MZ. This may relate to the presence of mutated IgM MBC in the MZ observed in human spleens (98); *Ehrlichia*-induced MBC seem to mirror that phenomenon and may represent an example of how human MZ becomes naturally populated with mutated IgM MBC.

There is a great deal of literature on the effects of an infection with one pathogen on subsequent infection with a different pathogen, with many potential mechanisms having been invoked. Given the importance of MZ B cells in the acute response to infection, the remodeling of the MZ by *E. muris*, and potentially other similar infections, could be a previously unappreciated mechanism by which an initial infection could alter or impair the response to subsequent infection. This bears further exploration in this and other systems.

Taken together, these studies reveal a novel intra-parenchymal B cell immune responses in the liver. Our data document how this local response disseminates and interchange with parallel responses in SLT. We further show that these GC-independent responses undergo SHM with clonal expansion and diversification, ultimately generating MBC that also disseminate. They uncover and characterize T-bet$^+$ MBC in the liver as an aspect of the overall MBC compartment. They demonstrate unexpected plasticity and phenotypes of T-bet$^+$ MBC, altering our emerging concepts of these cells, which are important in pathogen responses and autoimmunity. In addition, they describe a process of MZ remodeling caused by infection that is predicted to substantially alter the response to subsequent infection by other pathogens.

# 3.0 The role of the actin cytoskeleton and BCR endocytosis in GCBC function

## 3.1 Introduction

Humoral immunity is crucial for clearance of infections and for generating memory to pathogens and vaccines. Typically, B cells differentiate into a GC phenotype, undergo clonal expansion, and SHM in their Ab gene. GCBC that have BCR with higher affinity towards an Ag get positively selected through this process. Moreover, the GC reaction also leads to the generation of Ag-experienced, long lived, B cell sub-types such as AFC and MBC.

A robust GC response requires the integration of signals from various receptors. Two of the most important signaling axes necessary for efficient GCBC function and output are the 1) B cell receptor signaling induced by antigen and 2) CD40 signaling, mediated by the interaction of GCBC with T follicular helper (Tfh) cells (99). These signaling axes are rewired in GCBC when compared to NBC and a synergy of BCR and CD40 signaling is necessary for positive selection of GCBC (99). There are many regulatory mechanisms that tightly control BCR signaling and thus GC phenotype and function. More details about BCR signaling and its regulation in the context of GC reaction are discussed as follows.

### 3.1.1 BCR signaling

Upon stimulation with antigen, cell-surface BCRs aggregate together. This leads to the phosphorylation of the immune receptor tyrosine-based activation motifs (ITAM) of Igα and Igβ by the Src family kinase Lyn (100), further leading to the recruitment of the cytosolic tyrosine

kinase Syk, which couples these initial events to various signaling effectors downstream of the BCR (101). Lyn also phosphorylates accessory receptor protein CD19, which in turn leads to the recruitment of the enzyme phosphatidylinositol-3-kinase (PI3K) (102, 103). This enzyme converts the plasma membrane lipid inositol phosphatidylinositol 4,5 bis-phosphate $PI(4,5)P_2$ to phosphatidylinositol 3,4,5 tris-phosphate ($PIP_3$). The generation of PIP3 is crucial for the recruitment of pleckstrin homology (PH) domain-containing effector proteins such as Bruton's tyrosine kinase (Btk), phosphoinositide-dependent kinase-1 (PDK-1) and serine/threonine Akt kinases (104, 105).

The activity of Akt and PDK-1 is linked to PI3K activity and the concentration of PIP3 (106). PDK-1 phosphorylates Akt1 at the threonine 308 (T308) site in a PI3K-dependent manner (106). Subsequently, Akt can be phosphorylated at serine 473 (S473); this double-phosphorylation of Akt is needed for maximal Akt activation (107). The mTOR signaling pathways are closely linked to the Akt signaling axis. mTOR kinases are found in large multi-protein complexes that constitute the functional enzyme (108). mTORC1 includes a protein subunit known as raptor and, leads to the activation of S6 kinases and phosphorylation of ribosomal protein S6 and 4EBP, in an Akt-dependent manner (109). mTORC2 includes the rictor subunit, among other proteins. mTORC2 can phosphorylate Akt at the S473 site (110). Thus, mTORC1 functions occur downstream of Akt, whereas, mTORC2 functions occur upstream of Akt kinase. Together, Akt, mTORC1 and mTORC2 regulate the pathways for B cell growth and proliferation (107). Akt kinase has several substrates one of which that is crucial for B cell biology is forkhead box, subgroup O (FOXO). These FOXO proteins are usually localized in the nucleus, where they cause cell cycle arrest (111). Upon Akt activation, FOXO is phosphorylated by Akt, which leads to the exit of FOXO proteins from the nucleus into the cytosol where they are eventually degraded (112).

Thus, the Akt-FOXO axis is crucial for B cell proliferation and as such plays a crucial role in the maintenance of the GC reaction (99, 113).

The generation of PIP3 leads to the recruitment of PH-domain containing protein Btk near the signaling complex. Together, PIP3 and Btk promote the recruitment and activation of the enzyme PLCγ2, in a process mediated by the adapter protein B cell linker (Blnk) (114-116). PLCγ2 catalyzes the breakdown of the lipid inositol $PI(4,5)P_2$ into two signaling effector molecules inositol triphosphate ($IP_3$), and diacylglyercol (DAG) (117). IP3 induces $Ca^{2+}$ influx in the cells and these elevated $Ca^{2+}$ levels lead to the activation of the transcription factors NF-κB via protein kinase C (PKC), and NFAT via $Ca^{2+}$ binding messenger protein calmodulin (118-120). DAG, on the other hand, can lead to the activation of the mitogen activated protein kinase (MAPK) family (121). Moreover, Blnk can form a complex with adapter proteins Grb2 and SOS and activate the small G proteins Rac and Ras, leading to the activation of MAPK pathways (121).

The MAPK family consists of mainly 3 different protein kinases known as extra-cellular signal-regulated kinase (Erk), c-Jun NH2-terminal kinase (JNK) and p38 MAPK. The activation of these kinases leads to the phosphorylation and activation of different transcription factors such as Elk-1, c-Myc, c-Jun and ATF-2 (122). As discussed above, NF-κB and NFAT are transcription factors that are important downstream mediators of the BCR signaling pathway (122). Upon activation, all the above-mentioned TFs translocate into the nucleus and carry out transcription of different proteins that can lead to B cell activation, proliferation, Ag presentation, morphological changes and cytokine production (122).

### 3.1.2 BCR signaling in GCBCs

In comparison to NBC, BCR signaling in GCBC is markedly dampened. Previously, our lab has shown through flow cytometry and western blot approaches that several signaling proteins downstream of the BCR in the GCBCs have reduced phosphorylation in comparison to NBs when receiving a BCR stimulation (60, 99, 123). Reduced tonic and inducible BCR signaling have been reported by other groups as well (124). However, use of a strong BCR stimulation can lead to restoration of the most proximal signaling to the BCR (125). This dampened signaling through the BCR in GCBC has been attributed to the enhanced activity of protein and lipid phosphatases such as Src homology region 2 domain-containing phosphatase-1 (SHP-1), SHIP-1 and PTEN (60, 123).

SHP-1 is a protein tyrosine phosphatase that can be activated by inhibitory receptors in B cells such as CD22 and paired immunglobulin-like receptor B (PIR-B) (122). SHP-1 can de-phosphorylate its substrates Syk, CD79, Vav, Blnk and Btk and dampen proximal BCR signals (126). In NBC, SHP-1 is co-localized with the BCR under resting conditions, however, it moves to the opposite pole of the cell upon receiving BCR stimulation (60). On the other hand, in GCBC SHP-1 is hyper-phosphorylated and remains co-localized with the BCR at the basal level and even after BCR ligation (60). These data suggest that constitutive association of SHP-1 with the BCR is a potential mechanism for dampened BCR signaling in GCBC. Moreover, inducible deletion of SHP-1 in GCBC during an ongoing GC reaction leads to a reduction in the number and frequency of GCBC, suggesting a prominent role for SHP-1 in sustaining the GC reaction (60).

SHIP-1 and PTEN are lipid inositol phosphatases that work on the substrate $PIP_3$. SHIP-1 de-phosphorylates $PIP_3$ to generate phosphatidylinositol 3,4-bisphosphate ($PI(3,4)P_2$) and PTEN de-phosphorylates $PIP_3$ to generate $PI(4,5)P_2$ (127). Classically, these phosphatases are thought to be negative regulators of BCR signaling because their activity reduces the levels of $PIP_3$, which is

an important secondary messenger necessary for coupling initial BCR signaling to effector proteins such as Btk and Akt (127). Moreover, SHIP-1 can also function as an adapter protein independent of its enzymatic activity (128). More details about the functions of SHIP-1 and its role in B cell biology are discussed in the Chapter 4.

GCBC exhibit a different lipid inositol profile upon receiving BCR stimulation when compared to NBCs (123). Upon BCR ligation with anti-μ, NBC generate significant amounts of $PIP_3$ and $PI(3,4)P_2$ within five minutes of stimulation. On the contrary, GCBC generate minimal amount of $PIP_3$ and $PI(3,4)P_2$ and generate a substantial amount of $PI(4,5)P_2$ in comparison to NBC within few minutes (123). These data suggest a prominent role for PTEN in the regulation of the levels of $PIP_3$ and thereby proximal BCR signaling in GCBC. Treatment of B cells using a PTEN inhibitor (SF1670) leads to increase in the production of $PIP_3$ and reduction in the levels of $PI(4,5)P_2$ in both NBC and GCBC (123). Moreover, treatment with PTEN inhibitor also leads to restoration in the phosphorylation of Akt at the S-473 site and pS6 in GCBC to the magnitude observed in NBC (123). This data suggests that PTEN is a major regulator of BCR signaling in GCBC that dampens the Akt-S6 axis of BCR signaling by reducing the amount of the available $PIP_3$ (123).

Recently, a novel feedback loop involving Akt kinase has been discovered in GCBC that is not found in NBC (123). Akt kinase specifically targets the phosphatases Csk, HPK-1 and SHP-1 enhancing their functions thus negatively regulating the BCR signaling pathway (123). Taken together, these data demonstrate the different ways in which BCR signaling is rewired in GCBC in comparison to NBC. A summary of the all the signaling effector molecules that are differentially expressed/phosphorylated/generated in GCBC when compared to NBC upon BCR stimulation is presented in the table below.

| Number | Signaling molecules | Signaling status in GCBC upon BCR stimulation in comparison to NBC | References |
|---|---|---|---|
| **Signaling effector molecules** | | | |
| 1 | Lyn | Dampened phosphorylation of activating site (Tyr 396) and enhanced phosphorylation of inactivating site (Tyr 507). | Unpublished data |
| 2 | Syk | Dampened phosphorylation. Upon inducible deletion of Syk, GC collapses and loss of LZ GCBC. | (60, 99) |
| 3 | Btk | Dampened phosphorylation. | (99) |
| 4 | Blnk | Dampened phosphorylation. | (60, 99) |
| 5 | PLCγ2 | Dampened phosphorylation. | (99) |
| 6 | Akt | Dampened phosphorylation of Serine 473, Increased phosphorylation of Threonine 308. Akt targets and enhances activity of Csk, HPK-1, SHP-1 in GCBC but not in NBC. | (99, 123) |
| 7 | S6 | Dampened phosphorylation. | (99) |
| 8 | IκBα | Dampened phosphorylation. | (99) |
| 9 | Erk | Dampened phosphorylation. | (99) |
| 10 | $Ca^{2+}$ flux | Dampened. | (60) |
| **Transcription Factors** | | | |
| 11 | FOXO1 | Increased phosphorylation. | (99, 129) |
| 12 | NF-κB | Dampened phosphorylation. | (99) |
| 13 | NFAT | Dampened nuclear localization. | (99) |
| **Lipid Inositols** | | | |
| 14 | $PIP_3$ | Reduced generation. | (123) |
| 15 | $PI(4,5)P_2$ | Significantly increased generation. | (123) |
| 16 | $PI(3,4)P_2$ | Reduced generation. | (123) |

| Protein/Lipid Phosphatases | | | |
|---|---|---|---|
| 17 | SHP-1 | Constitutive association with the BCR, hyperphosphorylated, GC collapse in the absence of SHP-1. | (60) |
| 18 | SHIP-1 | Increased expression, hyperphosphorylated, cell cycle defects in GC in the absence of SHIP-1. | (60) and Chapter 4 |
| 19 | PTEN | Increased expression, GC collapse in the absence of PTEN. | (123, 130, 131) |

**Table 2 Signaling status of effector molecules in GCBC upon BCR stimulation in comparison to NBC**

### 3.1.3 Cytoskeletal regulation of BCR signaling

The importance of the actin cytoskeleton in immune cells was first recognized by studying the basis for certain autoimmune conditions. Wiskott-Aldrich syndrome, an immunodeficiency that often leads to systemic autoimmunity, is caused by mutations in Wiskott-Aldrich syndrome protein (WASp), which is an actin regulator (132). In murine hematopoietic cells two isoforms of this protein, WASp and neural-WASp (N-WASp), are ubiquitously expressed (133). B cells deficient in N-WASp have elevated BCR signaling and higher numbers of self-reactive B cells, suggesting a role for N-WASp in negatively regulating B cell activation and preventing autoimmunity (133). Moreover, WASp deficient animals also have elevated signaling responses to BCR and Toll-like receptor (TLR) signals, spontaneous GC formation, class-switched auto-Abs and renal disease (134, 135). These findings established the importance of the actin cytoskeleton in regulation of immunity and specifically B cell signaling and function (132, 136, 137). Moreover, knock out mouse models of several other cytoskeletal regulators such as WASp interacting protein family member 1 (Wipf1), dedicator of cytokinesis protein 8 (Dock 8) and ezrin, are also known

to impair B cell development or responses to Ags (138). The different components of the cortical cytoskeleton are discussed next.

#### 3.1.3.1 Components of the cortical cytoskeleton

The cortical cytoskeleton in B cells consists of several different components such as globular actin (G-actin), filamentous actin (F-actin), myosin, actin nucleating proteins Arp2/3 and formin; actin severing proteins cofilin, gelsolin, and destrin and several other actin regulators (138, 139). Actin exists in the cells in its monomeric globular form as G-actin which can be polymerized to form F-actin (138, 139). Two major nucleation factors involved in this process are formin and Arp2/3 proteins (138). Arp2/3 nucleates a new filament at an oblique angle to an already existing filament (138). Formin, on the other hand, generates new F-actin from G-actin (138). The cortical cytoskeleton is made up of a meshwork of F-actin nucleated by Arp2/3 and formin. Arp2/3 activity is necessary for the generation of lamellipodia which are membrane extensions often found in GCBC (140, 141). The F-actin network can be de-polymerized by actin severing proteins such as gelsolin, cofilin and destrin, which can lead to rapid remodeling of the cortical cytoskeleton under different stimulus (138).

The F-actin network is linked to the plasma membrane via ezrin, radixin and moesin that are together known as the ERM proteins (142). The ERM proteins have a conserved threonine residue in the cytoplasmic tail (142), phosphorylation of which leads to a conformational change, exposing a FERM domain in the N terminus and an actin-binding domain in the C terminus (142, 143). The FERM domain in the N-terminus can bind to different molecules on the plasma membrane such as the lipid inositol $PI(4,5)P_2$ and transmembrane receptors such as CD44, CD43 and intracellular adhesion molecules (ICAM) have shown that disruption in the actin cytoskeleton adversely affects B cell activation, proliferation and function (138, 142, 143). Upon BCR

stimulation, the cortical actin cytoskeleton and the ERM proteins undergo rapid re-modelling that both positively and negatively regulates the BCR signaling.

#### 3.1.3.2 Actin cytoskeleton in regulation of BCR diffusion

The movement of BCRs can be tracked using single particle labeling with total internal reflection fluorescence (TIRF) microscopy (144-147). In their resting state, IgM BCRs on naïve primary B cells exist as monomers or nano-clusters with a diffusion coefficient of $0.03\mu^2/s$ (145, 148, 149). The meshwork of F-actin plays an important role in restricting the lateral mobility of the BCR (145, 148, 149). In resting B cells, the F-actin network creates compartments in the plasma membrane within which individual BCRs or BCR nano-clusters are restricted (145, 148, 149). The F-actin acts as a barrier that reduces the lateral mobility of the BCRs and accidental clustering of the BCRs (145, 148, 149). This is a proposed mechanism for regulation of tonic signaling in B cells (144, 145, 149). The diffusion coefficient of BCRs within actin-rich areas ($0.014\mu^2/s$) of the cells is significantly lower in comparison to that outside of actin-rich regions ($0.039\mu^2/s$) (145).

Upon treatment of B cells with actin de-polymerizing agents such as latrunculin-A (LatA) and cytochalasin D (Cyto-D), the F-actin undergoes rapid de-polymerization and that leads to increased diffusion of the BCR (145, 150). In the study by Treanor et al. treatment of NBC with 0.5μM LatA increased the BCR diffusion coefficient to $0.086\ \mu^2/s$ (145). Moreover, LatA-mediated actin disruption leads to BCR-like signaling in the B cells as measured by the phosphorylation of signaling proteins Akt and Erk, and induction of $Ca^{2+}$ flux (145). This BCR-like signaling induced by actin disruption does not occur in B cells that lack key BCR signaling effector proteins such as PLCγ2, Btk, Vav, Blnk and Lyn (145). These data provided evidence that

actin disruption changes the diffusion rate of BCRs and induces signaling in B cells, via a process that is dependent on effector proteins closely associated with BCR signaling.

#### 3.1.3.3 BCR activation remodels the actin cytoskeleton

Since actin acts as a barrier to BCR diffusion, actin re-modeling must be required for allowing efficient interactions among BCRs and formation of BCR clusters upon BCR stimulation. Indeed, the actin cytoskeleton undergoes dynamic changes when B cells are stimulated through the BCR (151, 152). In NBC, BCR stimulation leads to a rapid reduction in F-actin and the de-polymerization phase in F-actin network has been correlated to an increase in the lateral mobility of the BCRs (145, 152, 153). Upon BCR ligation, the lateral mobility of the BCR transiently increases to $0.05\mu^2/s$ from $0.03\mu^2/s$ (153). This de-polymerization phase is thought to be mediated through the actin-severing protein cofilin (152). Cofilin has a phosphorylation site at the Serine 3 residue, the phosphorylation of which, is inversely related to its actin severing function (154). Cofilin undergoes rapid dephosphorylation upon BCR ligation in primary B cells and this dephosphorylation allows cofilin to sever F-actin around the plasma membrane (152). This F-actin depolymerization leads to increased movement of the BCR, which eventually leads to BCR clustering and enhancement of signaling (145, 152, 153). Another actin-severing protein known as gelsolin also co-localizes with the BCR upon BCR ligation and may also play a role in actin remodeling in B cells (155).

As mentioned previously, the F-actin network is linked to the plasma membrane by ERM family proteins (142). This attachment of the plasma membrane to the cortical cytoskeleton via ERM contributes in the formation of compartments that restrict the diffusion of BCRs (143, 153). However, upon BCR ligation, ERM proteins undergo de-phosphorylation and the plasma membrane transiently detaches from the F-actin (143, 153, 156). At the same time, the overall

levels of F-actin reduce because of the activity of actin severing proteins (153). This process allows for increased lateral mobility and diffusion of the BCRs on the plasma membrane within seconds of BCR ligation (143, 145, 153).

This increased diffusion leads to the formation of BCR micro-clusters from the association of individual BCRs and BCR nano-clusters (152, 153). The lateral mobility of the BCR within these clusters reduces and the BCR micro-clusters move to one pole of the cell with a diffusion coefficient of $0.01\mu^2/s$ (148, 157). This movement eventually leads to the fusion of BCR micro-clusters to form a "BCR cap" on one pole of the cell (155, 157). When NBCs are stimulated using soluble Ags, BCR caps can be detected within 5 minutes of stimulation (60). When NBCs are stimulated through membrane-tethered Ags, BCR central cluster is detected at the contact zone of Ag presentation (155, 157, 158). The BCR clustering process stabilizes the lipid rafts and brings signaling effector molecules closer to the BCR and leads to further propagation of the signaling events (159). During the later stages of BCR clustering, de-novo actin polymerization occurs around the BCR clusters and ends up surrounding the BCR cap (155, 157). At this point, ERM proteins also become phosphorylated and the linkage between the cortical cytoskeleton and the plasma membrane is reestablished (145, 153, 160).

### 3.1.4 BCR Endocytosis

Apart from triggering a signaling cascade, BCR ligation also induces the internalization of the BCR. Upon endocytosis, BCR-containing endosomes co-localize with MHC II-containing compartments (161). The endocytosed Ag is then proteolyzed and some of the resultant peptides are presented on the surface of B cells by MHC II. Ag presentation leads to efficient B-T

interactions and allows B cells to receive helper signals from T cells. These helper signals are crucial for B cell differentiation and for positive selection of GCBC (99).

The endocytic process is thought to require both clathrin and dynamin (162, 163). The plasma membrane around the Ag clusters invaginates and the Ag-BCR complexes accumulate in clathrin-coated pits (164). The BCR is linked to the clathrin via the adapter protein AP2 (165). The adapter protein Abp1 links the endocytic machinery with F-actin by binding to F-actin and dynamin simultaneously (165). Dynamin creates a restriction around the neck of the clathrin-coated pits and the vesicle detaches from the plasma membrane because of the force generated by F-actin filaments around the neck of the vesicle (162, 163). Recently, in GCBC, a different mechanism of endocytosis has been described. Using membrane-tethered Ag and high-throughput imaging, the authors show that upon extraction, Ag in GCBC is transported along the sides of the cells and is subsequently endocytosed from the cell periphery (166). This is unlike the mechanism described in NBC, where endocytosis occurs through the central cluster (166). It is proposed that using these unique pod-like structures GCBC internalize the Ag in an affinity-dependent way (166). These data suggest that GCBC have rewired their endocytic machinery, perhaps to match their unique functions in the competitive GC environment. In agreement with this, previously our lab has shown that BCR organizes differently upon BCR stimulation in GCBC compared to NBC. BCR capping is not observed in GCBC, unlike in NBC (60). In the studies described in this chapter, we extend these findings and compare the dynamics and requirements of BCR endocytosis and Ag presentation between NBC and GCBC.

### 3.1.5 Study goals

Previous work from our lab has shown in a series of papers that several axes of BCR signaling are selectively dampened in GCBC in comparison to NBC (60, 99, 123). The reason for this phenomenon has been attributed to higher activity of phosphatases like PTEN, SHP-1 and SHIP-1 in GCBC and the recently discovered Akt-mediated feedback loop that enhances the activity of phosphatases SHP-1, Csk and HPK1 in GCBC (60, 123). Given that actin is a known negative regulator of early BCR signaling in NBC (144, 145, 149, 153), we sought to determine if F-actin was also acting as a negative regulator of BCR signaling in GCBC by restricting the movement of the BCR.

We used LatA-mediated actin disruption to demonstrate that GCBC had higher resistance to actin de-polymerization and that actin disruption restored signaling in GCBC along the Akt-S6 signaling axis. Moreover, we found through single particle tracking on live cell TIRF microscopy, that individual BCR on GCBC moved at a lower speed in comparison to that on the NBC. Future experiments will determine whether this is actin-dependent or not by TIRF imaging of individual BCRs on untreated and LatA treated NBC and GCBC.

We also wanted to determine if the lack of clustering of the GCBC BCRs led to differential endocytosis and Ag presentation. Using standard flow cytometry and imaging cytometry we demonstrated that BCR endocytosis occurred more rapidly in GCBC in comparison to NBC. Moreover, Ag presentation also occurred more rapidly in GCBC like the enhanced endocytosis. In addition, we found that Ag presentation in both NBC and GCBC was dependent on the function of tyrosine kinase Syk and the lipid phosphatase PTEN. These data have provided new insights into how GCBC interpret BCR signals differently than NBC and how the process of BCR

internalization and Ag presentation is enhanced in GCBC. Moreover, it sheds light on the previously unknown role of the phosphatase PTEN in B cell Ag presentation.

## 3.2 Methods

**Mice and immunizations**: All mice were maintained under specific pathogen free conditions in accordance with guidelines issued by University of Pittsburgh Institutional Animal Care and Use Committee. 6-16 weeks old B18 BCR knock in Balb/c, IgM B18i BCR transgenic Balb/c (referred to as MEG), WT C57BL/6, and B18+/- Vκ8R+/- CD45.1/2 C57BL/6 mice were used as sources of NBC and GCBC as mentioned in the figure legends. MEG mice carry IgM B18i transgene and are bred to the JHD-/- background and as a result all B cells in these mice have the IgM B18i heavy chain(60). MEG mice do not undergo isotype switching. MEG mice were immunized using 50μg of Nitrophenyl-Chicken Gamma Globulin (NP-CGG) precipitated in Alum. The C57BL/6 strains were immunized using 75ug of NP-CGG precipitated in Alum. Mice were analyzed between day 10-16 post immunization.

**B cell purification and treatment**: Total B cells, or GCBC were purified from relevant strains as mentioned in the figure legends using streptavidin beads based negative selection method as described previously (99, 123). The cells were re-suspended in B cell media (RPMI 1640 medium supplemented with 5% Fetalplex (Gemini bio-products), penicillin/streptomycin, glutamine and 50 μM β-mercaptoethanol) and warmed to $37^{O}$C in 5% CO2 for at least 15m before the following treatments. For experiments using LatA, 2μm or 5μm of LatA (Abcam) dissolved in ethanol or ethanol alone was added to the cells. For BCR stimulation, 20μg/mL of endotoxin free anti-μ was added to the cells. For experiments using inhibitors, 20μm of 3AC (SHIP-1 inhibitor,

Echelon Biosciences) dissolved in ethanol or 20μm of SF1670 (PTEN inhibitor, Calbiochem) dissolved in DMSO or 20μm of BAY 61-3606 (Syk inhibitor, Calbiochem) or the respective diluents were added to the cells. For Ag presentation assays, 25μg/mL EαGFP dissolved in PBS, 25μg/mL NIP-EαGFP dissolved in PBS, 25μg/mL NP-BSA or PBS alone was added to the cells for 1 or 2 hours.

**Reagent Preparation and Conjugations**: For BCR labeling, Fab fragments were prepared from home-made rat anti mouse IgM (clone: B7-6) by papain digestion using the Pierce Fab Preparation kit (Thermo fisher scientific; 44985). The digestion was performed as per the recommended protocol from the manufacturer. Anti-IgM Fab was conjugated to Alexa 647 as previously described. Plasmid expressing EαGFP was a generous gift from Mark Jenkins (167). The Eα peptide gets processed by the endocytic machinery and presented on the surface in the context of MHC II (167). This peptide-MHC II complex can be detected on the surface by an antibody known by the clone name YAe (167). The plasmid was transformed into TOP10 competent cells. The expression of EαGFP was induced by 1mM IPTG and the purification of the His tagged protein was done using Ni-NTA spin kit (Qiagen, 31314). The purified EαGFP was conjugated to NIP using Alexa 647 NHS Ester (Thermofisher A 2006).

**Flow Cytometry**: The stimulations and/or treatments were stopped by fixing the cells using 1.5% paraformaldehyde (PFA) at room temperature for at least 15 minutes. The cells were permeabilized using BD Perm Wash buffer or 0.1% Triton X-100 at room temperature for at least 20 minutes. Fc receptors were blocked using anti-CD16/32 (home-made 2.4G2 antibody clone). Phalloidin A488 (Santa Cruz Biotechnology, sc-363791) was used to label F-actin. For flow cytometry, the following conjugated reagents and antibodies were used, PNA (Vector laboratories), anti-lambda (Goat polyclonal; Southern Biotechnology), anti-CD95 (clone: Jo-2;

BD Pharmigen), anti-CD45R (clone RA3-6B2; BD Pharmigen), anti-CD19 (clone 1D3; BD Horizon), anti-CXCR4 (clone- L276F12; Biolegend), anti-CD86 (clone GL-1; Biolegend), anti-IgM (clone B7-6; home-made) and anti- I-A/I-E (clone M5/114.15.2; Biolegend). For Ag presentation assays, anti-Ea52-68 peptide bound to IA-b (clone YAe; Ebioscience) was used. For signaling assays, conjugated antibodies to p-S6 (S235/236; clone: D57.2.2E; Cell Signaling Technology), p-AKT (S473; clone: M89-61; BD Biosciences), p-AKT (T308; clone: 244F9; Cell Signaling Technology), p-Btk (Y223/Itk pY180; clone: N35-86; BD Biosciences), p-PLC-γ2 (Y759; clone: K86-689.37; BD Biosciences), p-Syk (Clone 17A/P-ZAP70; BD Biosciences), Cofilin (D3F9; Cell Signaling Technology), and p-Cofilin (S3, clone: 77G2; Cell Signaling Technology) were used.

**Imaging flowcytometry**: Cells were labeled as described earlier for flow cytometry assay. For BCR clustering and endocytosis, data were collected using Amnis ImageStream®X Mark II Imaging Flow Cytometer. Data were analyzed by gating on focused, singlet cells using the IDEAS software. The cells were further gated as $B220^+$ $PNA^+$ $Lambda^+$ (GCBC) and $B220^+$ $PNA^-$ $Lambda^-$ (NBC) or $B220^+$ $PNA^+$ $CD95^+$ (GCBC) and $B220^+$ $PNA^-$ $CD95^-$ (NBC). For BCR clustering analysis the "Delta Centroid" feature was used and for BCR endocytosis "Internalization" feature was used (EMD Millipore). For defining the internalization feature, B220 was used as the cell surface mask.

**TIRF Imaging**: For single BCR labeling, bead purified NBC and GCBC were labeled using 0.2μg/mL anti-IgM Fab A647 and 0.8μg/mL unlabeled anti-IgM Fab. Labeled cells were then allowed to adhere to Mattek dishes (Mattek Corporation P35G-1.5-14-C) coated with 5μg/cm2 Fibronectin (Millipore Sigma F1141) for at least 30 minutes at $37^OC$ and 5% CO2. The cells were imaged on a Nikon Eclipse Ti inverted microscope (Nikon, Melville, NY, USA) with a

100 × 1.49 NA oil-immersion objective using 647 nm laser line. All experiments were performed at 37°C and 5% CO2 in R10 medium. Images were collected using Nikon Elements software (version 4.30, Nikon, Melville, NY) and an Andor (Belfast, Ireland) Zyla 5.5 camera; at full resolution under these conditions the pixel size with a 1 × coupler matches Nyquist sampling (120 nm xy exactly). The cells were imaged using Nikon Ti microscope. Data were de-convoluted in NIS Elements using 2D deconvolution by the Richardson-Lucy method. A647 signals were marked as spots. The spots were tracked over time with a maximum distance of movement set as 1μM per frame. The spots were converted into a channel and tracks were generated in Imaris 7.1 software (Bitplane INC, South Windsor, CT) based on the movement of the spots. Brownian motion particle-tracking algorithm was applied to trace objects through sequential frames and calculate track parameters such as mean speed, distance, length and displacement.

**RNA Sequencing analysis**: We utilized in house RNAseq data (NCBI's Gene Expression Omnibus database (GEO) accession ID GSE128710, n=3) for sorted naive, *in vivo* activated B cells, and GCBC cells (unpublished data). Cytoskeleton genes were taken from http://amigo.geneontology.org/amigo/term/GO:0005856. Gene-set enrichments were preformed using the rankSumTestWithCorrelation function in limma, which explicitly corrects for correlation among genes in the gene set being interrogated.

**Statistics**: Statistics for data were calculated by Graphpad Prism using Student's t-test or Two-way Anova as described in the figure legends. Symbols for levels of significance are * $p< 0.05$, * * $p<0.01$, * * * $p<0.001$, * * * * $p< 0.0001$.

## 3.3 Results

To study the role of the actin cytoskeleton in GCBC function, we first measured the amounts of polymerized filamentous actin (F-actin) by flow cytometry. We set a stringent gate around the forward scatter area (FSC-A), so as not to introduce any bias in the measurements based on cell size (figure 25 A-B). We observed that GCBC expressed higher levels of F-actin, in comparison to NBC (figure 25 C-D).

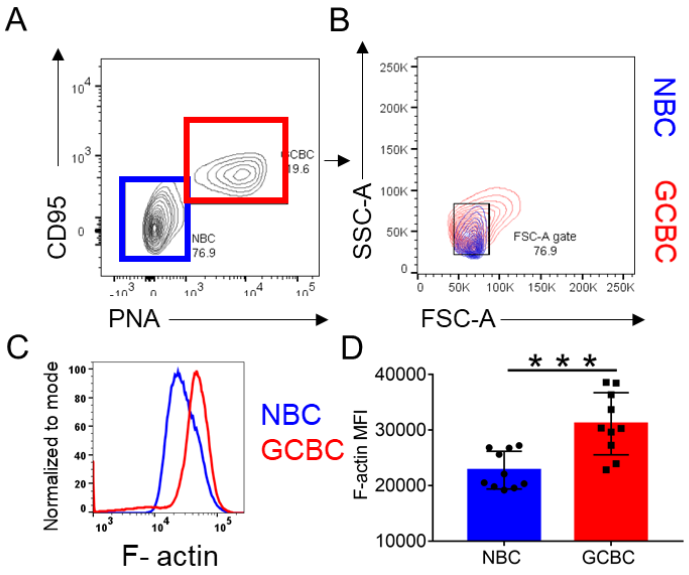


**Figure 25 GCBCs express higher levels of F-actin than NBCs**

**(A) Gating strategy of NBC and GCBC. The cells are pre-gated on B220+ cells. (B) Size gating based on FSC-A, (C-D) Histogram (C) and Quantification (D) for F-actin using phalloidin staining in NBCs and GCBCs. Data are representative of at least two independent experiments with and are represented as mean with SD of groups of at least two mice.**

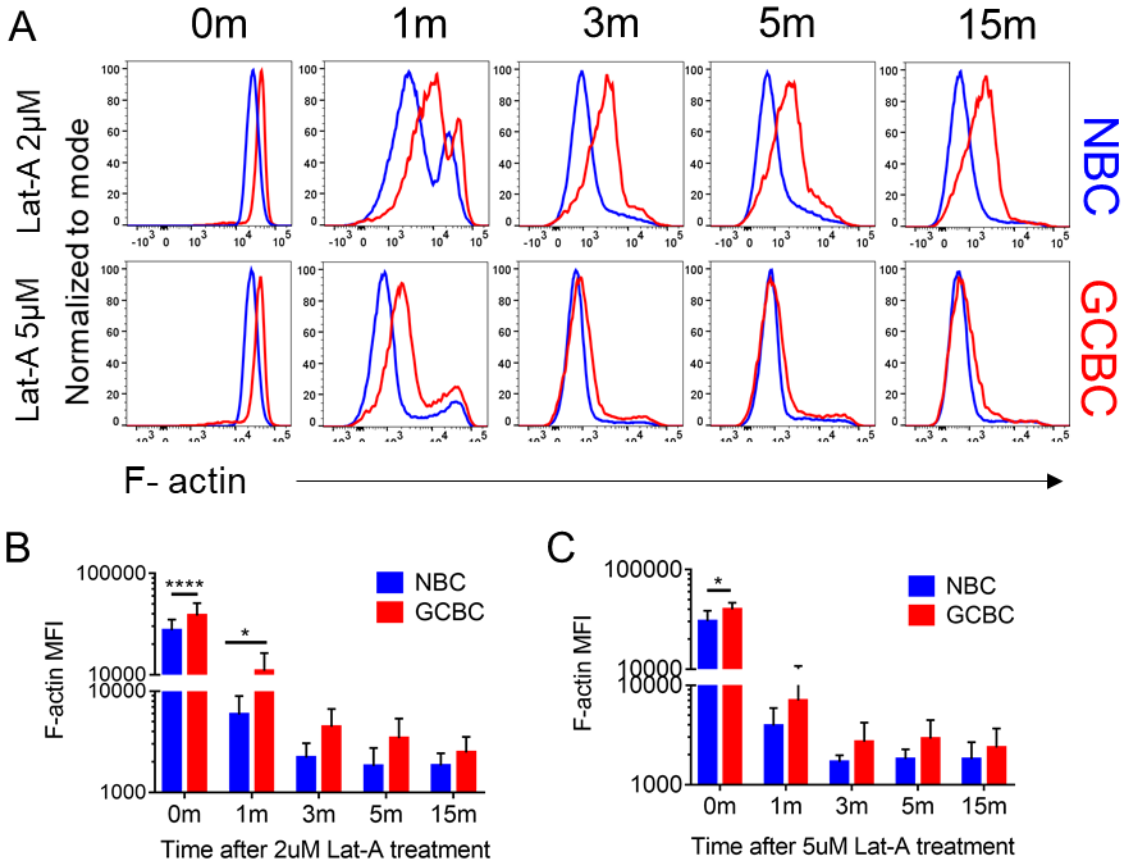


**Figure 26 GCBCs have higher resistance to actin de-polymerization in comparison to NBCs**

**(A-C) Histogram (A) and quantification (B,C) of phalloidin staining by flow cytometry in NBC and GCBC after 2uM (A,B) and 5uM (A,C) LatA treatment. Data are representative of at least two independent experiments.**

Previously it was shown that NBC undergo actin depolymerization when treated with LatA (145). To characterize the effects of actin depolymerization on GCBC, we treated both NBC and GCBC with 2μM or 5μM LatA; (figure 26A-C). GCBC required a higher dose of LatA and a longer treatment time to de-polymerize the F-actin network (figure 26A-C). Treatment with 2μM did not completely de-polymerize the F-actin in GCBC, but treatment with 5μM caused actin de-polymerization after 3 minutes of treatment (figure 26A-C). NBC, on the other hand, underwent complete de-polymerization after 3 minutes of treatment with 2μM LatA (figure 26A-C). Based

on these data, we conclude that GCBC have higher resistance to actin de-polymerization in comparison to NBC.

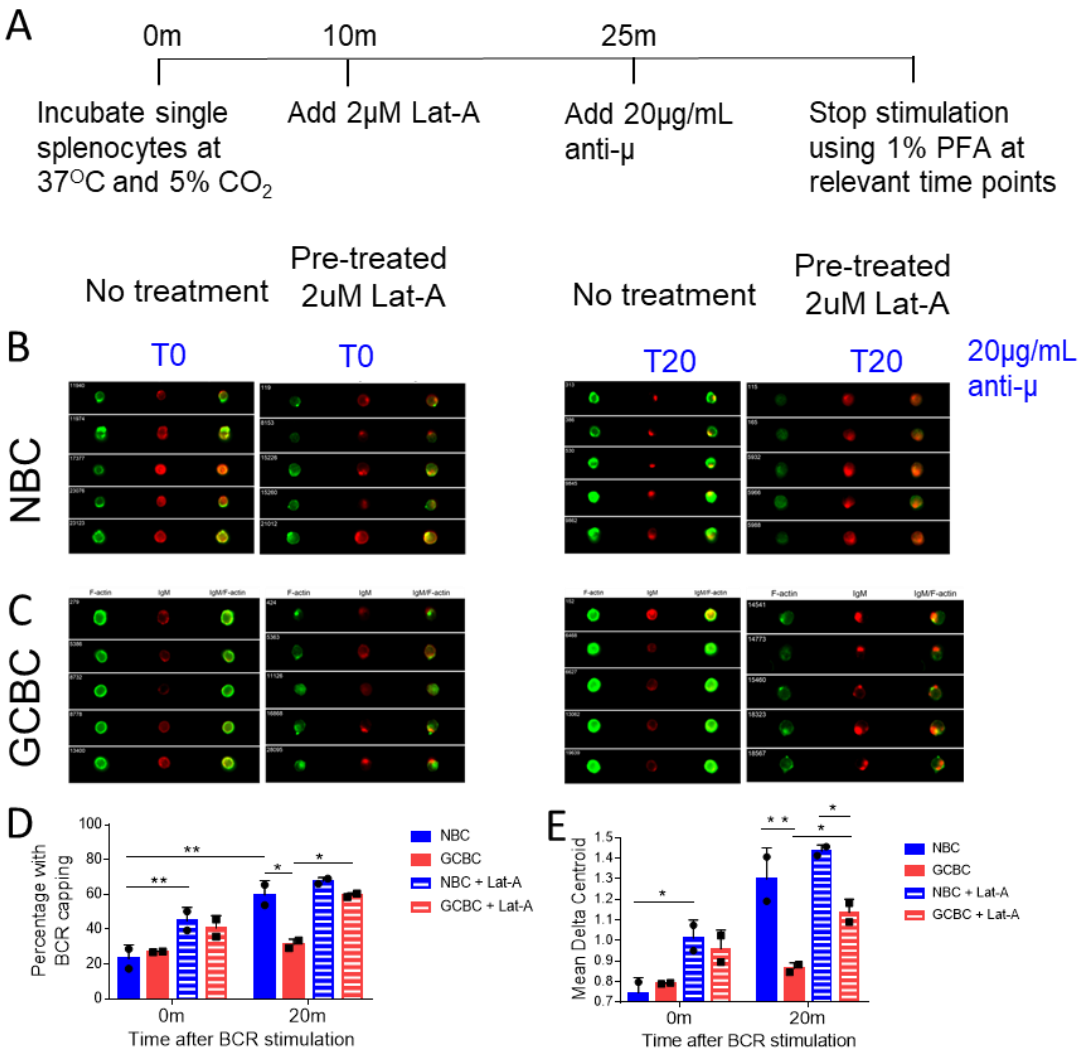


**Figure 27 Actin de-polymerization induces BCR clustering in B cells**

**(A)Schematic diagram of treatment and stimulation of B cells for data presented in figures 30-32. (B-E) Images (B-C) and quantification (D-E) of BCR clustering in NBC and GCBC either untreated or LatA treated and stimulated with 20ug/mL anti-μ stimulation. Quantification of BCR clustering was used by the Delta Centroid function in the IDEAS software and data are presented as percent cells with BCR caps (D) and mean delta centroid value (E) for each condition. At least 1000 cells were analyzed for each condition. Data are representative of at least two independent experiments.**

Actin de-polymerization leads to increased diffusion of the BCR in NBC (145, 153). To study the effect of actin-depolymerization in GCBC in BCR diffusion and clustering, we used the treatment regimen described above (figure 27A) and measured BCR clustering by Image stream. We used the delta centroid function from the IDEAS software to measure BCR clustering/capping. Our data showed that, actin de-polymerization mediated by LatA led to increased BCR clustering in NBC and GCBC (figure 27B-E). Upon BCR stimulation, there was a further increase in the magnitude of BCR clustering in NBC and GCBC (figure 27B-E). In NBC, BCR stimulation induced BCR clustering within 10 minutes of treatment (figure 27 B, D, E). BCR clustering was further enhanced upon treatment with LatA (figure 27 B, D, E). However, in the case of GCBC, as previously reported (60), BCR stimulation by itself did not induce BCR clustering (figure 27C-E). Instead, we observed that BCR clustering only occurred when the actin cytoskeleton was de-polymerized (figure 27C-E). These data suggest a role for polymerized actin in preventing BCR clustering in GCBC.

Next, to study the effect of actin-depolymerization on the BCR signaling we treated NBC and GCBC with a suboptimal dose of LatA for 15 minutes followed by BCR stimulation using anti-μ (figure 27A). This allowed us to study the change in BCR signaling in the absence of F-actin. Treatment with LatA induced BCR like PI3K signaling in NBC as previously reported (145) (figure 28 A-F). LatA treatment caused a moderate increase in the basal levels of p-Akt (S473) and significant increase in the basal levels of pAkt (T308) and pS6 in GCBC (figure 28A-F). Moreover, upon BCR stimulation, we observed a further increase in Akt (T308) phosphorylation in both NBC and GCBC (figure 28A-F). However, Syk, Btk and PLCγ2 phosphorylation was not significantly affected by LatA in GCBCs (figure 29A-F). In NBC, p-Btk and p-PLCγ2 had a similar trend as GCBC; however, Syk phosphorylation was slightly although not significantly

increased at 3m post-BCR stimulation in LatA-treated cells (figure 29A-F). GCBC have significantly higher SHP-1 activity compared to NBC. Since Syk is a known target of SHP-1 (168), increased SHP1 activity could prevent Syk phosphorylation induced by LatA in GCBC. Overall, these data demonstrate that GCBCR signaling can be partially restored by actin de-polymerization and, as previously reported, the absence of F-actin network leads to increased signaling along the Akt-S6 axis.

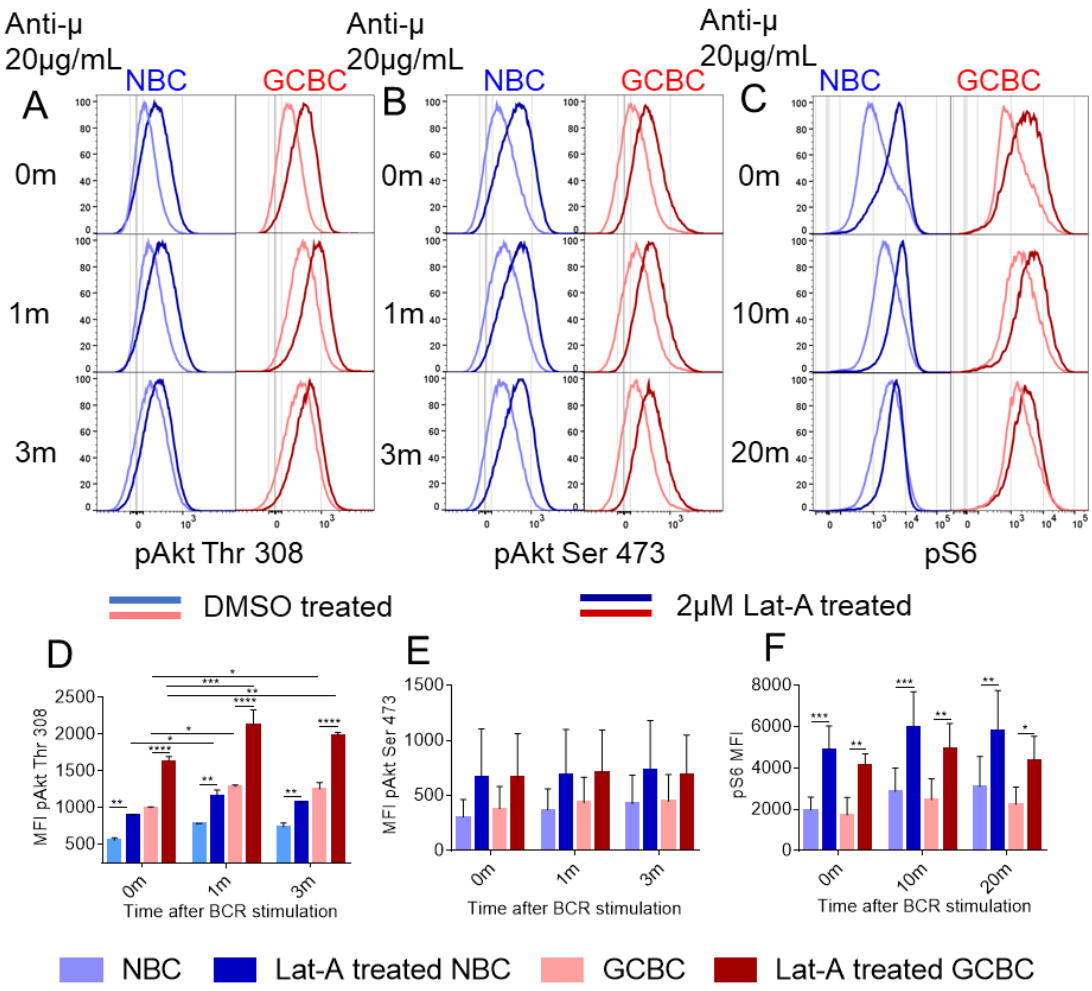


**Figure 28 Actin de-polymerization induces and enhances BCR signaling in B cells.**

**(A-F) Histograms and MFI of pAkt (T 308) (A, D), pAkt (S 473) (B, E) and pS6 (C,F) untreated or treated with 2μM LatA for 10m followed by BCR stimulation and measured by flow cytometry for time points mentioned in the legend. Data are representative of at least two independent experiments.**

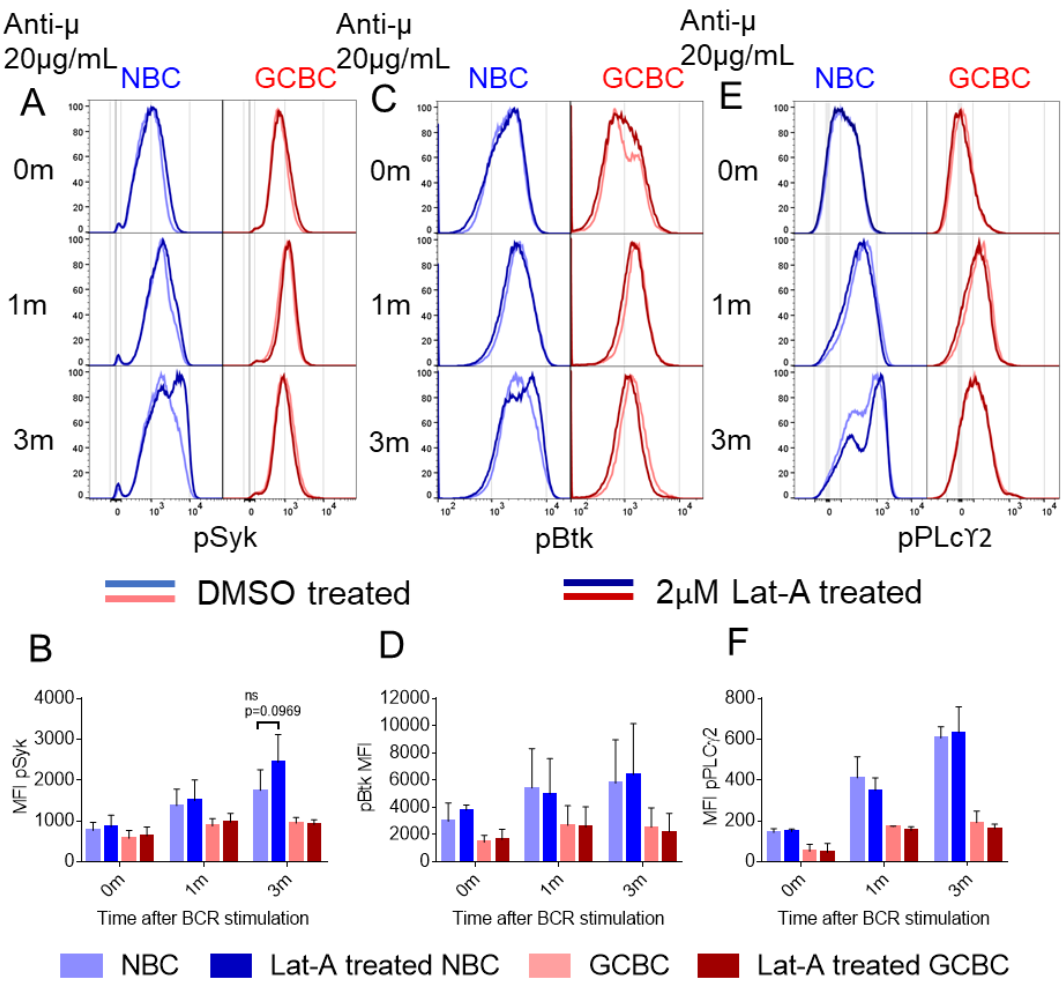


**Figure 29 Figure 29 Actin de-polymerization does not enhance signaling along the Syk-Btk axis.**

**(A-F) Histograms and MFI of pSyk (A, D), pBtk (S473) (B, E) and pPLcϒ2 (C,F) untreated or treated with 2μM LatA for 10m followed by BCR stimulation for the indicated time points. Data are representative of at least two independent experiments.**

Previously, it has been shown that the extent of actin network polymerization inversely corelates to BCR diffusion. GCBC have a more polymerized actin network compared to NBC. Also, the BCR expression is 5-fold lower in GCBC compared to NBC. There is more amount of F-actin per each BCR in GCBC. As in the Image Stream experiment described above, BCR clustering in GCBC seems to be restricted by the presence of F-actin, and upon actin de-

polymerization, GCBCR demonstrate clustering (figure 27). To study whether increased F-actin in GCBC influences BCR movement, we performed TIRF microscopy to track the movement of the BCR in NBC and GCBC. We used fibronectin coating to allow NBC and GCBC to adhere to the Mattek dishes. The BCRs were labeled by a mixture of unlabeled anti-IgM Fab (0.8μg/mL) and A647 conjugated anti-IgM Fab (0.2μg/mL). The cells were labeled with Fab fragments to avoid cross-linking the BCRs. We imaged bead-purified NBC and GCBC under basal conditions in the TIRF plane at 25 fps and recorded the movement of A647 signal. We created spots (referred to as "BCR spots") based on the intensity of the A647 signal in NIS Elements (figure 30A). In Imaris, we created tracks of the movement of the BCR-spots and measured the speed, distance, displacement and duration of the individual tracks (figure 30A-E). We observed that GCBCR had lower track speeds in comparison to Naïve BCR (NBCR) and a trend of higher track duration in GCBC compared to NBC (figure 30C, E). However, GCBCR were not different in track distance and displacement (figure 30B, D). These data demonstrate that under basal conditions, GCBCR moved significantly slower than NBCR which we theorize to be the product of its highly polymerized actin network. Future experiments will focus on measuring track statistics of BCRs in NBC and GCBC with or without LatA treatment to test the above-mentioned theory.

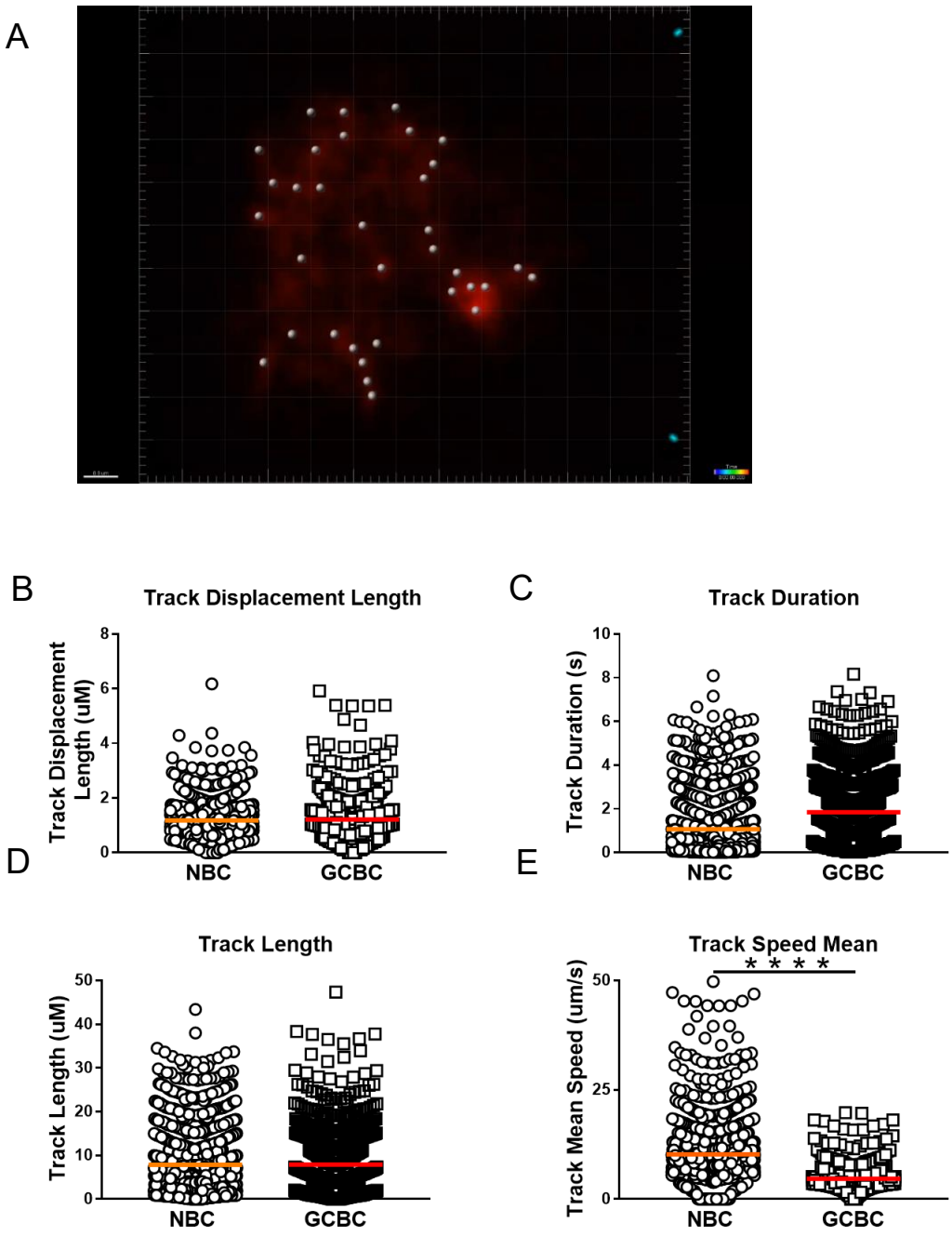


**Figure 30 BCRs on GCBCs move slower in comparison to NBCs at resting state**

**(A) Representative image from a GCBC of BCRs labeled with IgM Fab A647 (red dots), imaged at 25 fps in TIRF. The grey spheres and dragon tails represent tracks of the movement of BCR over time. (B-D) Track statistics from NBCs and GCBCs demonstrating displacement length (B), duration (C), length (D) and speed mean (E) of BCRs at resting state. Data is from one TIRF experiment with 20 cells per each cell type.**

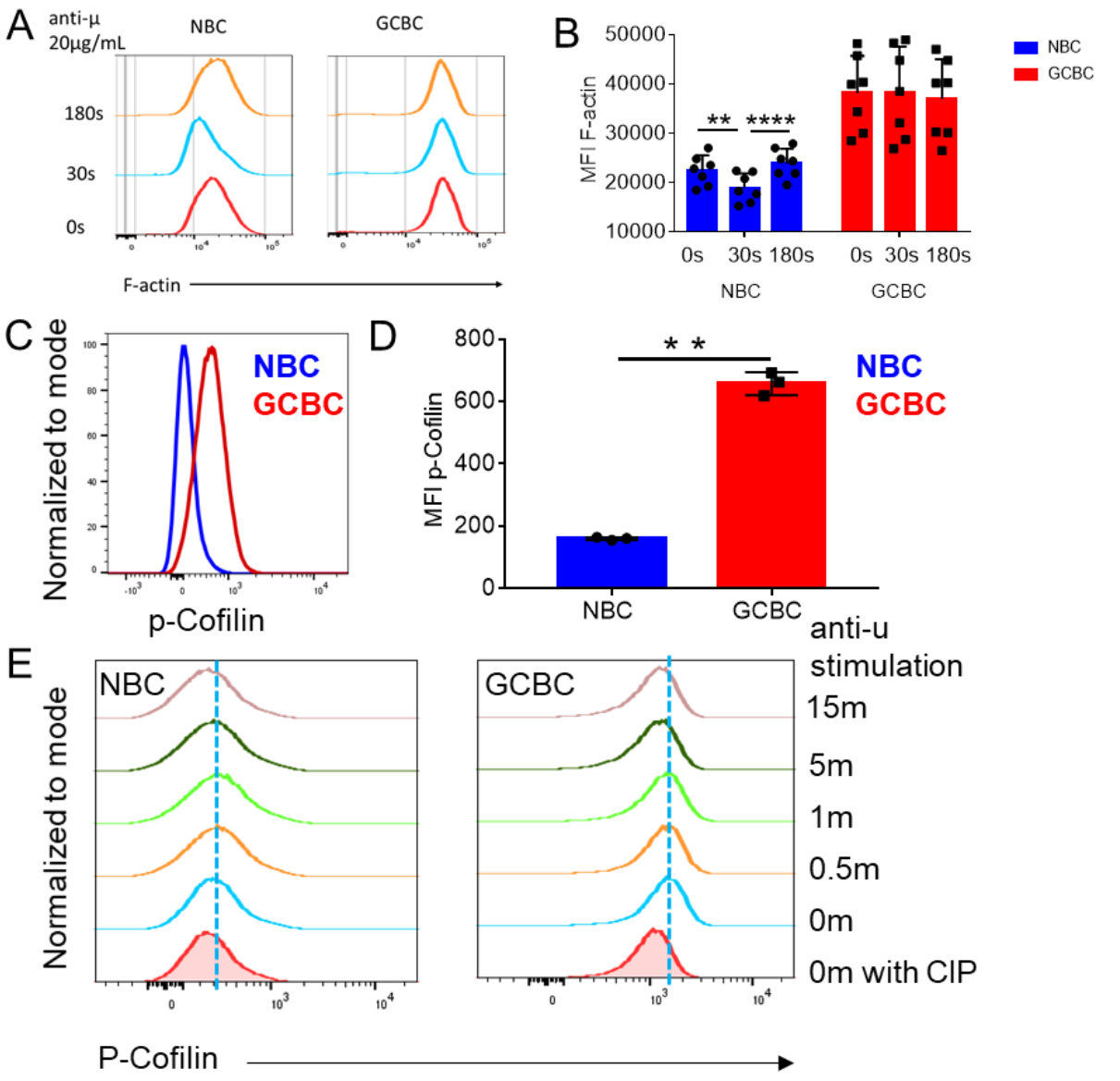


**Figure 31 Differential actin dynamics in GCBC upon BCR stimulation compared to NBC**

**(A-B) Histogram (A) and quantification (B) of F-actin in NBC and GCBC upon BCR stimulation. (C-D) Histogram (C) and quantification (D) of p-cofilin in NBC and GCBC at resting state. (E) Histogram of p-cofilin in NBC and GCBC after CIP treatment (shaded) and BCR stimulation. Data are representative of at least two independent experiments in A-B and is from one experiment in C-E.**

Previous studies have shown that B cells undergo a rapid and transient phase of actin de-polymerization upon receiving a stimulus through the BCR (151). This de-polymerization has been attributed to the actin-severing protein cofilin (152). Upon BCR stimulation, cofilin undergoes a transient de-phosphorylation which activates cofilin to perform its actin severing function (152). Since, GCBC have higher levels of polymerized actin at the resting state, we sought to determine if the F-actin dynamics in GCBC were any different from those in NBC.

Upon BCR stimulation, in agreement with published results (151), we observed a reduction in the global levels of F-actin as measured by flow cytometry for phallodin binding (figure 31A-B). Within 30 seconds of BCR stimulation, F-actin levels were significantly reduced in NBC compared to 0 seconds and 180 seconds, when the F-actin levels were restored to the basal levels (figure 31A-B). However, in GCBC, F-actin levels did not change after BCR stimulation (figure 31A-B). The transient de-polymerization of actin is critical for increasing BCR diffusion and to form a central BCR cluster (139). BCR clustering is not observed in GCBC as previously reported by our lab (60) and in figure 30. The lack of transient de-polymerization of actin offers a potential explanation as to why the BCR does not cluster in GCBC. It is possible that because of the continued restriction of the actin cytoskeleton, BCRs have limited contacts with other BCRs and therefore end up organizing into smaller clusters and not forming a cap like in NBC.

As described above, actin de-polymerization is directly correlated to cofilin de-phosphorylation and activation (152). In line with higher F-actin, p-cofilin levels were also significantly higher in GCBC compared to NBC (figure 31C-D). In fact, treatment of the cells using calf intestinal phosphatase (CIP) reduced p-cofilin levels in GCBC but not in NBC (figure 31E). These data suggested that cofilin is phosphorylated in GCBC in the resting state but has minimal phosphorylation in NBC. However, upon BCR stimulation, there was no significant

change in the phosphorylation status of cofilin in NBC or GCBC except a moderate reduction at 15m post-stimulation (figure 31E). Future studies will focus on understanding the role of cofilin and other actin severing proteins such as gelsolin and destrin that may be acting in a redundant manner with respect to actin dynamics in GCBC.

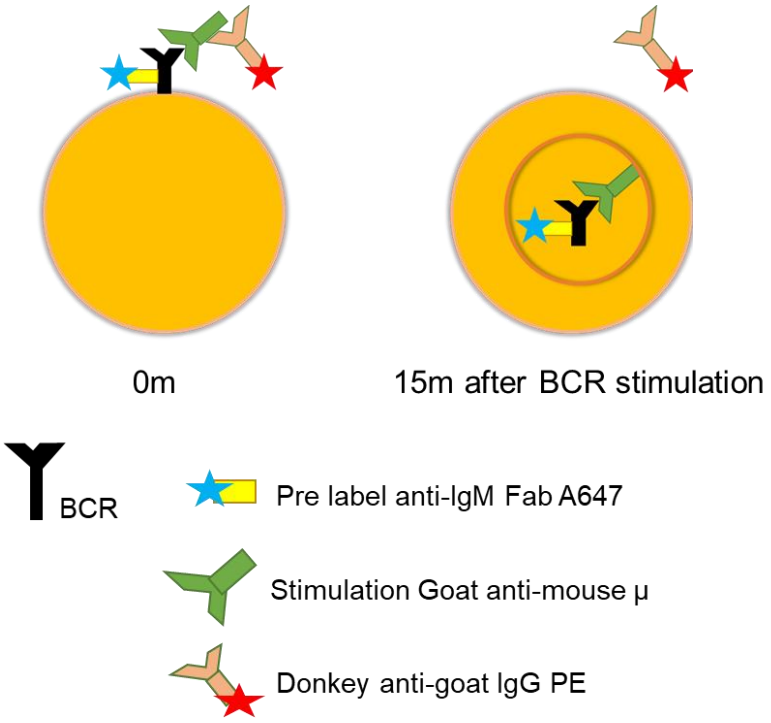


**Figure 32 Schematic diagram for BCR endocytosis assay by flow cytometry.**

Apart from BCR signaling, actin re-modeling has a major impact on BCR endocytosis. (139, 164, 165). To study the BCR endocytosis in GCBC, we designed an assay to measure BCR internalization by flow cytometry. We used anti-IgM Fab-A647 to pre-label the BCRs and

stimulated these cells using goat anti-mouse μ IgG antibody for different lengths of time

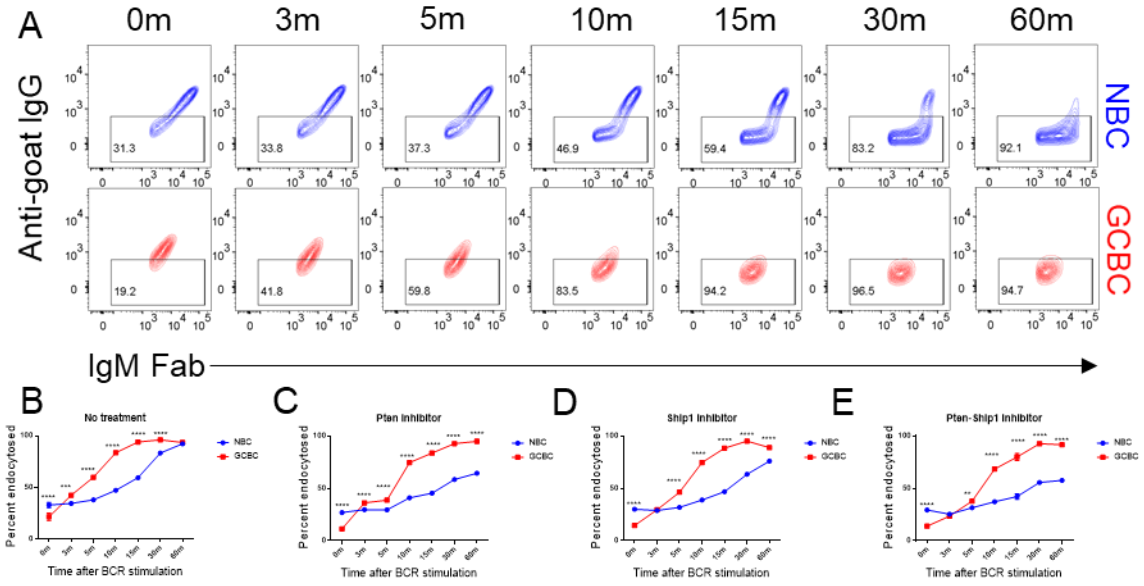


**Figure 33 Rapid BCR endocytosis in GCBC is partially dependent on lipid inositol phosphatases PTEN and SHIP-1.**

**(A) Contour plots of BCR endocytosis assay in NBC and GCBC at different time points after receiving BCR stimulation between 0 to 60 minutes. (B-E) Quantification of the BCR endocytosis assay in NBC and GCBC in cells pre-treated with DMSO (B), 20μM PTEN inhibitor SF1670 (C), 20μM SHIP-1 inhibitor 3AC (D) and both 20μM PTEN and 20μM SHIP-1 inhibitor (E). Data are representative of at least two independent experiments.**

as described in the legend section (figure 32). The stimulations were stopped by fixing the cells using 1.5% paraformaldehyde (PFA) (figure 32). The cells were later stained using donkey anti-goat IgG-PE (figure 32). Under basal conditions, the majority of the cells were labeled with A647 and PE (figure 32). However, over time, we observed that staining for PE decreased as the BCR was internalized (figure 32). We observed that GCBC had rapid BCR internalization based on reduced staining for PE in comparison to NBC (figure 33A-B). Specifically, GCBC demonstrated reduction in the PE labeling within 5 minutes of BCR stimulation, whereas NBC had bi-modal

populations that expressed different levels of labeling with PE (figure 33A-B). GCBC demonstrated maximal reduction in PE staining between 5 and 15 minutes, whereas NBC had maximal reduction in PE staining between 10 and 30 minutes (figure 33A-B). From these data, we conclude that GCBCRs undergo rapid internalization upon BCR stimulation.

As previously reported, upon BCR stimulation GCBC induce the production of different lipid inositols in comparison to NBC (123). NBCR stimulation generally leads to a rapid spike in $PIP_3$, whereas, GCBCs have higher basal levels of $PI(3,4)P_2$ and upon BCR stimulation generate more PI(4,5)P2 and relatively little PIP3 (123). These observations have been linked to the higher expression and function of lipid inositol phosphatases SHIP-1 and PTEN in GCBC (60, 123). Both $PIP_2$ species mentioned above have been implicated in receptor-mediated endocytosis. $PI(3,4)P_2$ is a known recruiter of endosome-associated protein Bam32 and sorting nexin 9 (snx9) (169, 170). Interestingly, Bam32 expression is upregulated in human GCBC (171) and we have observed that it is highly phosphorylated in GCBC in comparison to NBC (data not shown). On the other hand, $PI(4,5)P_2$ is known to interact with the adaptor protein AP2, which plays an important role in clathrin-mediated endocytosis (172). To analyze the role of these lipid inositol phosphatases in BCR endocytosis, we performed a flow cytometry-based endocytosis assay in the presence of inhibitors specific for these phosphatases. We observed that NBCR endocytosis is very sensitive to treatment with these inhibitors and endocytosis is significantly reduced in the presence of SHIP-1 or PTEN inhibitor (figure 33B-E). On the other hand, GCBC demonstrate a reduction in BCR endocytosis at 3-5m post-BCR stimulation after pre-treatment with SHIP-1 or PTEN inhibitor, compared to untreated controls. (figure 36 B-E). However, at 10 minutes after BCR stimulation, BCR endocytosis in SHIP-1 and/or PTEN inhibitor pre-treated cells is comparable to the levels in

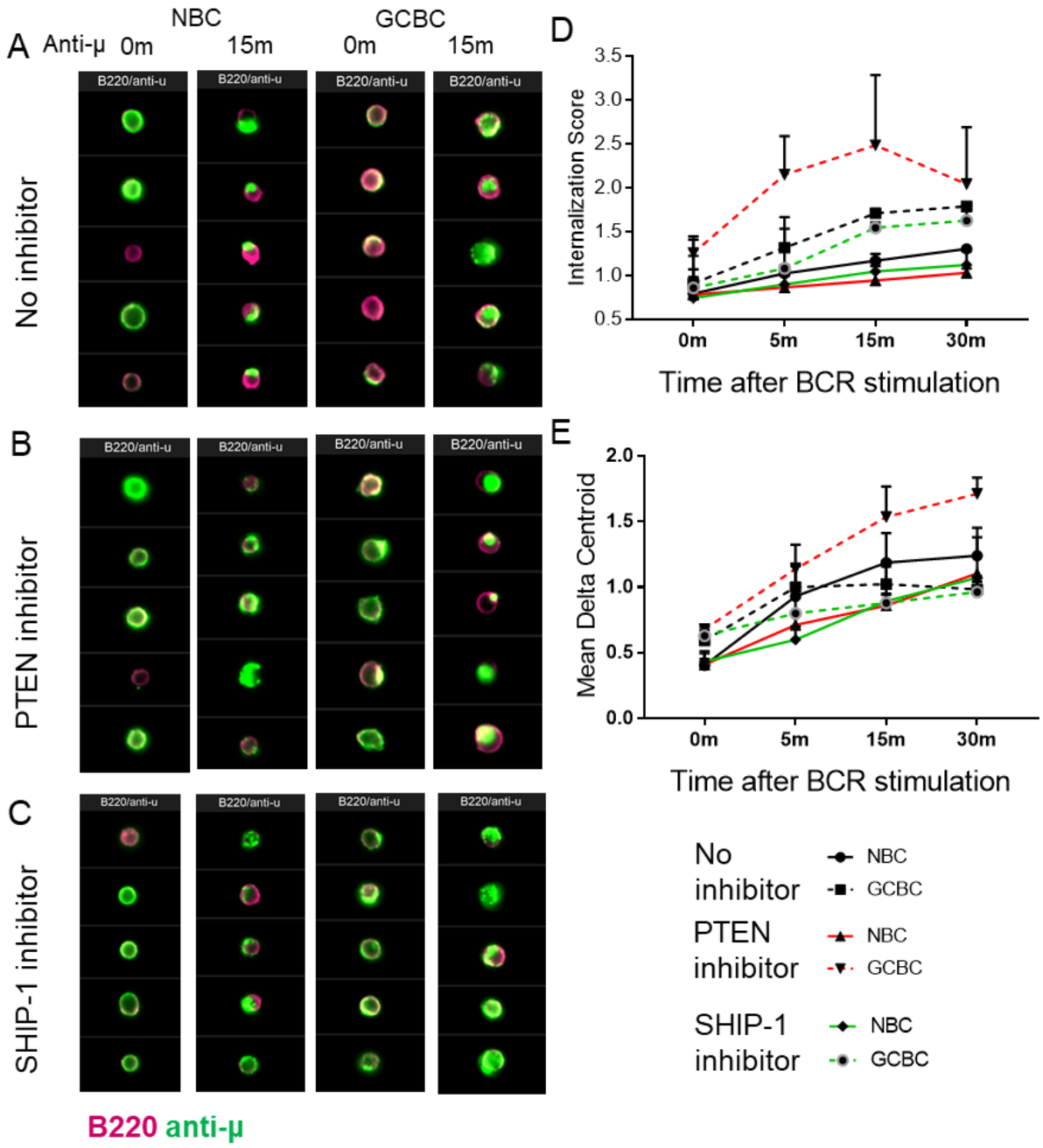


**Figure 34 Differential BCR clustering and internalization after SHIP-1 and PTEN inhibition**

**(A-C) Amnis images of B220 and anti-μ staining on NBC and GCBC at 0m and 15 m post-BCR stimulation treated by control (A), 20μ PTEN inhibitor (B) and 20μ SHIP-1 inhibitor (C). (D) Internalization score from analysis of Amnis data using IDEAS software for BCR internalization in B cells described as above. (E) Delta Centroid from analysis of Amnis data using IDEAS software for BCR internalization in B cells described as above. Data are representative of at least two independent experiments.**

un-treated cells (figure 33B-E). These data hint towards a strong endocytic machinery in GCBC and potentially the initial phase of BCR endocytosis is dependent on PTEN and SHIP-1 in GCBC, whereas NBCR endocytosis is completely dependent on these phosphatases.

To further study this, we performed Image Stream analysis to estimate the internalization of goat anti-mouse μ conjugated to A488. We stimulated the cells using goat anti-mouse μ A488 and fixed the cells at different time points with 1% PFA. We found that consistent with our flow cytometry data, the internalization feature of the IDEAS software revealed that GCBCR were rapidly endocytosed, compared to NBCR (figure 34A, D). As noted previously, NBC organized BCR as single clusters or caps, whereas GCBCRs were organized as smaller clusters, and several of these clusters were observed as microvesicles inside the cells (figure 34A, D). From these data, we conclude that BCR dynamics are fundamentally different in NBC and GCBC and this phenomenon potentially leads to different downstream functions. Interestingly, similar to the flow cytometry data, we observed a reduction of BCR internalization in NBC with SHIP-1 or PTEN inhibition and a reduction in BCR internalization in GCBC after inhibition of SHIP-1 (figure 34A-D). However, treatment with PTEN inhibitor led to enhanced internalization of the BCR in GCBC (figure 34A-D). This is contrary to our flow cytometry data, where we observed a moderate reduction in BCR endocytosis in GCBC with PTEN inhibition (figure 33C). To resolve this, we will perform confocal microscopy that will provide higher resolution images of B cells that are un-treated or treated with PTEN inhibitor and stimulated using anti-BCR.

Unexpectedly, we observed that upon BCR stimulation, GCBC treated with the PTEN inhibitor had significantly more BCR clustering than un-treated GCBC (figure 34A-C, E). NBC, on the other hand, had reduced BCR clustering when stimulated through the BCR in the presence of SHIP-1 or PTEN inhibitor (figure 34A-C, E). SHIP-1 inhibitor did not have a major impact on

BCR clustering in GCBC (figure 34A-C, E). Previously, we showed that treatment with PTEN inhibitor leads to restoration of BCR signaling in GCBC and there is enhancement of BCR signaling in NBC (123). The enhanced signaling and BCR clustering phenotype demonstrate the potent function of PTEN in dampening BCR signaling in GCBC. From these data, we conclude that PTEN and SHIP-1 control BCR endocytosis in NBC, whereas in GCBC, SHIP-1 has a modest control over BCR internalization. Most strikingly, PTEN prevents anti-BCR induced capping of the receptor in GCBC and its effect on BCR endocytosis will be studied further using confocal microscopy.

Positive selection of GCBC depends on their ability to present Ag to T cells (99). In fact, it has been shown that CD40 signaling is crucial for induction of c-Myc expression in GCBC, which is a strong signature of positive selection (99). As shown previously, GCBC have enhanced BCR endocytosis compared to NBC. To study whether enhanced endocytosis also translates to rapid Ag presentation, we used the peptide Eα, which when processed and presented on the surface in the context of MHC II I-$A^b$, can be detected by an antibody referred to as YAe (167, 173). The peptide Eα is linked to GFP so that the uptake of Eα can be tracked by GFP fluorescence. We further conjugated Eα-GFP to NIP to prepare a reagent, NIP-EαGFP, that can be taken up by NIP-specific B cells. We immunized B18+/- Vκ8R+/- CD45.1/2 with NP-CGG. These mice have 1-2% lambda positive cells in the resting state. Upon immunization, these lambda positive cells expand, and some enter the GC. We stimulated B cells using 25μg/mL EαGFP, 25μg/mL NIP-EαGFP, 25μg/mL NP-BSA or PBS alone for 1 or 2 hours *in vitro*. We fixed the cells with 1% PFA to stop the stimulation and surface stained for YAe to assess the Ag presentation in B cells. The combination of B18+/- heavy chain with lambda light chain is a good indicator of NIP reactivity.

Therefore, we used lambda staining to gate on NIP reactive B cells, and then further gated on CD95+ CD38- GCBC and CD95- CD38+ NBC as shown below (figure 35).

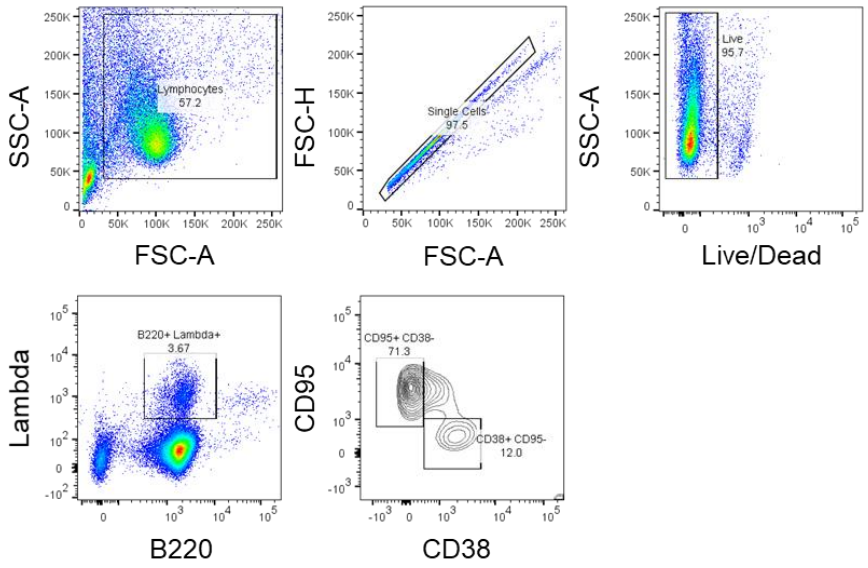


**Figure 35 Gating strategy for NBC and GCBC in B18+/- Vκ8R +/- (C57BL/6 mice) for BCR endocytosis assay.**

**Data are representative of at least two independent experiments.**

We observed that there was an increase in YAe staining within one hour of stimulation with NIP-EαGFP (figure 36A-D). Approximately 20% of NBCs and 40% of GCBC had higher YAe staining, compared to un-stimulated cells (figure 36A-D, figure 38A). Moreover, within 2 hours, 40% of NBC and about 65% of GCBC had higher YAe staining than un-treated groups (figure 36 A-D, figure 38A). These data suggested that a higher number of GCBC present Ag in a rapid manner compared to NBC.

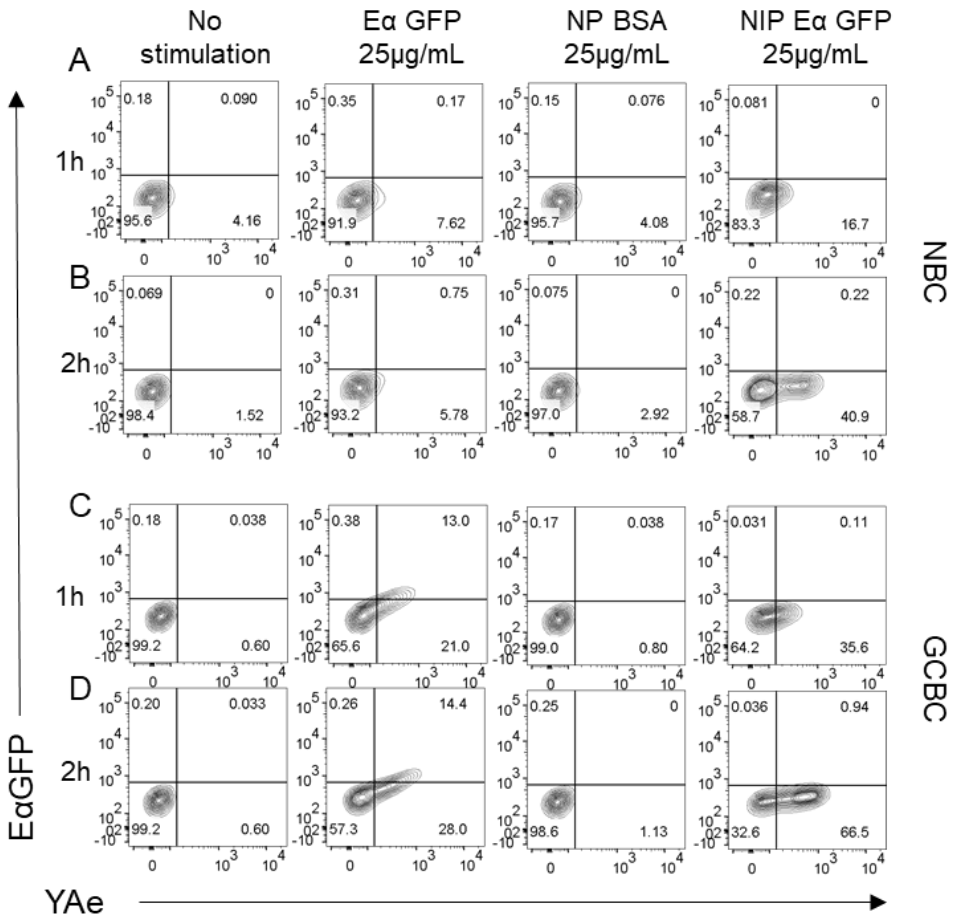


**Figure 36 Rapid Ag presentation in GCBCs compared to NBCs**

**(A-D) Contour plots of YAe and EαGFP staining in NBCs (A-B) and GCBCs (C-D) upon stimulation by control, 25μg/mL EαGFP, 25μg/mL NP BSA and 25μg/mL NIP-EαGFP (left to right columns) at 1 hour (A,C) and 2 hours (B,D) post stimulation. Data are representative of at least two independent experiments.**

Unexpectedly, we observed an increase in YAe staining in GCBC, but not in NBC, stimulated with EαGFP (figure 36A-D 2nd column). At 2 hours, about 30% GCBC had an increase in YAe staining but in NBC this staining remained at a basal level (figure 36A-D 2nd column). The uptake of EαGFP in GCBC was likely mediated by phagocytic or pinocytic pathways, since it was Ag-nonspecific. Interestingly, the pattern of YAe and anti-GFP FITC staining was different between the EαGFP and NIP-EαGFP stimulations (figure 36A-D 2nd and 4th column). GCBC

treated with EαGFP were double positive for YAe and anti-GFP FITC, whereas GCBC treated with NIP EαGFP only stained with YAe (figure 36A-D 2nd and 4th column). These unique staining patterns may be because of the different efficiencies of Ag processing in different endosomal compartments. Receptor mediated endocytosis may lead to faster Ag breakdown and processing followed by rapid Ag presentation. On the other hand, Ag taken up via phagocytosis or pinocytosis may be processed more slowly, leading to co-staining of GCBC with YAe and anti-GFP FITC, which is an indirect measure of un-processed Ag.

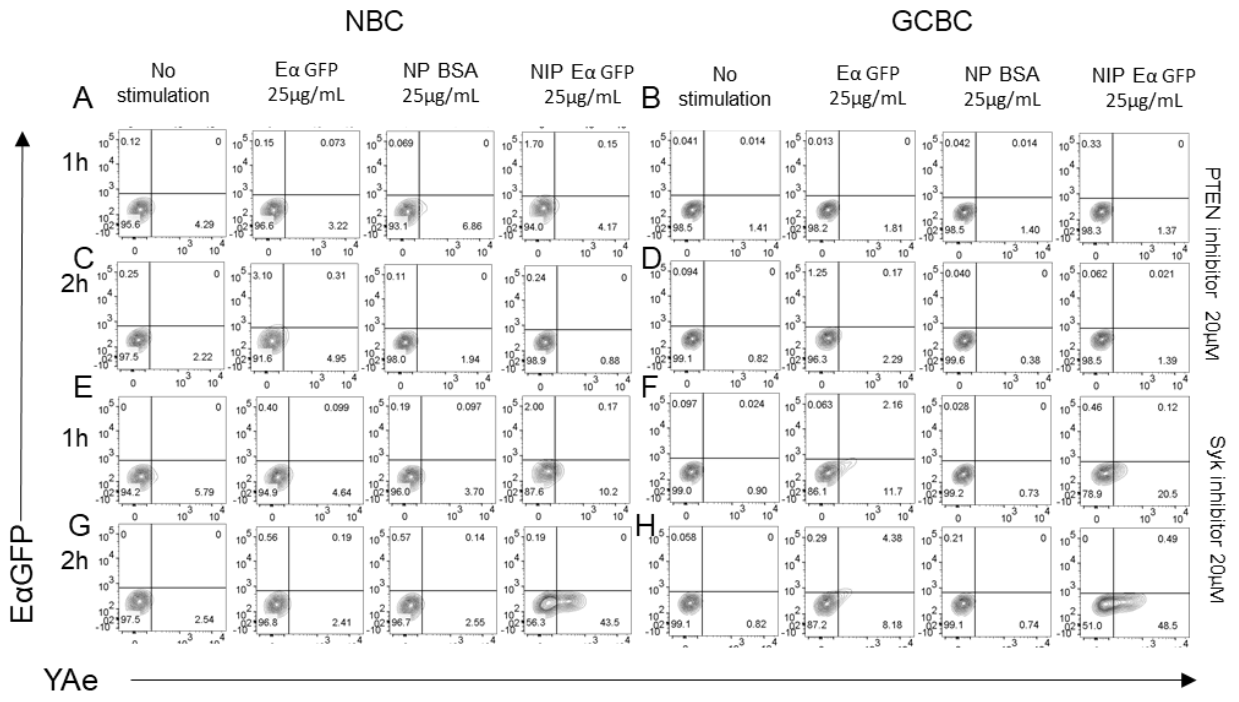


**Figure 37 B cell Ag presentation is PTEN dependent and partially dependent on Syk activity**

**(A-H) Contour plots of YAe and EαGFP staining in NBCs (A,C,E,G) and GCBCs (B,D,F,H) upon stimulation by control, 25μg/mL EαGFP, 25μg/mL NP BSA and 25μg/mL NIP EαGFP (left to right columns) at 1 hour (A-B, E-F) and 2 hours (C-D, G-H) post stimulation in cells treated by 20μM PTEN inhibitor (A-D) or 20μM Syk inhibitor. Data are representative of at least two independent experiments.**

Previously we showed that BCR endocytosis in NBC is sensitive to PTEN and SHIP-1 inhibition and, as per our flow cytometry data, GCBC have a partial impact on endocytosis with PTEN and SHIP-1 inhibition. Differences in endocytosis may delay Ag processing and presentation in B cells. The effector kinase Syk is also known to play a role in mediating endocytosis of the BCR (174). Therefore, we wanted to determine if treatment with Syk, PTEN or SHIP-1 inhibitors would change Ag presentation dynamics in B cells. We treated cells with 20μM PTEN inhibitor, 20μM SHIP-1 inhibitor or 20μM Syk inhibitor and measured endocytosis as described for figure 36. We observed that treatment with PTEN inhibitor completely abolished the Ag presentation in both NBC and GCBC within 2 hours of stimulation (figure 37A-D, figure 38B). Ag presentation did not occur in GCBC that were stimulated with 25μg/mL EαGFP either, the pathway that we suspect is mediated via phagocytosis or pinocytosis (figure 37A-D, figure 38B). This was an unexpected result because GCBC only have a minor reduction in endocytosis of the BCR upon PTEN inhibition, as assessed by flow cytometry; in fact, our Amnis data showed enhanced BCR internalization in GCBC upon PTEN inhibition (figure 33-34). We observed a different pattern of BCR clustering and enhanced signaling when PTEN activity was inhibited (figure 34). This data suggests that there is a previously unappreciated PTEN-dependent step that is necessary for efficient Ag processing and presentation in B cells.

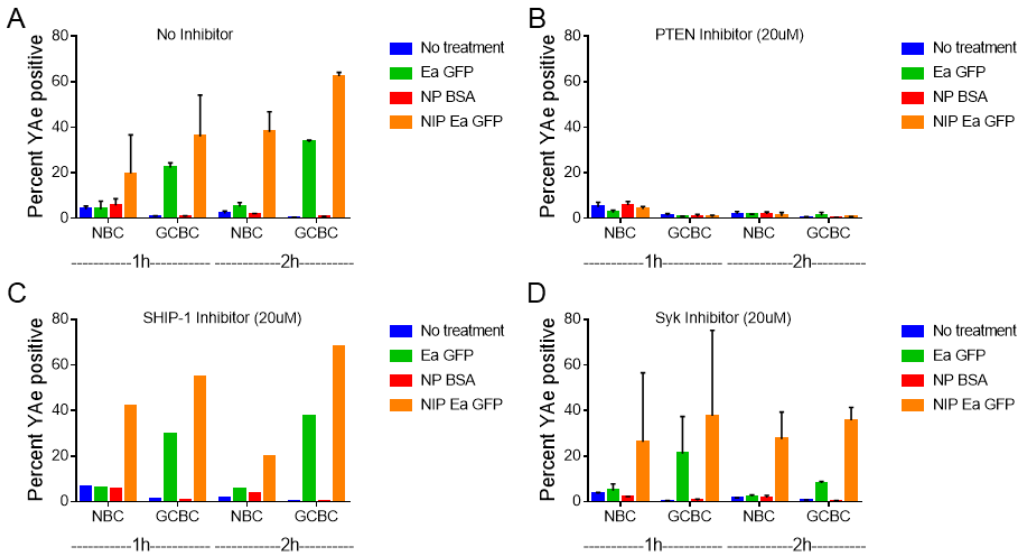


**Figure 38 B cell Ag presentation is PTEN dependent, partially dependent on Syk and independent of SHIP-1 activity**

**(A-D) Quantificationof YAe positive cells in NBC and GCBC upon stimulation by control, 25µg/mL EαGFP, 25µg/mL NP BSA and 25µg/mL NIP-EαGFP at 1 hour and 2 hours post stimulation in cells treated by 20µM PTEN inhibitor (B) or 20µM SHIP-1 inhibitor (C) or 20µM Syk inhibitor (D). Data are representative of at least two independent experiments.**

On the other hand, treatment with SHIP-1 inhibitor did not lead to any detectable change in the Ag presentation function of the B cells (figure 38C). However, treatment with Syk inhibitor had a partial effect of B cell Ag presentation (figure 37E-H, figure 38D), which was found to be reduced at 1 and 2 hours in Syk inhibitor-treated cells, compared to un-treated cells (figure 37E-H, figure 38D). The effects were more profound at 2 hours post-stimulation, suggesting a role for Syk function in sustained Ag presentation and MHC II turnover (figure 37E-H, figure 38D). Overall, these data showed that GCBC present Ag more rapidly than NBC and that the Ag presentation pathways are partially dependent on Syk activity and completely dependent on PTEN

activity. Future experiments will focus on determining the role of PTEN in Ag processing and presentation pathways.

Based on our earlier observations, we hypothesized that GCBC have significant alterations in the components of their cytoskeleton that leads to differential BCR signaling and endocytosis. To uncover these alterations, we performed RNA-sequencing analysis of purified NBC and GCBC and in vivo activated B cells. The in vivo activated B cells represent B cell blasts found at 48 hours post NP-Ficoll immunization and are control for activated B cell population. We created comparisons of GCBC to NBC and GCBC to B cells activated *in vivo* (figure 39A-B). Next, we performed gene set enrichment analysis (GSEA) of cytoskeleton-related genes (http://software.broadinstitute.org/gsea/msigdb/cards/CYTOSKELETON) with respect to the comparisons mentioned above (figure 39A-B). We observed that there was a significant enrichment of cytoskeleton-associated genes in GCBC compared to NBC and that a similar trend was observed in GCBC compared to in vivo activated B cells (figure 39A-B). Out of the 368 genes that were tested, 78 genes were differentially expressed to a significant degree in GCBC compared NBC and *in vivo* activated B cells (FDR < 0.01, fold change 2) (figure 39C).

As expected, genes regulating the actin cytoskeleton were found to be highly expressed in GCBC (figure 39C, figure 40A). Notably, genes involved in protrusions and filopodal extensions such as Aif1l and fascin 1 (*Fscn1*) were highly expressed in GCBC compared to NBC and *in vivo* activated B cells (figure 40A). *Lima* a gene known for inhibiting actin de-polymerization (175), was found to be highly expressed in GCBC compared to NBC and in vivo activated B cells (figure 40A). Interestingly, proteins involved in actin severing such as *Capg* and protein kinase C binding protein *Marcks* were found to have reduced in expression in GCBC in comparison to NBC and in vivo activated B cells (figure 40A). Interestingly, we also found higher expression of genes

associated with endocytosis in GCBC compared to NBC and in vivo activated B cells. Cortactin is a component of clathrin mediated endocytosis that facilitates actin nucleation and pinching off of endosomes from the cell surface by acting as a link between dynamin and Wasp proteins (176). We validated the higher expression of cortactin and fascin at the protein level in GCBC compared to NBC (figure 40B-C). Overall, the RNA-seq analysis demonstrated that the cytoskeleton is significantly remodeled in GCBC when compared to NBC and *in vivo* activated B cells and that these modifications may lead to differential GCBC function in the context of BCR signaling and endocytosis that have been observed earlier in this chapter.

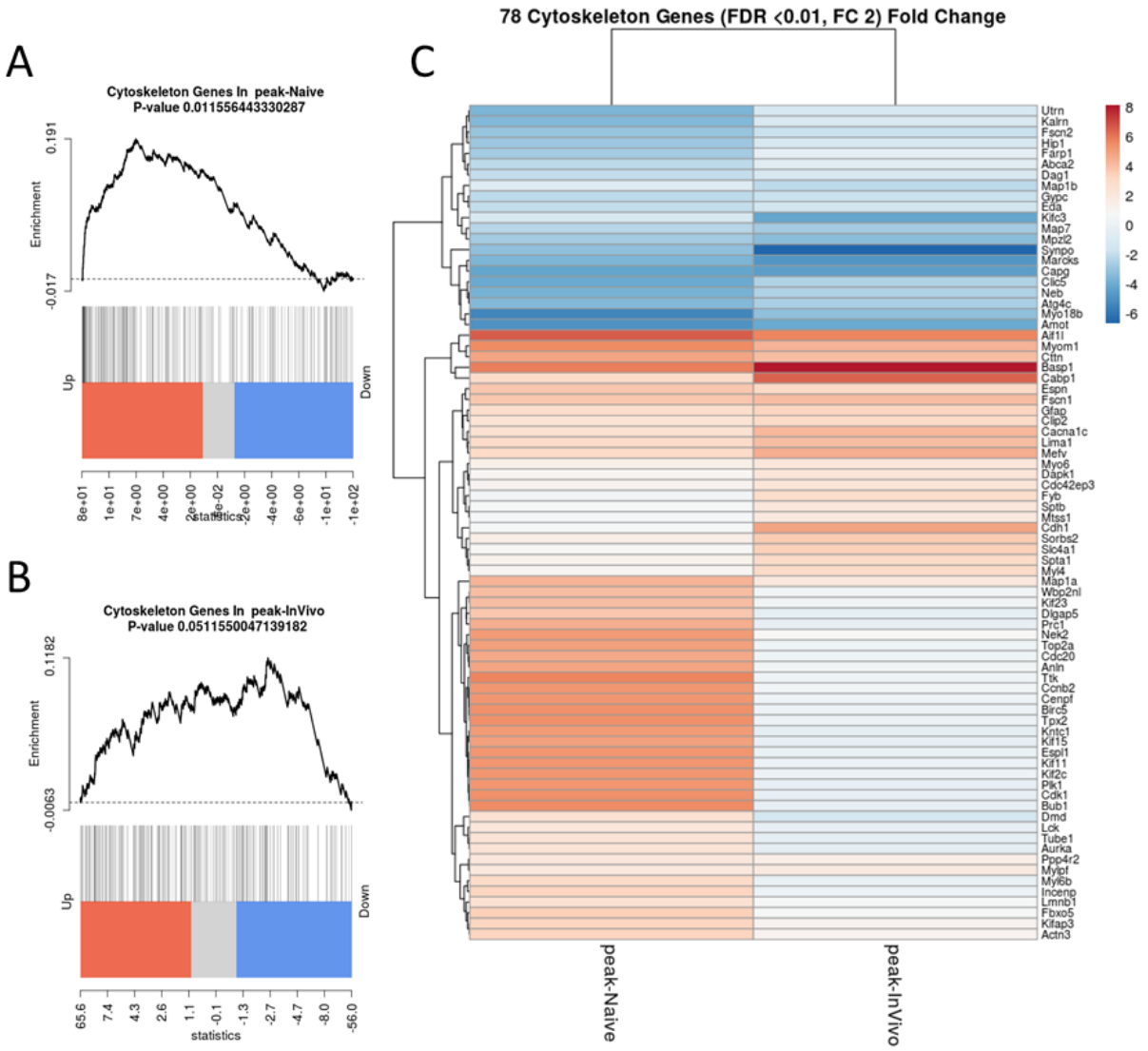


**Figure 39 RNA-seq analysis of cytoskeleton related genes in GCBCs in comparison to NBCs and in vivo activated B cells**

**(A-B) GSEA of cytoskeleton associated genes in GCBCs in comparison to NBCs (A) and invivo activated B cells (B). (C) Heat map of 78 differentially expressed genes in GCBCs compared to NBCs and activated B cells. Data are from one RNA-seq experiments with FACS sorted cells from at least 3 mice.**

It has been reported that Bam32 is highly expressed in human GCBC and that that BCR internalization does not occur efficiently in Bam32-/- B cells (171). Moreover, GC dissolve earlier than WT and the GCBC do not undergo efficient class switch in Bam32-/- mice (177, 178). We

observed higher expression of Bam32 in murine GCBC compared to NBC (figure 40D). Future experiments in this area will focus on knocking out Cortactin, Fascin and Bam32 and observing the effects on overall GC function and understanding the role of these proteins in BCR endocytosis.

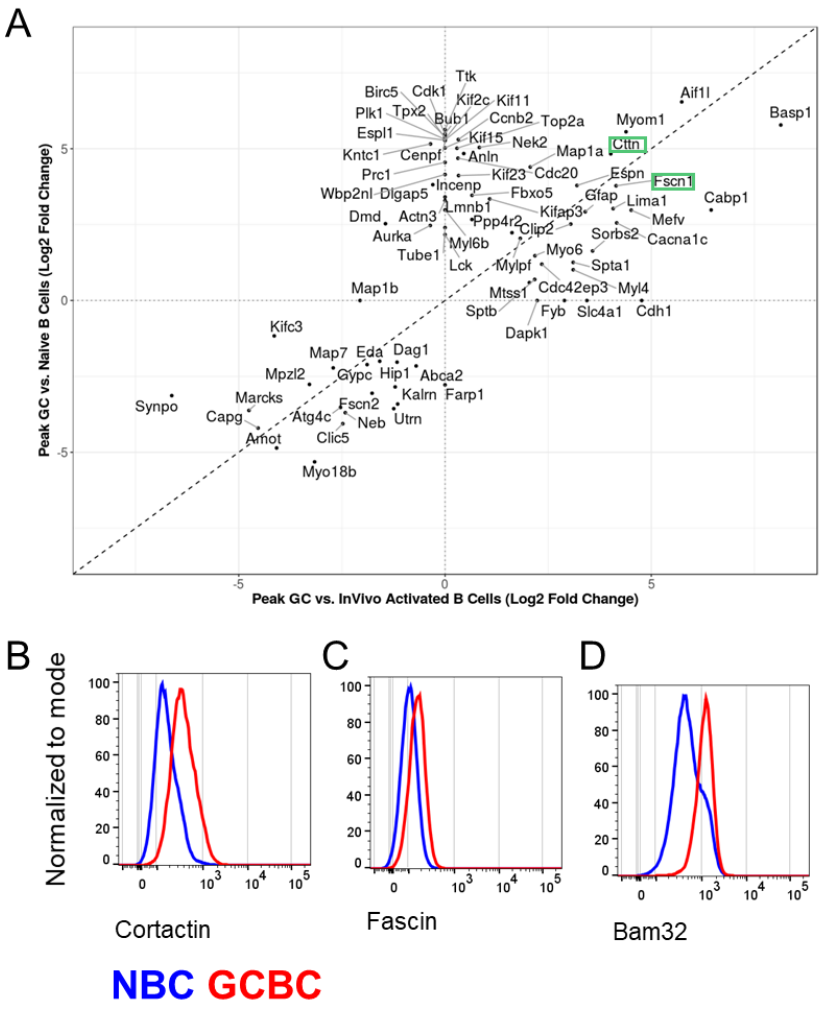


**Figure 40 Increased expression of cytoskeleton related genes Cortactin, Fascin and Bam 32 in GCBC in comparison to NBC**

**(A) X-Y plot demonstrating differential expression of cytoskeleton associated genes in GCBCs in comparison to NBCs and invivo activated B cells (B-D) Histogram of Cortactin (B), Fascin (C) and Bam32 (D) expression in GCBC (red) compared to NBC (blue). Data in A are from one RNA-seq experiments with FACS sorted cells from at least 3 mice. Data in B-D are representative of at least two independent experiments.**

## 3.4 Discussion

In this study we have shown that GCBC have significant re-modeling in how their BCR interpret Ag stimulation when compared to NBC. In terms of the actin cytoskeleton, we found that GCBC have significantly more F-actin and de-polymerization of the F-actin network led to BCR clustering and BCR-like signaling. These data are in agreement with others and they demonstrate that F-actin can act as a negative regulator of BCR signaling in GCBC and NBC (145, 153). In NBC, it has been shown earlier, that the amount of F-actin inversely correlate to the diffusion of the BCR (145, 153). Interestingly, in GCBC, we found that the BCR moved significantly more slowly than in NBC. We theorize that the highly polymerized actin cytoskeleton acts as a barrier to the movement and therefore reduces the speed of the BCR in GCBC. We will further test this theory by measuring the speed of BCR on GCBC and NBC before and after treatment with the actin de-polymerizing agent LatA.

Previously, it was shown that in NBC F-actin forms smaller compartments around the plasma membrane within which individual BCRs or BCR nano-clusters are trapped (139, 144, 145, 149, 150, 153). Upon receiving a BCR stimulation, the actin cytoskeleton transiently de-polymerizes allowing for free diffusion of the BCR which eventually leads to their clustering and propagation of the signal (151-153). We showed that GCBC had higher levels of polymerized actin at the basal level. Moreover, by flow cytometry, the expression of BCR on GCBC is 5-fold lower in comparison to NBC. So, in theory, for each BCR there is overall more F-actin available, which may contribute to further restriction in BCR movement and diffusion. In NBC, F-actin undergoes a temporary de-polymerization within 30 seconds of receiving a BCR stimulus. However, GCBC do not undergo a transient de-polymerization upon BCR stimulation. This effect can at least be attributed to the highly phosphorylated cofilin in GCBC. The actin severing protein, cofilin, is

inactive in its phosphorylated form (152, 154). We found that GCBC had higher basal levels of p-cofilin compared to NBC. However, contrary to published literature, in our study, NBC did not undergo a de-phosphorylation in cofilin, although NBC did undergo actin de-polymerization (152). These data may suggest redundant roles for actin severing proteins such as cofilin, destrin and gelsolin (155, 179). The function of other actin-severing proteins in context of GCBC remains to be elucidated.

Ag stimulation eventually leads to BCR internalization and Ag presentation in order to receive helper signals from T cells. Previous work has indicated that BCR signaling and BCR internalization are mutually exclusive processes (180). Non-ITAM and ITAM tyrosine residues are phosphorylated in the Igα cytosolic tail upon BCR stimulation and these phosphorylated BCRs are retained on the cell surface to initiate a signaling cascade (180). On the other hand, non-phosphorylated BCRs are rapidly internalized (180). The phosphorylation of these residues is mediated by kinases Lyn or Syk (180). We previously showed that both Syk and Lyn exhibit a dampened signaling state in GCBC compared to NBC after BCR stimulation (60, 99). This may be leading to reduced phosphorylation of tyrosine residues on the cytosolic tail of Igα and therefore the non-phosphorylated BCR get internalized rapidly in GCBC as we observed in our data. Future work will focus on mapping these phosphorylation sites on the BCR in GCBC and comparing their phosphorylation states to NBC.

It has also been that ubiquitination of Igβ is also crucial for proper endosomal sorting of the BCR and Ag presentation (181). Igβ ubiquitination leads to accumulation of $PIP_3$ in endosomal compartments which allows for sorting of BCR into Lamp1+ endosomes (181). BCR co-localize with $PIP_3$ in early endosomal Ag (EEA)+ and Lamp1+ endosomes, whereas no such co-localization has been reported between $PI(4,5)P_2$ and the BCR (181). From these data, the authors

have concluded that $PIP_3$ is necessary for endosomal sorting and processing of the BCR, however, Ag presentation was not measured in this study (181). Contrary to this finding, in our study, we observed that inhibition of PTEN led to reduced BCR clustering and internalization in NBC. In GCBC, as per our Amnis ImageStream data there was enhanced BCR internalization and BCR clustering. Inhibition of PTEN and BCR stimulation lead to an increase in the levels of $PIP_3$ within 5 minutes of stimulation in both NBC and GCBC (123). Thus, BCR endocytosis and sorting may not be entirely dependent on the levels of $PIP_3$ and we propose that there is a un-appreciated role for PTEN and $PI(4,5)P_2$ in this process.

Further supporting this theory, inhibition of PTEN led to complete abolishment of Ag presentation in both NBC and GCBC. In the Ag presentation assay, the Ag Eα is conjugated to GFP. Upon entry of GFP into acidic compartments, the fluorescence is lost, but we can still track it using an anti-GFP FITC antibody. However, in case of PTEN inhibitor-treated B cells, anti-GFP FITC signal was not detectable. And from the flow cytometry and Amnis data, it seemed that BCR do get internalized in PTEN inhibitor-treated B cells albeit to a lesser extent. So, we suspect that endocytosed Ag gets processed but is not efficiently presented on B cells. We stained for intracellular YAe, but it was not detectable in PTEN inhibitor-treated B cells, whereas it was detected in untreated cells that were stimulated with NIP-EαGFP (data not shown). Taken together, these data suggest a role for PTEN in MHC II processing and presentation. The exact role for PTEN in this process remains to be elucidated.

BCR-associated kinase Syk has been shown to play a major role in BCR endocytosis (174). BCR-mediated Syk activation leads to actin re-organization, which is necessary for BCR endocytosis and eventual Ag presentation (174). In agreement with these data, our Ag presentation data demonstrated that Syk inhibition does reduce the extent of Ag presentation both in NBC and

GCBC. In fact, this effect was more pronounced at 2 hours post-stimulation than at 1 hour, suggesting a role for Syk in sustained MHC II mediated Ag presentation and perhaps MHC II turnover.

The Ag presentation assay revealed an interesting pattern of anti-GFP FITC and YAe staining in GCBC. In the case of B cells stimulated with EαGFP for 2 hours, GCBC had approximately 30% cells that were YAe+. Within these YAe+ cells, 14% also stained for anti-GFP FITC. These data provide important insights into the GCBC function in several different ways. First, they highlight the phagocytic/pinocytic potential of GCBC that can lead to uptake of proteins from the surroundings in a non-BCR-mediated way. This may instead be mediated by certain scavenger receptors or by a non-receptor endocytic pathway. However, this process was not observed in NBC, reflecting a fundamental change in the biology of B cells upon differentiating into a GC phenotype. Secondly, the co-staining of anti-GFP FITC with YAe was only observed in EαGFP-treated GCBC and not in NIP-EαGFP-treated GCBC suggesting a difference in the dynamics of endocytic processing when a foreign protein is taken up by BCR-mediated endocytosis or by an alternative pathway. It is possible that specific signals associated with the BCR may direct the BCR-containing endosomes into MHC II containing compartments leading to efficient processing and rapid Ag presentation. The exact nature of these signals remains to be elucidated, although we provide strong evidence that PTEN could be a key player in this process.

Overall, from these data, we highlight the basic cell biological differences between NBC and GCBC that contribute to the phenotypical and functional differences with reference to BCR signaling, endocytosis and Ag presentation.

# 4.0 The role of SHIP-1 in GCBC function

## 4.1 Introduction

Upon encounter with antigen, the surface B cell receptor (BCR) initiates a signaling cascade that leads to B cell activation, proliferation, and differentiation. The classical BCR signaling pathway is discussed in detail in Chapter 3. The quality and quantity of BCR signaling is tightly regulated in B cells by means of different phosphatases such as SHP-1, PTEN, SHIP-1, among others. Generally, these phosphatases associate with an inhibitory receptor that triggers their function in dampening the BCR signaling.

### 4.1.1 Inhibitory Receptors

The magnitude and duration of BCR signaling can be negatively regulated by many transmembrane receptors such as CD22, Fcgamma receptor 2b (FcγR2b), siglec-G, CD31 and CD72 (122). Most of these inhibitory receptors possess an immunoreceptor tyrosine-based inhibition motif (ITIM), a tyrosine -containing consensus sequence, in their cytoplasmic region. ITIM tyrosines are phosphorylated by Src family kinases; e.g. the ITIMs in FcγRIIb and CD22 can be phosphorylated by the Src family kinase Lyn upon BCR ligation (122, 126). Phosphorylated ITIMs recruit and activate phosphatases such as SHP-1, SHP-2, SHIP-1 or SHIP-2 depending on the receptor (122). Additionally, tyrosine-protein phosphate non-receptor type 2 (PTNP22), tyrosine-protein phosphate non-receptor type 12(PTP-PEST) and phosphatase and tensin homolog

(PTEN) are also known to play a role in BCR regulation (182, 183). These phosphatases modulate BCR signaling by de-phosphorylating key molecules in the signaling cascade.

SHIP-1 can be recruited to the surface by formation of a quaternary complex between CD22, SHIP-1, Shc1 and Grb2 to regulate $Ca^{+2}$ flux response (184). When Ag binds to an existing IgG, the BCR and FcϒR2B become co-ligated (185, 186). In this case SHIP-1 gets recruited to the ITIM on FcϒR2B and negatively regulates BCR signaling (185, 186). However, SHIP-1 can also be recruited directly to the BCR by binding to ITAMs on CD79a/b (187, 188). The membrane recruitment of SHIP-1 is dependent on the activity of Syk (189). Upon recruitment, SHIP-1 interacts with different signaling proteins and lipid inositols using different protein domains in its structure.

### 4.1.2 Structure of SHIP-1

SHIP-1 is a 145 KDa protein with 1189 amino acids (190), including a central catalytic domain responsible for the phosphatase activity (191). PKA mediated phosphorylation at serine 440 can enhance the phosphatase activity as can binding of $PI(3,4)P_2$ at the C2 domain (192-194). Thus, Ser440 and C2 domain are allosteric activation sites (192-194). The phosphatase domain is flanked by a PH-R domain that can interact with $PIP_3$ (189). The SH2 domain at the N-terminus of SHIP-1 mediates interim with ITIM-containing receptors such as FcϒR2B and CD31, and ITAM-containing receptors and cytosolic proteins such as Shc1 and Dok-3 (128). The SH2 domain is responsible for the localization of SHIP-1 within the cytoplasm (195). The C-terminus of SHIP-1 has proline rich regions that can mediate interaction with Grb2 and tyrosine residues that can mediate interaction with Shc1, Dok-1 and Dok-3 (128). The structure of SHIP-1 reveals its role not only as an enzyme but also as a scaffolding protein that mediates interactions with various

signaling effectors. A schematic diagram of SHIP-1 and its protein domains is presented in figure 41.

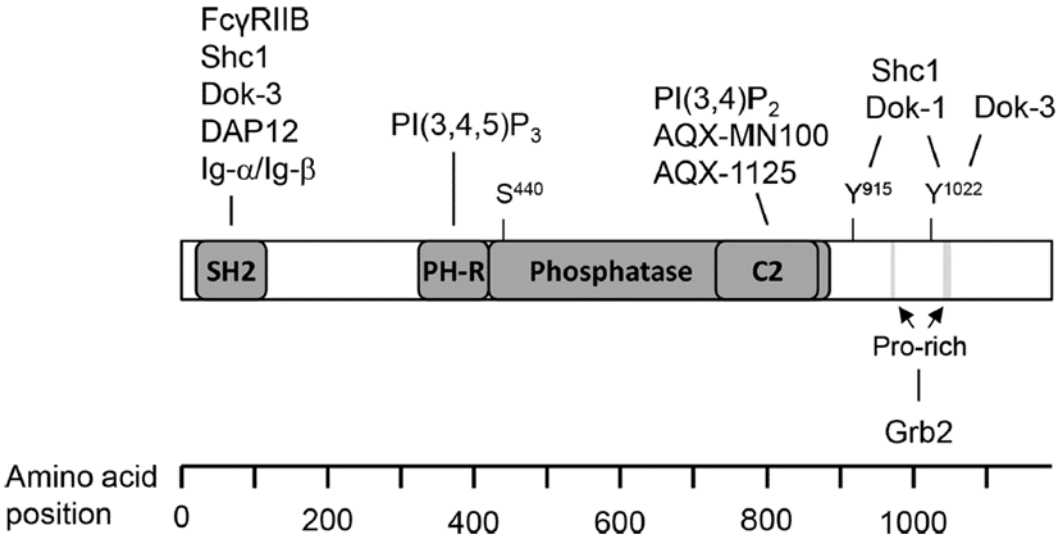


**Figure 41 Schematic diagram showing different protein domains of SHIP-1**

**Adapted from Eur. J. Immunol. 2017. 47: 932–945**

### 4.1.3 SHIP-1 as a regulator of signaling

As a lipid inositol phosphatase, SHIP-1 de-phosphorylates $PIP_3$ into $PI(3,4)P_2$ and reduces $PIP_3$ mediated signaling (196). As discussed earlier, PIP3 can recruit signaling effector proteins such as Akt, Btk, Bam32 and Vav (196). FcϒR2B mediated inhibition of $Ca^{+2}$ flux is dependent on the ability of SHIP-1 to reduce the levels of $PIP_3$, which in turn reduces the recruitment and phosphorylation of Btk and PLCϒ2 (189, 191). A SHIP-1 mutant that lacks phosphatase function cannot inhibit $Ca^{+2}$ flux in DT40 B cells (197). SHIP-1 can also function in a phosphatase-

independent manner as an adaptor, by binding to proteins such as Shc. The interaction of Shc with SHIP-1 limits Shc interaction with Grb2 and SOS, the latter being which is critical for Ras activation (198, 199). The interaction of SHIP-1 with Dok-1 and Dok-3 is known to inhibit Ras activation. Thus, SHIP-1 is a negative regulator of MAPK and PI3K pathways (200, 201).

The product of SHIP-1 enzymatic activity - $PI(3,4)P_2$ - can also recruit distinct effector proteins, including: tandem PH domain containing protein (TAPP) 1/2, lammellipodin (Lpd), Bam32, snx9 and Akt (196). Lpd and snx9 are proteins involved in actin regulation, cell migration and clathrin-mediated endocytosis (196). As shown in Chapter 3, treatment with SHIP-1 inhibitor led to a significant reduction in BCR endocytosis in NBC and literature suggests that this process may be dependent on the SHIP-1 enzymatic product $PI(3,4)P_2$. The interaction between TAPP and $PI(3,4)P_2$ is particularly interesting in the control of Akt signaling and has been extensively studied in TAPP KI mice (202, 203), which express a mutant form of TAPP that does not interact with $PI(3,4)P_2$ (202, 203). TAPP KI mice have high serum auto Abs, kidney pathology and spontaneous GC formation. Moreover, B cells from these mice are hyper-responsive and have higher Akt phosphorylation in comparison to controls (202, 203). Two mechanisms have been proposed to explain this phenotype: 1) TAPP-$PI(3,4)P_2$ interaction leads to recruitment of phosphatase PTPL1, which reduces Akt phosphorylation; or 2) Since $PI(3,4)P_2$ can bind and activate Akt directly, the interaction of TAPP proteins with $PI(3,4)P_2$ indirectly reduces Akt activation (202, 203).

Akt has been shown to directly bind $PI(3,4)P_2$ and $PIP_3$ but not $PI(4,5)P_2$ (204). The crystal structure of Akt also demonstrates its ability to bind directly to $PI(3,4)P_2$ (205). Co-incubation of Akt with synthetic phosphor-inositides $PIP_3$, $PI(4,5)P_2$ and $PI(3,4)P_2$ show that $PI(3,4)P_2$ has the highest potential to activate Akt (204). Moreover, addition of exogenous $PI(3,4)P_2$ to bone marrow derived mast cells and rat astrocytes increased Akt phosphorylation at the S473 site (206).

Consistent with these findings, the SHIP-1 inhibitor 3AC leads to reduced Akt phosphorylation at the T308 and S473 sites in hematopoietic cancer cell lines (207). These data hint towards a role for PI(3,4)$P_2$ and indirectly SHIP-1 in positively regulating signaling in certain scenarios (figure 42).

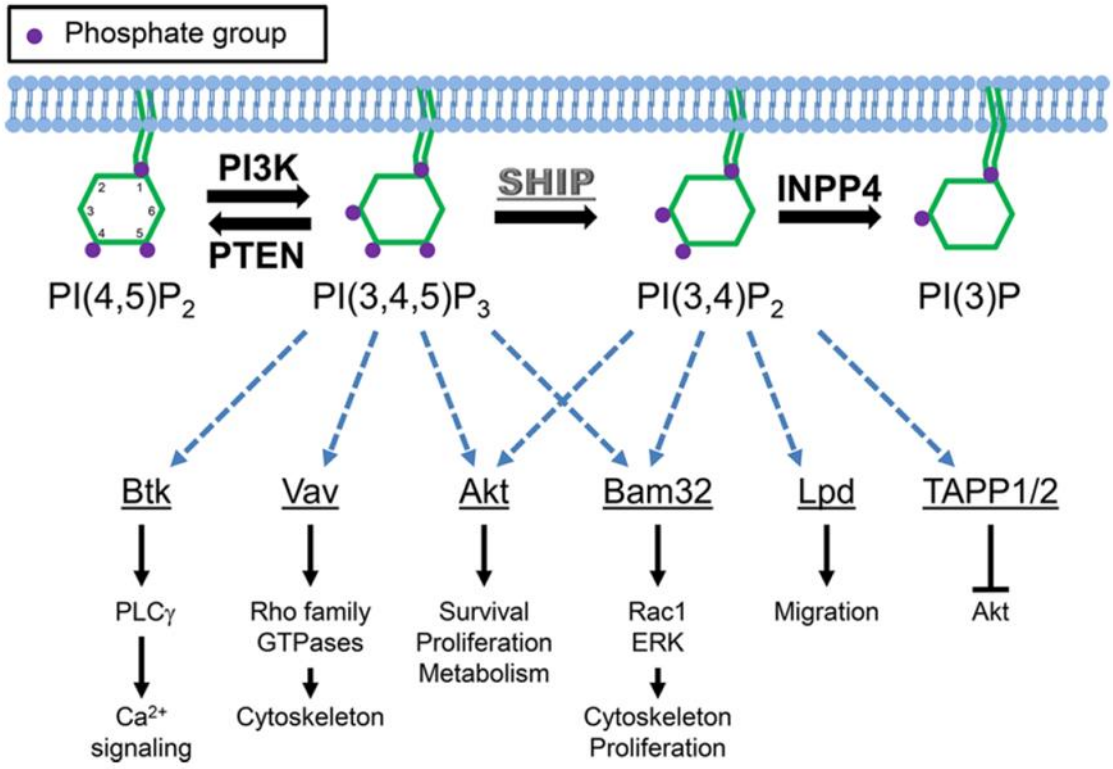


**Figure 42 Overview of SHIP-1 in regulating PI3K signaling**

**Adapted from Eur. J. Immunol. 2017. 47: 932–945**

### 4.1.4 Role of SHIP-1 in immunity

Consistent with the crucial role of SHIP-1 as a signaling regulator, deletion or mutation in SHIP-1 is known to disrupt immune functions. SHIP-1 deficient mice develop splenomegaly, autoimmunity and inflammation in the gut and lungs, and their survival rate at 14 weeks of age is

only 40% (208). Cell-specific deletion of SHIP-1 has been used to study its role within different immune compartments. Re-constitution of mast cell-deficient mice using SHIP-1 +/+ or SHIP-1 -/- mast cells, showed that SHIP-1 -/- mast cells are hyperresponsive and cause allergic asthma pathology (209). In the case of T cells, SHIP-1 deficiency leads to reduced differentiation into a Th17 phenotype and increased differentiation into Treg phenotype suggesting a role for SHIP-1 in maintaining balance between different T cell subsets and regulating immune homeostasis (210). Also, T cell specific SHIP-1 deletion reduces the Ab response to NP-CGG-Alum and Th2 immune responses to *Schistosoma masoni* infection (211). Moreover, macrophages from SHIP-1 -/- mice are skewed towards M2 phenotype because of constitutive high levels of arginase I (212). However, during helminth infection, myeloid-specific deletion of SHIP-1 leads to excessive production of IL-12 by macrophages, which generates a non-protective Th1 response instead of a protective Th2 response (213). Taken together, these finding suggest that SHIP-1 plays a crucial role in programming macrophages and mast cells and regulating T cell responses in infection and autoimmunity.

As discussed above, SHIP-1 plays a crucial role in regulating BCR signaling and by extension B cell functions. SHIP-1 deletion in B cells specific for Ars-1 or HEL leads to reversal of the anergic state of these B cells and restoration of BCR signaling (214, 215). Study of AID Cre/+ SHIP-$1^{fl/fl}$ mice revealed that SHIP-1 is necessary for the maintenance of IL-10 competent B cells and for the production of IL-10 and in the absence of SHIP-1, B cell dependent lupus-like autoimmunity develops (216). B cell-specific deletion of SHIP-1 using $CD19^{Cre/+}$ SHIP-$1^{fl/fl}$ mice resulted in reduced numbers of immature B cells and MZ B cells, but increased numbers of spontaneous GCBC (217). Moreover, SHIP-1 deficient B cells demonstrated increase isotype switching to IgG2a/2b because of increased expression of T-bet and STAT1 in these cells. SHIP-

1 deficient B cells have lower IgG1 and IgG2a serum titers in response to NP-CGG immunization (217). Moreover, total GCBC numbers were lower in the absence of SHIP-1 and SHM within the GCBC was also reduced compared to the controls (217). We have previously shown that SHIP-1 is hyperphosphorylated in GCBC and remains constitutively associated with the BCR in the resting state (60). The enhanced activity of SHIP-1 in GCBC may be a mechanism for dampening BCR-induced PI3K signaling. Here, we sought to further understand the role of SHIP-1 in control of GCBC signaling and function.

### 4.1.5 Study Goals

To ascertain the role of SHIP-1 in survival and selection of GCBC we used a tamoxifen inducible Cre system to delete SHIP-1 from B cells during an ongoing GC response to NP-CGG. SHIP-1 deletion led to bi-modal expression of SHIP-1 in GCBC expressing intermediate (SHIP-1 int) and low levels of SHIP-1 (SHIP-$1^{lo}$) compared to WT controls (SHIP-$1^{WT}$). SHIP-$1^{med}$ GCBC showed reduced phosphorylation of signaling proteins S6 and increased phosphorylation of Btk upon BCR crosslinking with anti-μ antibody. SHIP-$1^{lo}$ cells were un-responsive to BCR crosslinking and had the highest frequency of dead cells and caspase 3 positive cells among all three groups. This data suggests that SHIP-1 expression and activity is crucial to GCBC signaling and survival. The role of $PIP_2$ in regulating BCR signaling in GCBC remains to be elucidated.

## 4.2 Methods

**Mice, immunizations and treatments:** All mice were maintained under specific pathogen free conditions in accordance with guidelines issued by University of Pittsburgh Institutional Animal Care and Use Committee. 6-16 weeks old IgM B18i BCR transgenic Balb/c (referred to as MEG), huCD20 TamCre C57BL/6 (60), SHIP-$1^{fl/fl}$ C57BL/6 (218), and huCD20 TamCre SHIP-$1^{fl/fl}$ C57BL/6 mice were used as sources of NBCs and GCBCs as mentioned in the figure legends. MEG mice were immunized using 50μg of NP-CGG precipitated in alum and the C57BL/6 strains were immunized using 75ug of NP-CGG precipitated in alum. MEG mice were analyzed between day 12-16 post immunization and the C57BL/6 strains were analyzed between day 10-11. Mice were treated with 1 mg dose of tamoxifen in corn oil orally at day 6 and day 8 after immunization.

**In vitro Treatment:** The cells were re-suspended in B cell media (RPMI 1640 medium supplemented with 5% Fetalplex, penicillin/streptomycin, glutamine and 50 μM β-mercaptoethanol) and warmed to $37^{O}$C in 5% CO2 for at least 15m before the following treatments. For treatment with the SHIP-1 inhibitor, cells were treated with either ethanol or 20μM 3AC in ethanol for different time as mentioned in the figure legend.

**Flow Cytometry:** The stimulations and/or treatments were stopped by fixing the cells using 1.5% paraformaldehyde (PFA) at room temperature for at least 15 minutes. The cells were permeabilized using BD Perm Wash buffer or 0.1% Triton X-100 at room temperature for at least 20 minutes. Fc receptors were blocked using anti-CD16/32 (home-made 2.4G2 antibody clone). For B cells and GCBCs, the following conjugated reagents/ antibodies were used, PNA (Vector laboratories), anti-SHIP-1 (Mouse IgG1; Biolegend), anti-lambda (Goat polyclonal; Southern Biotechnology), anti-CD95 (clone: Jo-2; BD Pharmingen), anti-CD45R (clone RA3-6B2; BD Pharmingen), anti-CD19 (clone 1D3; BD Horizon), anti-CXCR4 (clone- L276F12; Biolegend),

and anti-CD86 (clone GL-1; Biolegend), anti-IgM (clone B7-6; home-made). For signaling assays, conjugated antibodies to p-S6 (S235/236; clone: D57.2.2E; Cell Signaling Technology), p-AKT (S473; clone: M89-61; BD Biosciences), p-AKT (T308; clone: 244F9; Cell Signaling Technology), p-Btk (Y223/Itk pY180; clone: N35-86; BD Biosciences), and p-Syk (Clone 17A/P-ZAP70; BD Biosciences) were used.

**ELISpots:** NP2-BSA (5µg/mL), and NP16-BSA (5µg/mL) were used as coating antigens to measure AFCs that were NP specific. Kappa (5µg/mL) was used as a coating antigen to measure total AFCs. 96 well 4HBX plates were coated using the above-mentioned antigens overnight at $4^{O}$C. On the day of experiment, plates were blocked using PBS + 1% BSA. Following blocking, splenocytes from different strains of mice as mentioned in the figure legend, were added to the plates and incubated overnight at $37^{O}$C. AFC were detected by using alkaline phosphatase-conjugated secondary antibodies (to IgG or IgM, Southern Biotech) and 5-bromo4-chloro-3-indolyl-phosphate in agarose.

**Imaging cytometry:** Cells were labeled as described earlier for flow cytometry assay. For BCR clustering and endocytosis, data were collected using Amnis ImageStream®X Mark II Imaging Flow Cytometer. Data were analyzed with IDEAS software using the "Delta Centroid" feature for BCR clustering and "Internalization" feature for endocytosis (EMD Millipore).

**Statistics:** Statistics for data were calculated by Graphpad Prism using Student's t-test or Two-way Anova as described in the figure legends. Symbols for levels of significance are * $p< 0.05$, * * $p<0.01$, * * * $p<0.001$, * * * * $p< 0.0001$.

## 4.3 Results

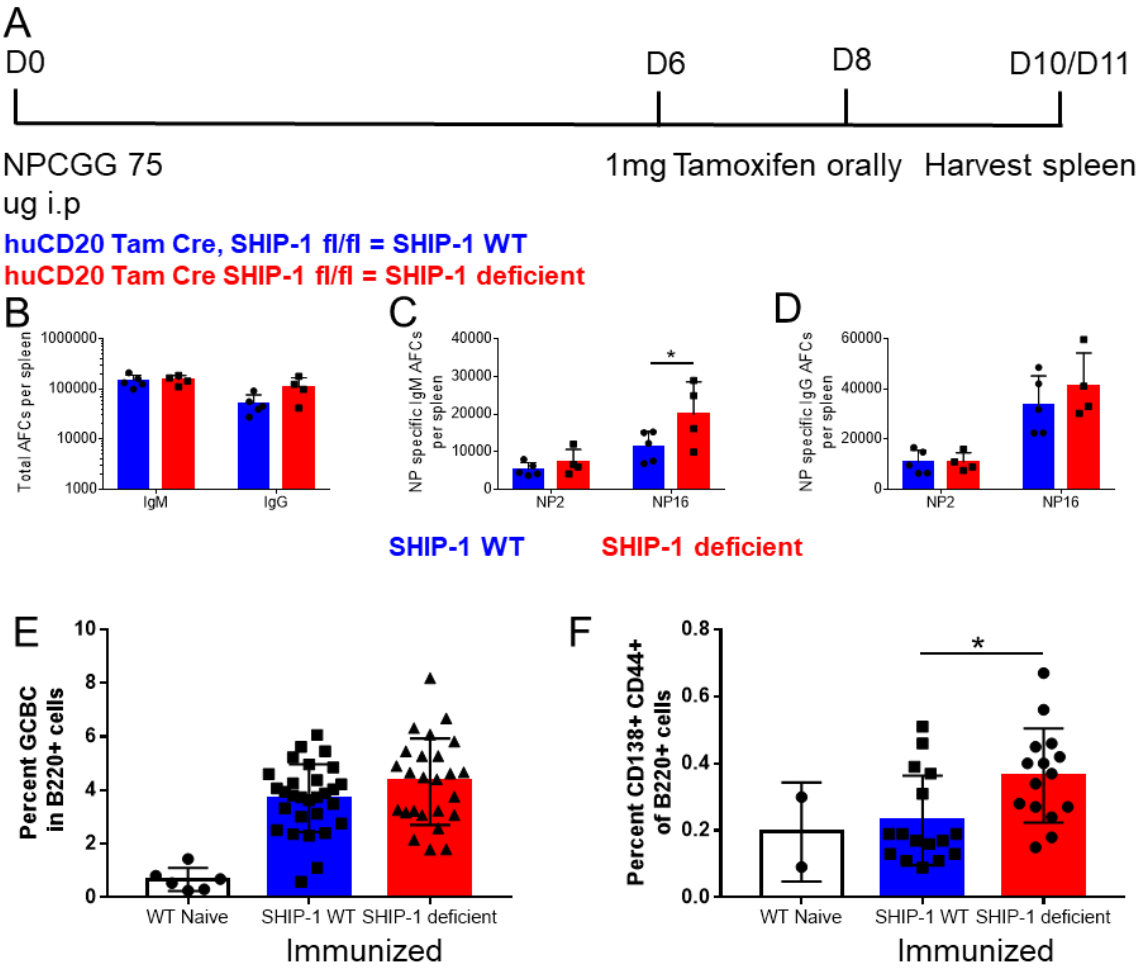


**Figure 43 SHIP-1 deletion leads to enhanced PB response**

**huCD20 Tam Cre and SHIP-1$^{fl/fl}$ mice were combined into a group as SHIP-1WT. huCD20 TamCre mice were referred to as SHIP-1 deficient group. (A) Schematic diagram of SHIP-1 deletion in B cell specific Tamoxifen inducible Cre system. (B-D) ELISpot assay for total (B), NP2 and NP16 (C-D) IgM (C) and IgG (D) AFC at D11 post NP-CGG immunization. (E-F) Percent GCBC (B220$^+$ PNA$^+$ CD95$^+$) (E) and Percent PB (B220$^+$, CD138$^+$ CD44$^+$) (F) in SHIP-1 WT and SHIP-1 deficient mice at D11 post NP-CGG immunization. Data are representative of at least two independent experiments with and are represented as mean with SD of groups of at least two mice.**

To study the role of SHIP-1 in GCBCs, we used a B cell specific tamoxifen inducible Cre system to delete SHIP-1 during an ongoing GC reaction. Mice were immunized with 75μg NPCGG and treated with 1mg/dose of tamoxifen at day 6 and day 8 post immunization and splenocytes were harvested at day 10-11 post immunization (figure 43A). huCD20 TamCre mice and SHIP-$1^{fl/fl}$ mice were combined into a group referred to as SHIP-1 WT and huCD20 TamCre SHIP-$1^{fl/fl}$ mice were referred to as SHIP-1 deficient. We performed ELISpot assays to assess the AFC response in SHIP-1 WT and SHIP-1 deficient groups. We observed that NP16 specific IgM AFCs were significantly increased in the SHIP-1 deficient group, and NP16-specific IgG AFCs had a similar trend (figure 43 B-D). However, there was no significant difference in NP2 specific IgM or IgG AFCs, or the numbers of IgM or IgG producing total AFCs (figure 43 B-D). The percentage of GCBC was comparable between SHIP-1 WT and SHIP-1 deficient groups (figure 43 E). In line with the ELISpot data, we observed an increase in the percentage of PBs in the SHIP-1 deficient group compared to WT group. These data agree with previously published results on AFC response in B cell specific SHIP-1 deficiency (217).

We observed that the SHIP-1 deficient mice (huCD20 TamCre SHIP-$1^{fl/fl}$ group) had bi-modal expression of SHIP-1 (figure 44 A-B). The GCBC in these mice had one peak that had slightly lower expression of SHIP-1 (SHIP-$1^{med}$) and another peak that expressed lower SHIP-1 (SHIP-$1^{lo}$) when compared to the WT expression of SHIP-1 (SHIP-$1^{WT}$) (figure 44 A-B). We suspect that the SHIP-$1^{med}$ group has deleted only allele of SHIP-1 and SHIP-$1^{lo}$ group has deleted both alleles of SHIP-1. Further comparisons in these studies were done on these 3 groups (SHIP-$1^{WT}$, SHIP-$1^{med}$ and SHIP-$1^{lo}$) based on their differential SHIP-1 expression. We observed that SHIP-1 deletion led to reduced numbers of $CD86^{high}$, CXCR4 low LZ GCBCs in comparison to CD86 low, CXCR4 high DZ GCBCs (figure 44 C-D). This increase in the DZ-LZ ratio was found

to be inversely co-related to the SHIP-1 expression (figure 44 C-D). From these data we conclude that SHIP-1 deletion disrupted cycling of GCBC between LZ and DZ.

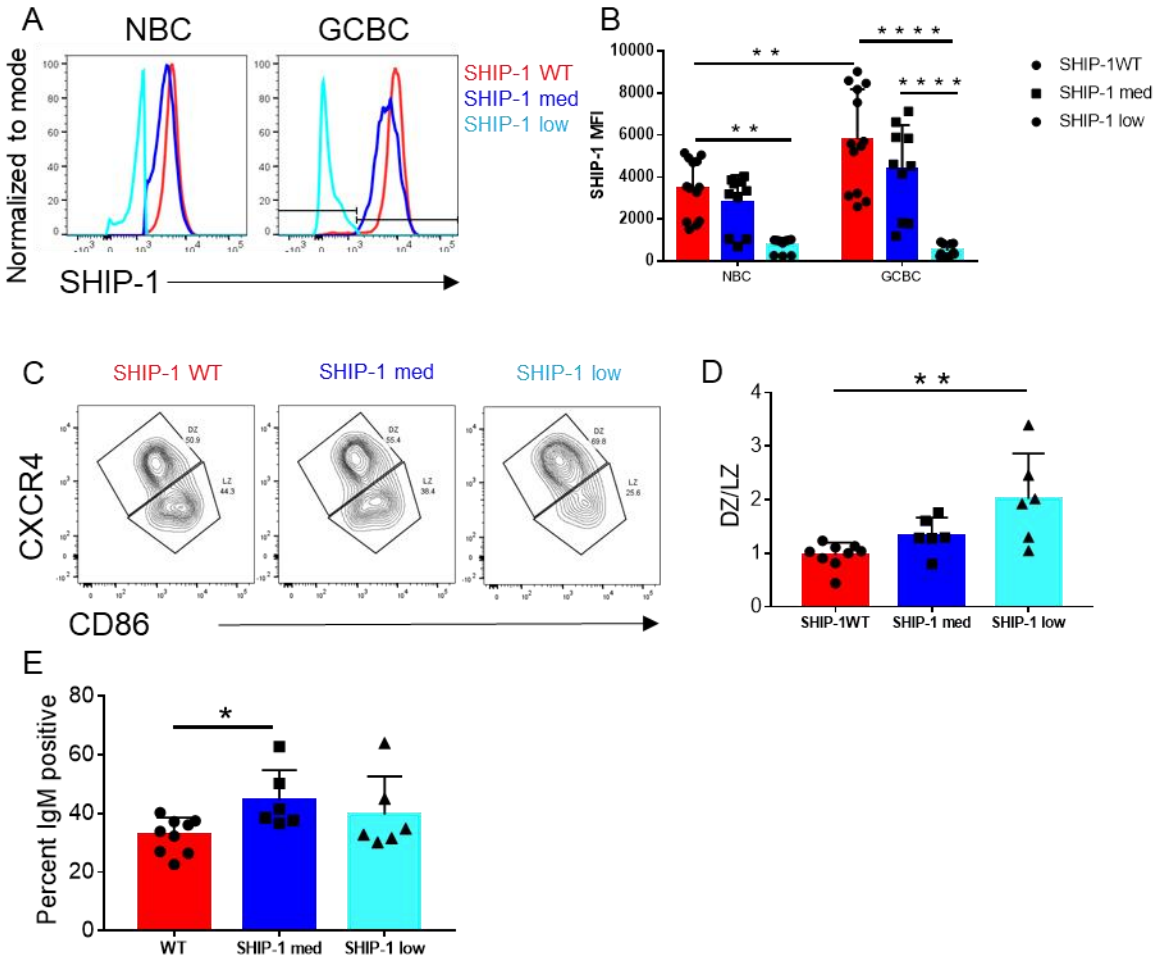


**Figure 44 SHIP-1 deletion led to bi-modality in SHIP-1 expression in B cells**

**huCD20 Tam Cre and SHIP-1$^{fl/fl}$ mice expressed WT levels of SHIP-1 and were referred to as SHIP-1$^{WT}$. HuCD20 TamCre SHIP-1$^{fl/fl}$ expressed bi-modal levels of SHIP-1 and were divided into SHIP-1$^{med}$ and SHIP-1$^{lo}$ based on the expression of SHIP-1.(A-B) Histogram (A) and (B) quantification of SHIP-1 MFI in NBC and GCBC. (C-D) Contour plots of CD86 and CXCR4 expression (C) and quantification (D) of DZ to LZ ratio in SHIP-1 WT, SHIP-1$^{med}$ and SHIP-1$^{lo}$ NBC and GCBC. (E) IgM expression in SHIP-1 WT, SHIP-1$^{med}$ and SHIP-1$^{lo}$ GCBC at D11 after NP-CGG immunization. Data are representative of at least two independent experiments with and are represented as mean with SD of groups of at least two mice.**

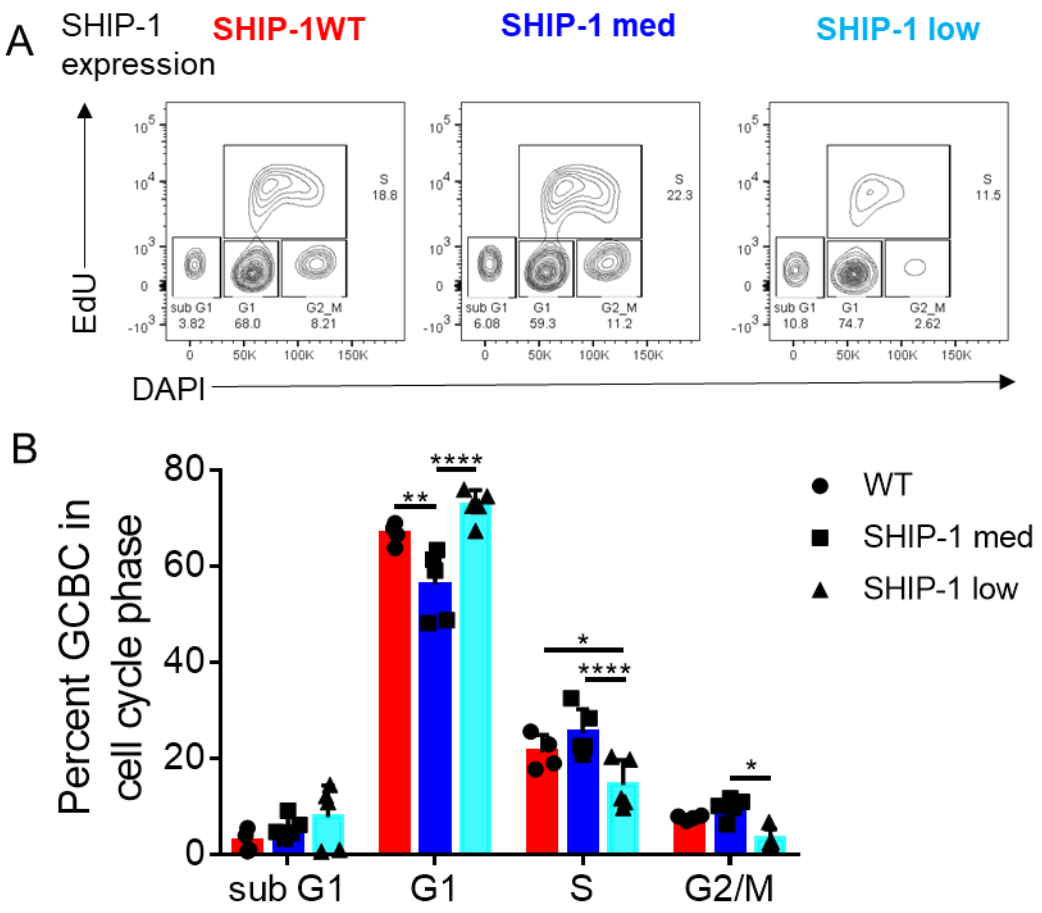


**Figure 45 SHIP-1 deletion led to cell cycle disruption in GCBC**

**(A) Contour plots of EdU and DAPI labeling in SHIP-1 WT, SHIP-1$^{med}$ and SHIP-1$^{lo}$ GCBC populations at D10/11 post NP-CGG immunization. (B) Quantification of SHIP-1 WT, SHIP-1 med and SHIP-1 low GCBC populations in subG1, G1, S and G2M phases of cell cycle. Data are representative of at least two independent experiments with and are represented as mean with SD of groups of at least two mice.**

GCBC are highly proliferative B cells that cycle between LZ and DZ to obtain appropriate signals related to cell proliferation and death. Since SHIP-1$^{lo}$ GCBC accumulated in the DZ we wanted to determine if SHIP-1 deletion disrupted GCBC proliferation. We treated the mice with 1mg of EdU 30 minutes prior to sacrifice, to label cells that were in the S phase of the cell cycle and performed cell cycle analysis of SHIP-1$^{WT}$, SHIP-1$^{med}$ and SHIP-1$^{lo}$ GCBC. We observed a

significantly higher percentage of SHIP-1$^{lo}$ cells in the G1 phase of the cell cycle in comparisons SHIP-1$^{med}$ group and SHIP-1$^{lo}$ cells in the sub-G1 phase showed a similar trend (figure 45 A-B). The sub-G1 phase reflects dead or dying cells and this data may suggest that SHIP-1$^{lo}$ GCBC have increased cell death. Moreover, a significantly lower percentage of the SHIP-1$^{lo}$ cells were found in the S phase and SHIP-1$^{lo}$ cells in the G2-M phase showed a similar trend (figure 45 A-B). In contrast to SHIP-1$^{lo}$ cells, SHIP-1$^{med}$ cells had a significantly lower percentage of cells in the G1 phase of the cell cycle and a higher percentage of cells in S and G2-M (figure 45 A-B). Overall these data show that a moderate decrease in SHIP-1 expression may increase cell cycle efficiency. However, extremely low levels of SHIP-1 are incompatible with efficient cell cycle progression and GCBC lacking SHIP-1 accumulate in the G1 and sub G1 phases. Taken together, these data indicate a role for SHIP-1 in regulating GCBC proliferation.

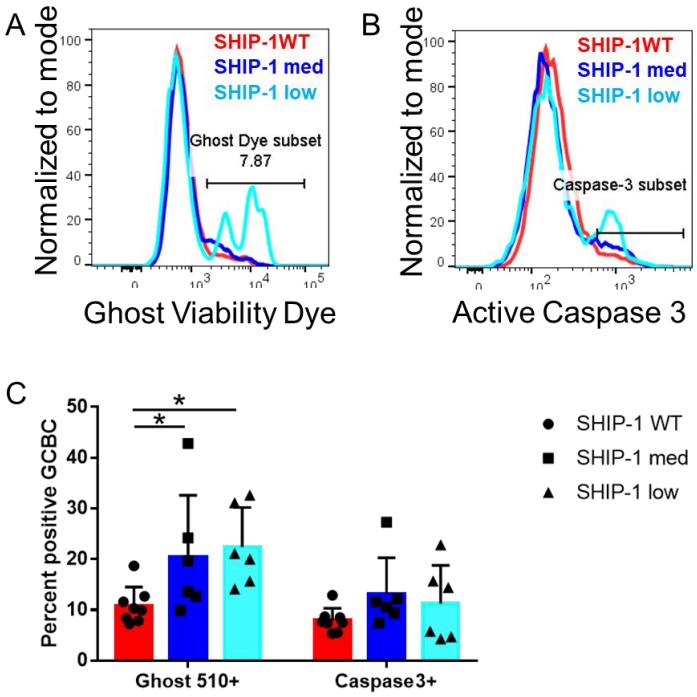


**Figure 46 SHIP-1 deletion led to increased cell death in GCBC**

**(A-B) Histograms of ghost viability dye (A) and active Caspase 3 staining (B) in SHIP-1$^{WT}$, SHIP-1$^{med}$ and SHIP-1$^{lo}$ GCBC populations at D10/11 post NP-CGG immunization. (C) Quantification of ghost viability dye and active Caspase 3 staining in SHIP-1$^{WT}$, SHIP-1$^{med}$ and SHIP-1$^{lo}$ GCBC populations at D10/11 post NP-CGG immunization. Data are representative of at least two independent experiments with and are represented as mean with SD of groups of at least two mice.**

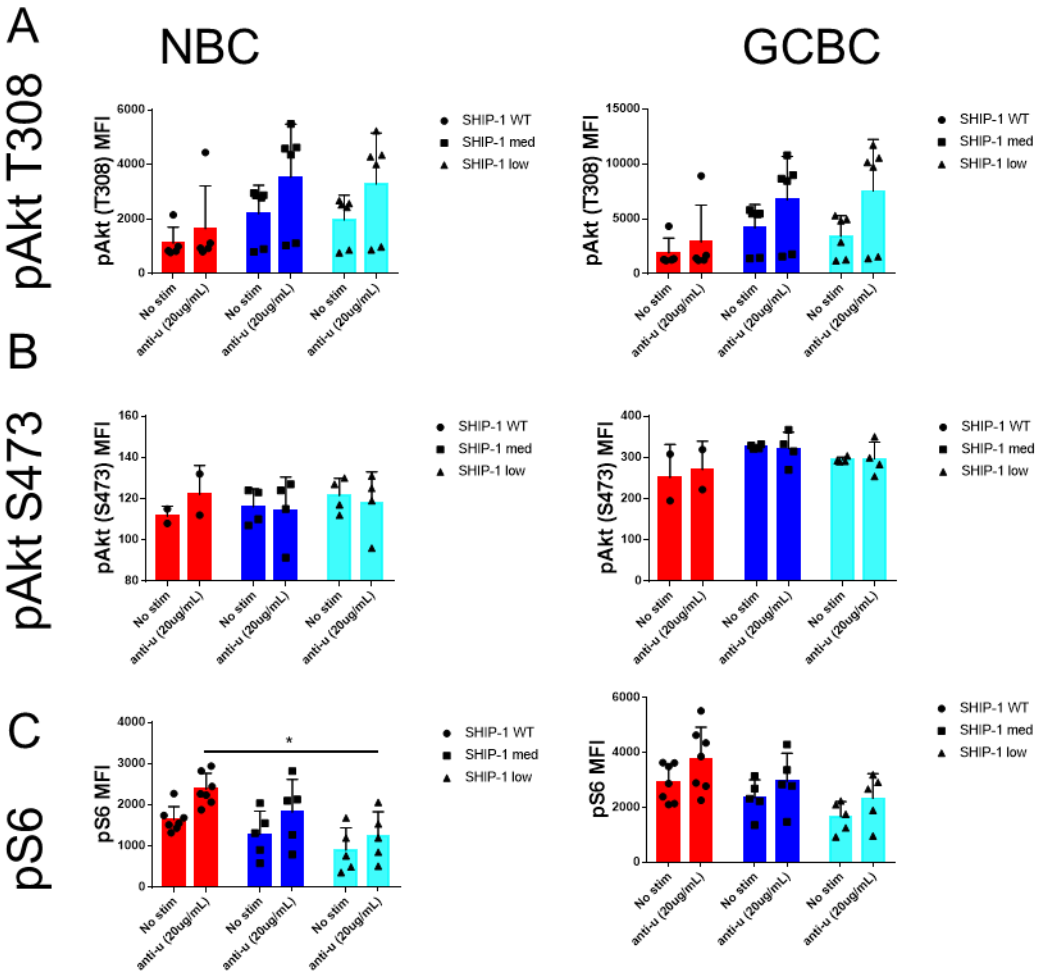


**Figure 47 SHIP-1 deletion led to moderate reduction in S6 phosphorylation in B cells**

**(A-C) Phosphorylation of Akt (T308) (A), Akt (S473) (B) and S6 (C) upon 20µg/mL anti-µ stimulation at 0 and 3m for for (A-B) and 0 and 20m for (C) in NBC and GCBC in SHIP-1$^{WT}$, SHIP-1$^{med}$ and SHIP-1$^{lo}$ populations. Data are representative of at least two independent experiments.**

Since we observed an increased percentage of SHIP-1$^{lo}$ GCBCs in the sub-G1 phase of the cell cycle, we suspected increased cell death with loss of SHIP-1 expression. We observed that in comparison to the SHIP-1$^{WT}$ group and SHIP-1$^{med}$ groups, SHIP-1$^{lo}$ group had a significant increase in the percentage of dead GCBCs (figure 46 A, C). Also, there was a trend toward increased active caspase 3 with loss of SHIP-1 expression (figure 46 B-C). Overall, these data

support our findings from the cell cycle analysis and demonstrate a correlation between the lack of SHIP-1 and increased cell death.

Since SHIP-1 is known to be a negative regulator of BCR signaling, it is possible that the absence of SHIP-1 leads to increased BCR signaling, which eventually leads to cell death in GCBC. To analyze the signaling aspects of SHIP-1, we performed phospho-flow analysis of Akt (T308; S473) and S6 phosphorylation in SHIP-$1^{WT}$, SHIP-$1^{med}$ and SHIP-$1^{lo}$ B cells. BCR-induced Akt phosphorylation at either T308 or S473 was not significantly altered with differential expression of SHIP-1 (figure 47A-B). Counter to our expectations, we observed that the reduction of SHIP-1 expression led to reduced pS6 in NBCs and a similarly consistent trend in GCBCs (figure 47C). This finding was surprising because, the absence of SHIP-1 expression generally leads to enhanced phosphorylation of proteins in the PI3K axis. To further study this effect, we treated the cells with an inhibitor of SHIP-1. We observed that BCR induced phosphorylation of Syk, Btk, Akt (T308; S473) was unaffected by SHIP-1 inhibition; however, S6 phosphorylation was moderately reduced in both NBC and GCBC (figure 48A-E).

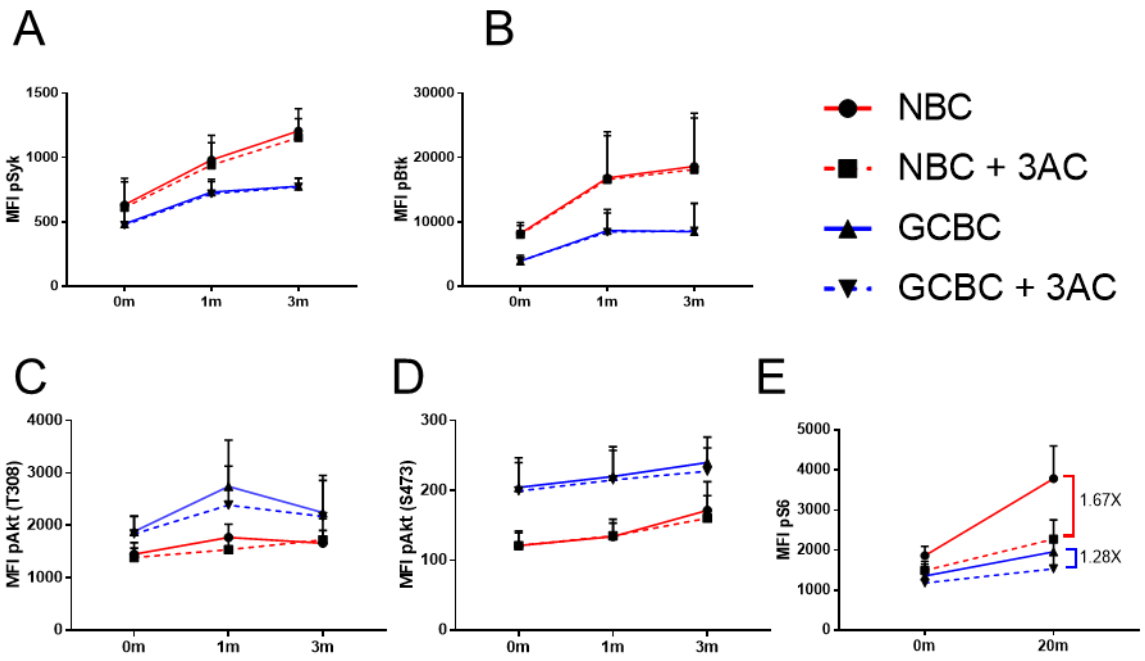


**Figure 48 SHIP-1 inhibition led to moderate reduction in S6 phosphorylation**

**(A-E) Phosphorylation of Syk (A), Btk (B), Akt (T308) (C), Akt (S473) (D) and S6 upon 20µg/mL anti-µ stimulation at 0-3 minutes for (A-D) and 0-20 minutes for (E) in NBC and GCBC in SHIP-1 WT, SHIP-1$^{med}$ and SHIP-1$^{lo}$ populations. Data are representative of at least two independent experiments.**

Both $PIP_3$ and $PI(3,4)P_2$ can recruit Akt kinase to the plasma membrane. It is possible that SHIP-1 deletion leads to reduced production of $PI(3,4)P_2$ which may lead to reduced recruitment of Akt to the plasma membrane and lower S6 phosphorylation. To assess the levels of $PI(3,4)P_2$, we stained the WT and SHIP-1 deficient B cells using anti-$PI(3,4)P_2$ and analyzed them by imaging cytometry. We observed that in the resting state, GCBC have higher staining MFI of $PI(3,4)P_2$ compared to NBC (figure 49 A-C). Upon anti-µ treatment, $PI(3,4)P_2$ staining increases in both NBC and GCBC (figure 49 A-C). However, in the SHIP-1 deficient B cells, $PI(3,4)P_2$ levels were unaffected in both the basal state and after BCR stimulation (figure 49 A-C). These data are inconsistent with results obtained from a similar experiment we performed, in which lipids were

extracted from NBC and GCBC that were stimulated using the anti-μ antibody and PI(3,4)P2 levels were measured by ELISA. In these experiments, upon stimulation, NBC generate a substantial amount of $PI(3,4)P_2$, however, GCBC generated minimal $PI(3,4)P_2$. By Image Stream analysis, both NBC and GCBC generated $PI(3,4)P_2$ upon BCR stimulation (figure 49 A-C). In this case, since we used antibody to stain $PI(3,4)P_2$ in fixed cells, it is possible that if $PI(3,4)P_2$ is bound by another effector protein, it may not be available to bind to the antibody. This would lead to a gross underestimation of the levels of $PI(3,4)P_2$ and therefore the Image Stream data may not accurately reflect total $PI(3,4)P_2$. However, this approach does provide useful information regarding the localization of $PI(3,4)P_2$, with the caveat that some $PI(3,4)P_2$ might not be detectable. In this regard, we observed that $PI(3,4)P_2$ showed a punctate expression pattern in the resting state; upon BCR stimulation, $PI(3,4)P_2$ localization was more diffuse, and was punctate in certain regions (figure 49 A-B). Future experiments in this study will be focused on measuring the levels of $PI(3,4)P_2$ by ELISA in SHIP-$1^{WT}$, SHIP-$1^{med}$ and SHIP-$1^{lo}$ GCBC and NBC.

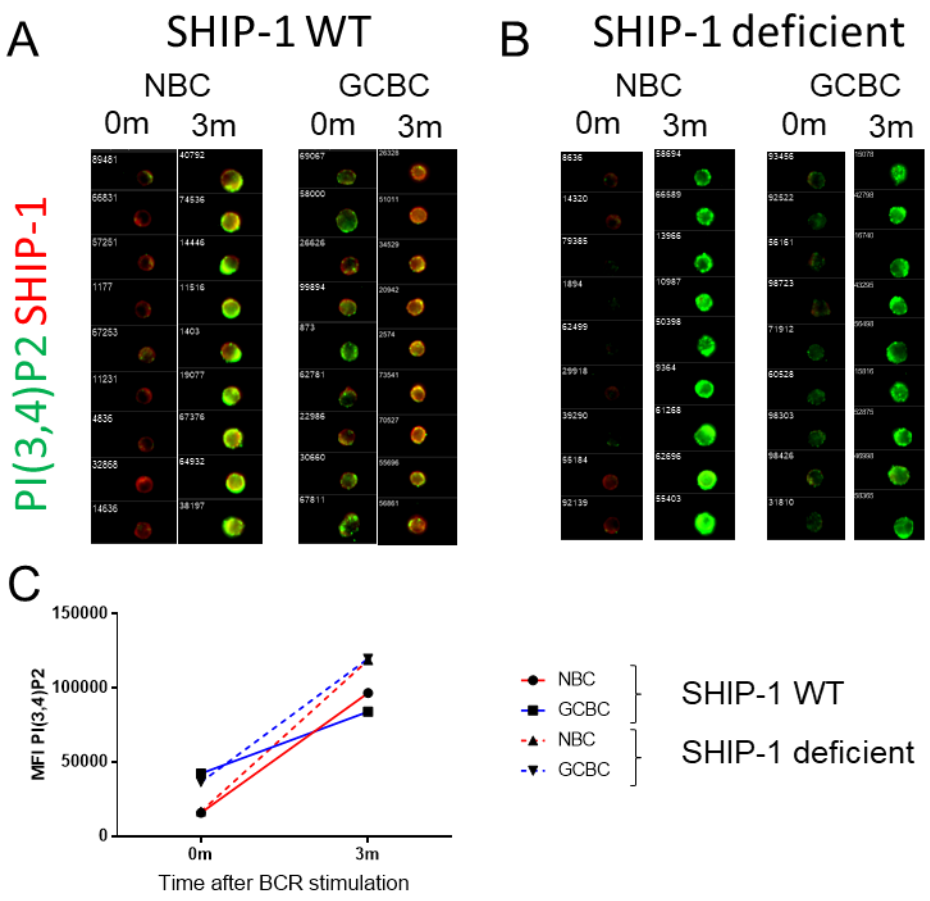


**Figure 49 BCR induced PI(3,4)$P_2$ production was unaffected by SHIP-1 deletion**

**(A-B) Image stream images of PI(3,4)$P_2$ and SHIP-1 in NBC and GCBC from SHIP-1 WT (A) and SHIP-1 deficient mice (B) at 0m and 3m post 20µg/mL anti-µ stimulation. (C) Quantification of PI(3,4)$P_2$ intensity in NBC and GCBC from SHIP-1 WT (A) and SHIP-1 deficient mice (B) at 0m and 3m after stimulation with 20µg/mL anti-µ. Data are from one Imaging flow cytometry experiment.**

## 4.4 Discussion

BCR signaling is dampened in GCBC, with limited generation of the key effector lipid inositol $PIP_3$ (123). SHIP-1 is a key regulator of $PIP_3$ levels and is highly expressed in GCBC in comparison to NBC (60). It is possible that higher SHIP-1 activity may be dampening BCR signaling in GCBC. However, in our study, SHIP-1 deletion or SHIP-1 inhibition did not enhance BCR signaling in the PI3K pathway or the Syk-Btk axis. In fact, there was a moderate reduction in S6 phosphorylation upon BCR stimulation in the absence of SHIP-1. This may hint towards the role of $PI(3,4)P_2$, a product of SHIP-1's enzymatic activity, in the recruitment of Akt. However, Akt phosphorylation at T308 and S473 sites were unaffected by SHIP-1 deletion or inhibition. So, $PI(3,4)P_2$ mediated Akt recruitment seems to be an unlikely explanation in this case. Overall, these data show that in NBC and GCBC, SHIP-1 may not a major regulator of the levels of $PIP_3$ and therefore may not contribute directly to the dampened BCR signaling observed in GCBC. Previously, we have shown that PTEN is a potent regulator of $PIP_3$ levels and PI3K signaling in NBC and GCBC (123). PTEN is highly expressed in GCBC and upon BCR stimulation, $PIP_3$ is not generated in GCBC but $PI(4,5)P_2$ is significantly generated compared to NBC (123). These results thus established a dominant role for PTEN in GCBC as the key regulator for PI3K signaling.

Contrary to our expectations, SHIP-1 deficiency led to an arrest of GCBC in the G1 phase of the cell cycle, followed by cell death. This was consistent with the fact the GCBCs that expressed the lowest SHIP-1 levels made up the highest percentage cells in sub-G1 phase of the cell cycle, as well as having the most active caspase 3 and dead cells. However, this did not affect the overall GC reaction and the percentage of GCBC was also comparable in WT and SHIP-1 deficient mice. These data suggest that in the competitive GC environment SHIP-1 sufficient cells are probably preferentially selected and continue to proliferate and maintain the GC. In B cell-

specific SHIP-1 deletion using $CD19^{+/Cre}$ $SHIP\text{-}1^{fl/fl}$ mice, the number of NP-specific GCBC is reduced upon NP-CGG immunization (217). These data further support our theory that SHIP-1 deletion can be detrimental to the GC, however, since with the tamoxifen-inducible system SHIP-1 is not completely deleted, which may allow for GC maintenance.

It has been shown before that B cells deficient in SHIP-1 generate more spontaneous PBs (217). These data are consistent with our study, where upon NP-CGG immunization we observed higher numbers of NP16 specific AFC and an increased percentage of PBs in the SHIP-1 deficient mice. These data suggest that apart from cell cycle maintenance, SHIP-1 may also play a role in regulating GCBC differentiation into PB phenotype. The mechanisms responsible for these functions of SHIP-1 in GCBC remain to be elucidated. We analyzed SHIP-1's enzymatic functions by measuring its product $PI(3,4)P_2$ and by assessing its effect on the PI3K signaling. However, SHIP-1 is also a scaffolding protein that can bind to several different signaling effectors such as Dok-1, Dok-3, Shc1 and DAP12 (198-201). These pathways lead to Ras mediated Erk and MAPK signaling, which is an axis that we did not investigate in our studies (198, 199). Erk signaling is known to control cell cycle progression and proliferation (219). Future studies will focus on dissecting out the role of SHIP-1 in the MAPK signaling pathways.

## 5.0 Inhibitory Receptor PIR-B

In previous chapters we went over the BCR signaling pathway and the different processes that regulate it. Here we focus on an inhibitory receptor PIR-B that is known to act as a negative regulator of immune cell signaling by recruitment of the phosphatases SHP-1 and SHP-2 (220).

## 5.1 Introduction

PIR-B belongs to the paired immunoglobulin like receptor family that is closely related to human leukocyte immunoglobulin-like receptor (220). Activating receptor PIR-A has positively charged residues in its transmembrane domain that facilitate its interaction with FcRϒ. Inhibitory receptor PIR-B is a glycoprotein that has six extracellular immunoglobulin like domains, a hydrophobic transmembrane domain and four ITIM-like sequences in its cytoplasmic tail that facilitate the recruitment of SHP-1 (220). There are many known ligands for PIR, including MHC I and the neural protein Nogo (220). Constitutive phosphorylation of PIR-B is reduced in β2 microglobulin-deficient mice, suggesting a role for MHC I in PIR-B activation (221). Surface plasmon resonance studies have also shown the ability of PIR-B to bind to H2 monomers (222). PIR-B ectodomains can bind to MHC I molecules in cis or trans (220).

PIR-A and PIR-B are expressed on various immune cells, such as B cells, T cells, macrophages, mast cells, dendritic cells (DCs) and granulocytes (220). PIR-B is constitutively phosphorylated in macrophages and is involved in integrin signaling in macrophages and neutrophils (223, 224). In macrophages, $Pirb^{-/-}$ cells show hyper-adhesiveness and spreading upon

cross-linking β2 integrins compared to WT controls (223, 224). In neutrophils, Lyn phosphorylates PIR-B, which in turn recruits SHP-1 to dampen integrin signaling. Lyn-deficient neutrophils are hyperactive, presumably due to the absence of this proposed mechanism that is mediated by PIR-B (223, 224). Consistent with these data, PIR-B$^{-/-}$ neutrophils are also hyperactive and hyper-adhesive (223, 224). Other Src family kinases such as Hck and Fgr maintain PIR-B phosphorylation to modulate responsiveness to chemokine signaling (223-225). In line with these data, Pirb$^{-/-}$ neutrophils and DCs show enhanced chemokine signaling in comparison to WT controls (225). In mast cells, PIR-B co-ligation with IgE receptor inhibits IgE-mediated mast cell activation and the release of serotonin (226). However, the process seems to be independent of SHP-1 as PIR-B mediated inhibition is intact in SHP-1 deficient mast cells (226). This hints towards a role for PIR-B in negatively regulating signaling pathways independently of SHP-1 by associating with other phosphatases.

PIR-B plays an important inhibitory role in the regulation of BCR signaling. In splenic B cells, PIR-B is constitutively phosphorylated because of presumed interactions with H2 molecules on the cell surface (222). Pirb$^{-/-}$ mice have normal B cell development except for the CD5$^{+}$ IgM$^{+}$ peritoneal B1 cell compartment, which accumulates in enhanced numbers with age (227). Pirb$^{-/-}$ B cells are hype-responsive and hyper-proliferative in response to BCR stimulation (227). Immunization with TNP-KLH leads to enhanced serum IgG1 and IgE antibodies in Pirb$^{-/-}$ mice (227). This is mainly attributed to the immature DCs that produce significant IL-4 following immunization (227). Pirb$^{-/-}$ mice do not develop autoantibodies and autoimmunity as observed in CD22$^{-/-}$ mice (228). However, Pirb$^{-/-}$ mice with the *Fas*$^{lpr}$ mutation make significant anti-rheumatoid factor IgM and IgG Abs and anti-DNA Abs in the serum and develop autoimmune glomerulonephritis (229). The peritoneal B1 cells in these mice are hyper-responsive to CpG DNA

stimulation as measured by Btk and p65 phosphorylation (229). Taken together, these data suggest an important role for PIR-B in humoral immune responses.

Given the enhanced activity of SHP-1 in GCBC and its constitutive association with the BCR, it is likely that inhibitory receptors such as PIR-B could be mediating this process (60). Here we sought to determine the role of PIR-B in the initiation and maintenance of GC reaction. We generated $Pirb^{-/-}$ mice on the C57BL/6 background and used NP-CGG and sheep red blood cell (SRBC) immunization to induce a GC response. We measured the GC and AFC response to immunizations and found that PIR-B deficiency leads to a moderate reduction in the long-lived IgG AFC response in the bone marrow (BM) compartment.

## 5.2 Methods

**Generation of PIR-B deficient mice:** It was not possible to find unique Cas9 targeting site and genotyping primers in the genomic region containing the sequence of exon 1 through 8 because of segmental duplication. Instead, a pair of sgRNA was identified; Pirb_sgRNA8 5'-3' ACTCCAGGCTGCCGAATCTGGGG and Pirb_sgRNA9 ACTGAGTGGACATTACTCGAGGG. These pairs mediated deletion of genomic DNA from within intron 8 to within exon 15 (deleting exon 15 splice acceptor sites), thus preventing exon 8 to splice and resulting in translation of a truncated proteins up to exon 8 and into intron 8 where it encountered a stop codon. Note that this truncated protein is likely not functional, since it corresponds to the extracellular domain, the transmembrane domain is located in the deleted exon 10, and the whole cytoplasmic domain is deleted.

The methods for the targeting strategy and the generation of CRISPR-Cas9 edited mice by recombination-mediated mutagenesis have been described (230). Briefly, PCR-generated sgRNA template was using for sgRNA synthesis using MEGAshortscript T7 Kit (ThermoFisher Scientific). The Cas9 mRNA was produced using a linearized plasmid as template for the in vitro transcription mMESSAGE mMACHINE T7 Ultra Kit (ThermoFisher Scientific) as previously (230). Both sgRNA and Cas9 mRNA were purified using MEGAclear Kit (ThermoFisher Scientific) following manufacturer's instructions.

C57BL/6J pronuclear-stage zygotes, obtained by natural mating of superovulated females, were microinjected with sgRNA (50 ng/µl, each) and Cas9 mRNA (100 ng/µl). Injected zygotes were cultured overnight and 2-cell embryos were transferred to pseudopregnant CD1 to obtained potential founder mice. The mice were routinely genotype with a three primers genotyping strategy using the following primers. Pirb-F52 GCATGAATCACTTCCATACTGTAGC, Pirb-F32 CCCAGGGAGAGACTTATGCC and Pirb-R32 GGGGGTCATTGCTCCATGT.

**Mice and immunizations:** All mice were maintained under specific pathogen free conditions in accordance with guidelines issued by University of Pittsburgh Institutional Animal Care and Use Committee. 6-24 weeks old IgM WT C57BL/6, $Pir^{+/-}$ (PIR-B Het) and $Pirb^{-/-}$ (PIR-B KO) were used as mentioned in the figure legends. The mice were immunized using 50µg of NP-CGG precipitated in Alum or $10^8$ sheep red blood cells (SRBC). Spleen and BM were harvested from mice and single cell suspensions were made and counted for flow cytometry and ELISpot experiments.

**Flow Cytometry:** The stimulations were stopped by fixing the cells using 1.5% paraformaldehyde (PFA) at room temperature for at least 15 minutes. The cells were permeabilized using BD Perm Wash buffer or 0.1% Triton X-100 at room temperature for at least 20 minutes. Fc

receptors were blocked using anti-CD16/32 (home-made 2.4G2 antibody clone). For B cells, GCBCs and PBs, the following conjugated reagents/ antibodies were used, PNA (Vector laboratories), anti-lambda (Goat polyclonal; Southern Biotechnology), anti-CD95 (clone: Jo-2; BD Pharmigen), anti-CD45R (clone RA3-6B2; BD Pharmigen), anti-CD19 (clone 1D3; BD Horizon), anti-CXCR4 (clone- L276F12; Biolegend), anti-CD86 (clone GL-1; Biolegend), anti-IgM (clone B7-6; home-made), anti-CD138 (clone 281-2; Biolegend), anti-CD44 (clone IM7; Biolegend) and anti-PIR (clone 6C1; Thermofisher). For signaling assays, conjugated antibodies to p-Btk (Y223/Itk pY180; clone: N35-86; BD Biosciences), and p-Syk (Clone 17A/P-ZAP70; BD Biosciences) were used.

**ELISpots:** NP16-BSA (5μg/mL) and CGG (5μg/mL) were used as coating Ags to measure AFCs that were NP and CGG specific. Kappa (5μg/mL) was used as a coating antigen to measure total AFCs. 96 well 4HBX plates were coated using the above-mentioned antigens overnight at $4^{O}$C. On the day of experiment, plates were blocked using PBS + 1% BSA. Following blocking, splenocytes from different strains of mice as mentioned in the figure legend, were added to the plates and incubated overnight at $37^{O}$C. AFC were detected by using alkaline phosphatase-conjugated secondary antibodies (to IgG or IgM, Southern Biotech) and 5-bromo4-chloro-3-indolyl-phosphate in agarose.

**Statistics:** Statistics for data were calculated by Graphpad Prism using Two-way Anova as described in the figure legends. Symbols for levels of significance are * $p< 0.05$, * * $p<0.01$, * * * $p<0.001$, * * * * $p< 0.0001$.

## 5.3 Results

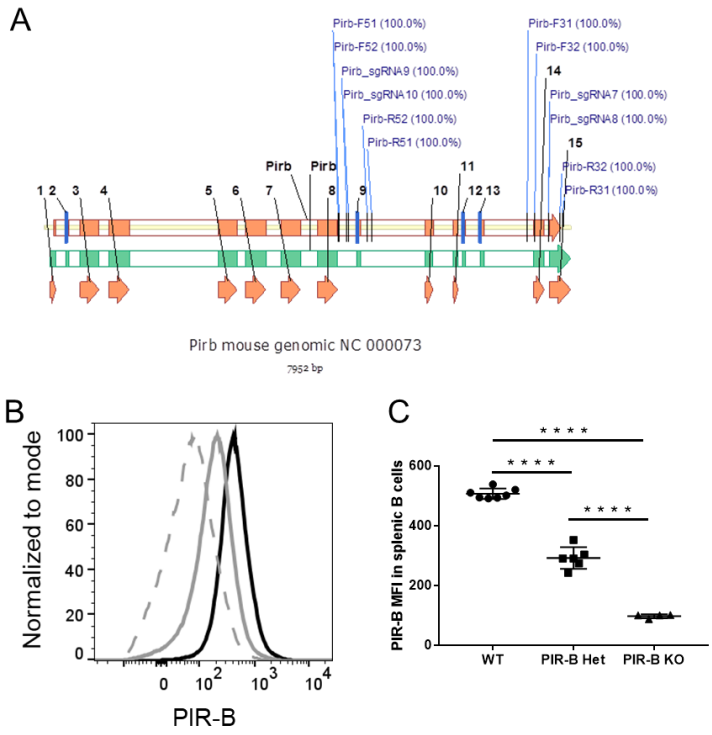


**Figure 50 Generation of PIR-B KO mice**

**(A) Schematic diagram showing the sgRNA target sites for generating PIR-B KO mice. (B-C) Histogram (B) and (C) quantification of PIR-B expression in WT C57BL/6 (black line), PIR-B Het (grey line), and PIR-B KO (grey dashed line). Data in B-C are representative of at least two independent experiments with and are represented as mean with SD of groups of at least two mice.**

To study the effect of PIR-B deficiency in GC function we generated PIR-B deficient mice using the CRISPR Cas9 targeting strategy as described in the Methods section. Briefly, a pair of sgRNA were used (Pirb_sgRNA8 and Pirb_sgRNA9) to delete genomic DNA from within intron 8 to within exon 15 (deleting exon 15 splice acceptor sites), thus preventing exon 8 from splicing and resulting in translation of a truncated proteins up to exon 8 and into intron 8, ending there with a stop codon (figure 50A). This truncated protein is likely not functional, since it corresponds to

the extracellular domain alone; the transmembrane domain is located in the deleted exon 10, and the whole cytoplasmic domain is also deleted. We assessed the expression of PIR-B on splenic B cells and found that $Pirb^{+/-}$ cells expressed medium levels of PIR-B and $Pirb^{-/-}$ cells did not express PIR-B compared to WT counterparts (figure 50B-C).

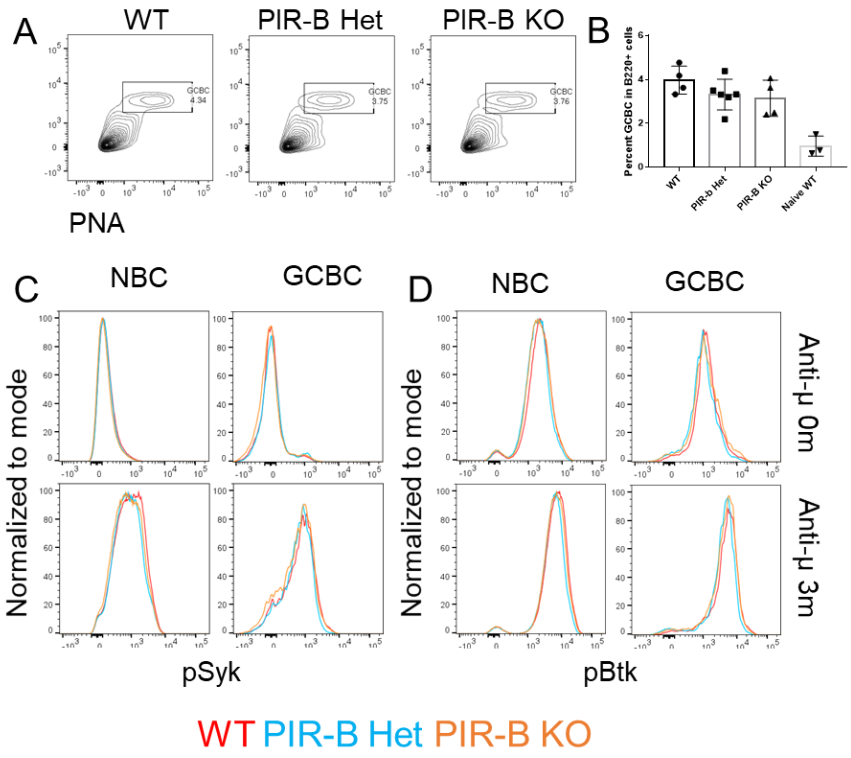


**Figure 51 PIR-B deficiency does not affect GC signaling**

**(A-B) Contour plots (A) and quantification (B) of GCBC in WT, PIR-B het and PIR-B KO mice. The cells are pre-gated on lymphocytes, singlets and B220 positive cells. (C-D) Histogram showing Syk and Btk phosphorylation in NBC and GCBC upon treatment with 20μg/mL anti-μ antibody. Data in A-B are representative of at least two independent experiments with and are represented as mean with SD of groups of at least two mice. Data in C is from one flow cytometry experiment.**

Next, we immunized WT C57BL/6, PIR-B Het and PIR-B KO mice using SRBC and observed the there was no significant difference in the percentage of GCBC between these strains (figure 51A-B). Because PIR-B recruits the phosphatase SHP-1, we wanted to determine whether PIR-B deficiency had an impact on BCR signaling. Unexpectedly, we observed that Syk and Btk phosphorylation were not altered among the three strains described above that have differential PIR-B expression (figure 51C-D). Both Syk and Btk are known targets for SHP-1 and therefore if PIR-B and SHP-1 mediation dampened BCR signaling then PIR-B deficiency would reverse that (126). However, it is possible that because of the redundancies in inhibitory receptors that recruit SHP-1, the deficiency of PIR-B may not influence BCR signaling.

In the spleen, the overall numbers of total kappa positive AFC were not significantly different in PIR-B sufficient and deficient mice (figure 52C). The splenic CGG-specific IgM AFC were significantly reduced in PIR-B KO mice compared to their WT counterparts at D10 post immunization (figure 52B left panel). However, there were no differences in the CGG-specific IgG AFC or the NP-specific IgM and IgG AFC (figure 52A-B). In the bone marrow (BM) compartment, the CGG specific IgM AFC were significantly reduced in PIR-B Het and PIR-B KO mice in comparison to the WT counter parts at 10 days post-mmunization (figure 52F, left panel). However, no other differences were found between the total AFCs, NP-specific AFCs, CGG-specific IgG AFCs in PIR-B deficient and sufficient mice (figure 52D-F). These findings were unexpected and contrary to the hyper-responsiveness of PIR-B humoral responses published earlier (227).

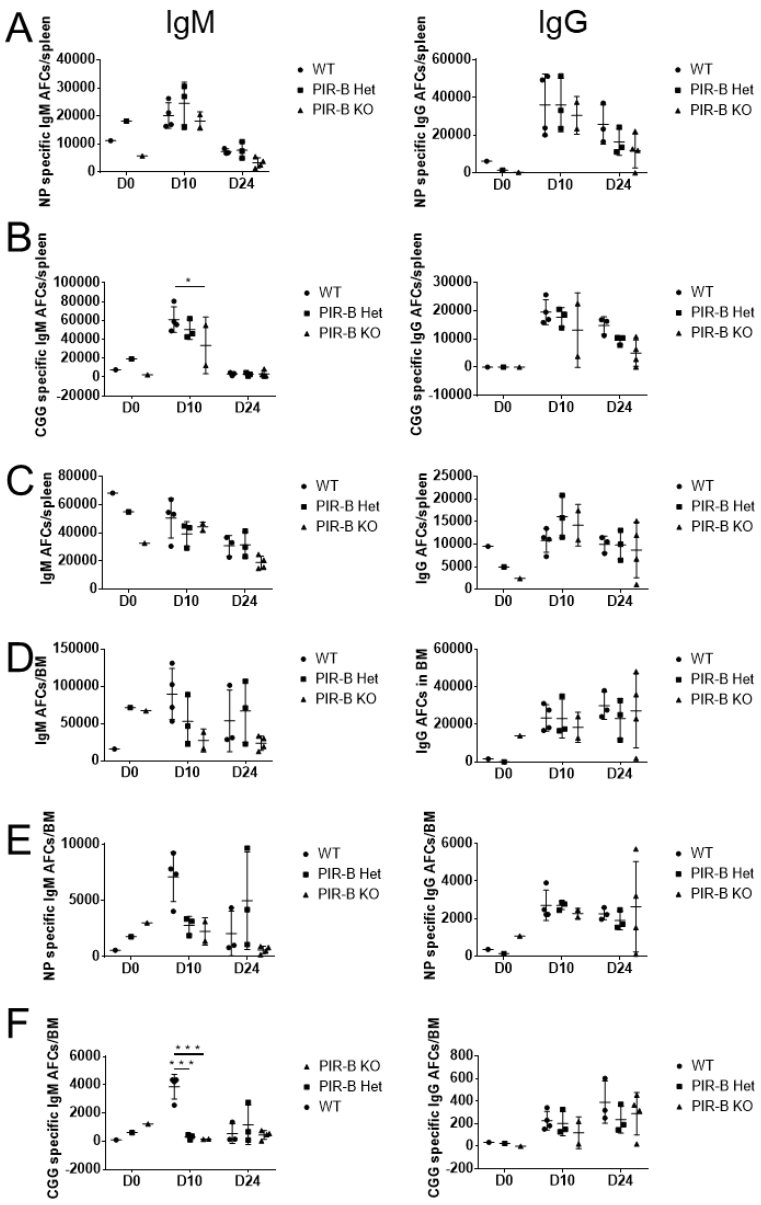


**Figure 52 PIR-B deficiency moderately affects acute AFC production**

**(A-C) Splenic IgM (left panel) and IgG (right panel) AFC to coating antigens NP (A), CGG (B), and kappa (C) at different time points post NP-CGG immunization. (D-F) Bone marrow IgM (left panel) and IgG (right panel) AFC to coating antigens NP (E), CGG (F), and kappa (D) at different time points post NP-CGG immunization. Data are from one ELISPOT experiment.**

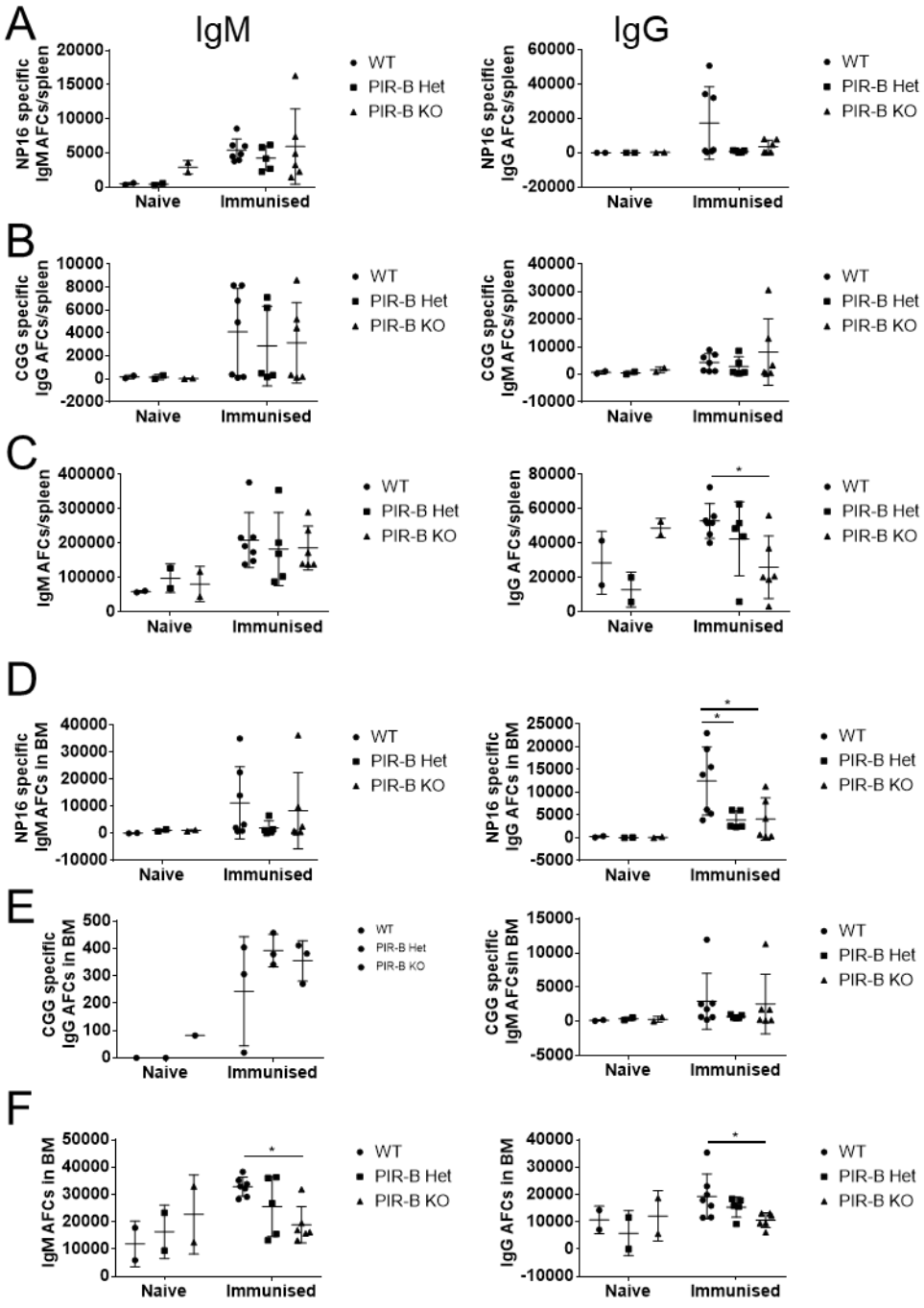


**Figure 53 PIR-B deficiency reduces long-lived AFCs in BM**

**(A-C) Splenic IgM (left panel) and IgG (right panel) AFC to coating antigens NP (A), CGG (B), and kappa (C) at 8 weeks post NP-CGG immunization. (D-F) Bone marrow IgM (left panel) and IgG (right panel) AFC to coating antigens NP (D), CGG (E), and kappa (F) at 8 weeks post NP-CGG immunization. Data are**

**representative of at least two independent experiments with and are represented as mean with SD of groups of at least a mouse.**

In order to further investigate the B cell response, we measured the long-lived AFC response to NP-CGG immunization in spleen and BM. Overall, we observed no differences in the IgM AFC compartment (figure 53A-C, left panels). The NP-specific IgG AFC showed a trend of reduced AFCs in the PIR-B KO compartment; however, CGG-specific IgG AFCs did not have this trend (figure 53A-B, right panels). The total IgG AFCs were significantly reduced in the PIR-B KO mice compared to the WT controls (figure 53C, right panel). In the BM, total IgM AFCs were significantly reduced in PIR-B KO mice compared to the WT control, whereas the Ag-specific IgM AFCs were not significantly different (figure 53E-F, left panels). However, both NP-specific and total IgG AFCs were significantly reduced in the PIR-B KO mice compared to the WT controls, whereas the CGG specific IgG AFCs were not significantly different (figure 53E-F, right panels). Overall, these data suggest that the absence of PIR-B moderately affected the long-lived AFC compartment in a negative manner. This is contrary to the hyper-responsiveness that had been reported in serum ELISAs during acute responses to immunization in PIR-B deficient mice (227).

Lastly, we wanted to assess spontaneous GC formations as a means to assess autoimmunity, similar to what has been reported in deficiency of inhibitory receptors such as in $CD22^{-/-}$ mice (228). We observed that the total number, percentage of GCBC was not significantly different in > 6-month old PIR-B sufficient and deficient mice (figure 54A-B). Moreover, the total number of B cells and spontaneous PBs was also not altered with PIR-B deficiency (figure 54C-D). This is in line with previous findings and it shows that PIR-B deficiency does not lead to autoimmunity in aged mice.

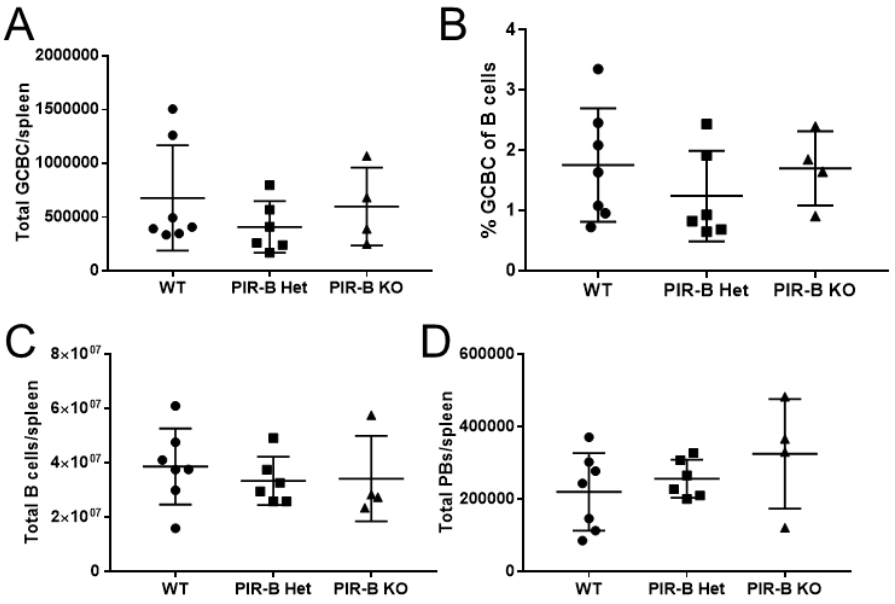


**Figure 54 PIR-B deficiency does not induce spontaneous GC or PB formation**

**(A-B) Total numbers (A) and percentage (B) of GCBC in > 6-month-old WT, PIR-B Het and PIR-B KO mice**

**(C-D) Total B220$^{+}$ B cells (C) and CD138$^{+}$ CD44$^{+}$ PB (D) in > 6-month-old WT, PIR-B Het and PIR-B KO mice. Data is from one flow cytometry experiment.**

## 5.4 Discussion

PIR-B is an inhibitory receptor on B cells that is known to regulate BCR signaling. Here we generated mice deficient in PIR-B and assessed B cell responses to T-dependent immunization. We found that the acute response to SRBC or NP-CGG immunization was not significantly altered in the absence of PIR-B. Moreover, proximal BCR signaling was also not affected by PIR-B deficiency. However, unexpectedly, we found that long-lived AFC compartment in PIR-B deficient mice showed reduced AFC numbers in the BM and moderately affected the splenic AFCs.

Previously, it was shown that PIR-B deficiency increases humoral IgG1 and IgE responses to TNP-KLH immunization (227). However, we did not observe this phenotype when we measured the AFC response in the spleen and BM at D10 and D24 after NP-CGG immunization. We probed this further by measuring NP-specific, GG-specific and total AFCs 8 weeks post-immunization to assess the long-lived AFC compartment. Surprisingly, the AFC responses were moderately reduced in the spleen and BM. However, unlike the study of Ujike et. al., we did not measure serum Abs (227). Also, the authors re-immunized the mice at 8 weeks and observed enhanced responses to re-immunization (227). The authors have attributed the hyper-responsive serum Abs to the IL-4 produced by DCs in lymph nodes of PIR-B deficient mice (227). Since we have not measured the serum or lymph node compartments or re-immunized the mice used in our studies, we have yet been able to assess those previous conclusions in the context of our data. From our study, we conclude that PIR-B positively regulates the long-lived IgG AFC compartment in the BM following immunization with T-dependent Ags.

PIR-B is known to recruit the phosphatase SHP-1 and dampen different signaling axes. However, PIR-B deficient B cells did not demonstrate any alteration in Syk or Btk phosphorylation upon BCR stimulation. These data suggest that while PIR-B may be playing a role in the recruitment of SHP-1, other inhibitory receptors such as CD22 and CD72 may have redundant roles in the recruitment of SHP-1 and the regulating of signaling (126). Overall, humoral immunity to NP-CGG and SRBC immunization was moderately reduced in the absence of PIR-B, but the mechanism remains to be elucidated.

# 6.0 Conclusion

Murine infection with *Ehrlichia muris* models human Ehrlichiosis, with prominent liver involvement. The B cell response is dominated by plasmablasts (PBs), with few GC, yet this response generates protective IgM MBC that express T-bet and harbor V region mutations. Here we have addressed the origins, specificity, and locations of these responses. B cells within infected livers were proliferating and undergoing SHM. Vh region sequencing revealed trafficking of B cell clones between the spleen and liver that was often followed by localized clonal expansion. A subset of T-bet$^+$ MBCs persisted in livers after infection. These cells resisted intravascular labeling and were observed at intraparenchymal locations. Hence, liver can be a generative site of B cell responses that include V region mutation, MBC generation, and long-term MBC localization. Further, T-bet$^+$ MBC expressed diverse surface phenotypes and colonized the splenic MZ, revealing unexpected plasticity of T-bet$^+$ MBC.

Distinct protein and lipid phosphatases that function exclusively in GCBC such as PTEN, SHIP-1, SHP-1, Csk and HPK1 dampen proximal BCR signaling. Here we have shown that actin also acted as a negative regulator of BCR signaling, although this regulation was observed in both GCBC and NBC. Upon Ag stimulation, GCBC displayed dampened BCR signaling and instead rapidly internalized the engaged BCR and processed and presented the Ag in the context of MHC II. This Ag presentation pathway in B cells was dependent on the activity of the lipid phosphatase PTEN. The mechanism of how PTEN regulates Ag presentation remains to be elucidated.

The lipid phosphatase SHIP-1 is highly expressed in GCBC and has a modest impact on BCR-induced PI3K signaling in B cells. However, SHIP-1 expression was crucial for GCBC proliferation and survival and may be dependent on the scaffolding functions of SHIP-1. Inhibitory

receptors also play a major role in regulating signaling events by recruiting phosphatases via their ITIM motifs. The inhibitory receptor PIR-B does not regulate proximal BCR signaling or GC reaction but may have an impact on long-term AFC generation. The redundant functions of different inhibitory receptors may be masking the role of PIR-B in GCBC biology.

Canonical B cell responses initiate a GC response pathway that is marked by differentiation of B cells into a unique phenotype. This differentiation into GC phenotype makes GCBC significantly different than NBC in signaling and cell biological aspects. These distinct features of GCBC allow for efficient GC reaction which is a major pathway for efficient generation of long-lived AFC and MBC. However, infection with certain pathogens such as *E. muris* can induce a non-GC response in lymphoid organs to generate long-lived AFC and MBC. Moreover, these non-canonical B cell responses can also occur in non-lymphoid organs. Overall, these studies provide insights into the mechanisms of GC and non-canonical B cell responses.

## Bibliography


1. Cunningham AF, *et al.* (2007) Salmonella induces a switched antibody response without germinal centers that impedes the extracellular spread of infection. *J Immunol* 178(10):6200-6207.
2. Elsner RA, Hastey CJ, & Baumgarth N (2015) CD4+ T cells promote antibody production but not sustained affinity maturation during Borrelia burgdorferi infection. *Infect Immun* 83(1):48-56.
3. Hastey CJ, Elsner RA, Barthold SW, & Baumgarth N (2012) Delays and diversions mark the development of B cell responses to Borrelia burgdorferi infection. *J Immunol* 188(11):5612-5622.
4. Elsner RA, Hastey CJ, Olsen KJ, & Baumgarth N (2015) Suppression of Long-Lived Humoral Immunity Following Borrelia burgdorferi Infection. *PLoS Pathog* 11(7):e1004976.
5. Victora GD & Nussenzweig MC (2012) Germinal centers. *Annu Rev Immunol* 30:429-457.
6. De Silva NS & Klein U (2015) Dynamics of B cells in germinal centres. *Nat Rev Immunol* 15(3):137-148.
7. Mesin L, Ersching J, & Victora GD (2016) Germinal Center B Cell Dynamics. *Immunity* 45(3):471-482.
8. Stebegg M, *et al.* (2018) Regulation of the Germinal Center Response. *Front Immunol* 9:2469.
9. MacLennan IC, *et al.* (2003) Extrafollicular antibody responses. *Immunol Rev* 194:8-18.

10. Malkiel S, Barlev AN, Atisha-Fregoso Y, Suurmond J, & Diamond B (2018) Plasma Cell Differentiation Pathways in Systemic Lupus Erythematosus. *Front Immunol* 9:427.

11. Di Niro R, *et al.* (2015) Salmonella Infection Drives Promiscuous B Cell Activation Followed by Extrafollicular Affinity Maturation. *Immunity* 43(1):120-131.

12. Racine R, *et al.* (2010) Impaired germinal center responses and suppression of local IgG production during intracellular bacterial infection. *J Immunol* 184(9):5085-5093.

13. Popescu M, Cabrera-Martinez B, & Winslow GM (2019) TNF-alpha Contributes to Lymphoid Tissue Disorganization and Germinal Center B Cell Suppression during Intracellular Bacterial Infection. *J Immunol* 203(9):2415-2424.

14. Ismail N, Bloch KC, & McBride JW (2010) Human ehrlichiosis and anaplasmosis. *Clin Lab Med* 30(1):261-292.

15. Ismail N & McBride JW (2017) Tick-Borne Emerging Infections: Ehrlichiosis and Anaplasmosis. *Clin Lab Med* 37(2):317-340.

16. Rikihisa Y (2015) Molecular Pathogenesis of Ehrlichia chaffeensis Infection. *Annu Rev Microbiol* 69:283-304.

17. Dumler JS, Madigan JE, Pusterla N, & Bakken JS (2007) Ehrlichioses in humans: epidemiology, clinical presentation, diagnosis, and treatment. *Clin Infect Dis* 45 Suppl 1:S45-51.

18. Moumene A & Meyer DF (2016) Ehrlichia's molecular tricks to manipulate their host cells. *Microbes Infect* 18(3):172-179.

19. Thomas S, Popov VL, & Walker DH (2010) Exit mechanisms of the intracellular bacterium Ehrlichia. *PLoS One* 5(12):e15775.

20. Luo T, Mitra S, & McBride JW (2018) Ehrlichia chaffeensis TRP75 Interacts with Host Cell Targets Involved in Homeostasis, Cytoskeleton Organization, and Apoptosis Regulation To Promote Infection. *mSphere* 3(2).

21. Thirumalapura NR, Crossley EC, Walker DH, & Ismail N (2009) Persistent infection contributes to heterologous protective immunity against fatal ehrlichiosis. *Infect Immun* 77(12):5682-5689.

22. McBride JW, Zhang X, Wakeel A, & Kuriakose JA (2011) Tyrosine-phosphorylated Ehrlichia chaffeensis and Ehrlichia canis tandem repeat orthologs contain a major continuous cross-reactive antibody epitope in lysine-rich repeats. *Infect Immun* 79(8):3178-3187.

23. Mohan Kumar D, *et al.* (2013) Ehrlichia chaffeensis uses its surface protein EtpE to bind GPI-anchored protein DNase X and trigger entry into mammalian cells. *PLoS Pathog* 9(10):e1003666.

24. Yang Q, Ghose P, & Ismail N (2013) Neutrophils mediate immunopathology and negatively regulate protective immune responses during fatal bacterial infection-induced toxic shock. *Infect Immun* 81(5):1751-1763.

25. Haloul M, *et al.* (2019) mTORC1-mediated polarization of M1 macrophages and their accumulation in the liver correlate with immunopathology in fatal ehrlichiosis. *Sci Rep* 9(1):14050.

26. Ismail N, *et al.* (2004) Overproduction of TNF-alpha by CD8+ type 1 cells and down-regulation of IFN-gamma production by CD4+ Th1 cells contribute to toxic shock-like syndrome in an animal model of fatal monocytotropic ehrlichiosis. *J Immunol* 172(3):1786-1800.

27. Habib S, El Andaloussi A, Hisham A, & Ismail N (2016) NK Cell-Mediated Regulation of Protective Memory Responses against Intracellular Ehrlichial Pathogens. *PLoS One* 11(4):e0153223.

28. Ismail N, Crossley EC, Stevenson HL, & Walker DH (2007) Relative importance of T-cell subsets in monocytotropic ehrlichiosis: a novel effector mechanism involved in Ehrlichia-induced immunopathology in murine ehrlichiosis. *Infect Immun* 75(9):4608-4620.

29. Winslow GM, *et al.* (2000) Antibody-mediated elimination of the obligate intracellular bacterial pathogen Ehrlichia chaffeensis during active infection. *Infect Immun* 68(4):2187-2195.

30. Winslow GM, Yager E, & Li JS (2003) Mechanisms of humoral immunity during Ehrlichia chaffeensis infection. *Ann N Y Acad Sci* 990:435-443.

31. Racine R, Chatterjee M, & Winslow GM (2008) CD11c expression identifies a population of extrafollicular antigen-specific splenic plasmablasts responsible for CD4 T-independent antibody responses during intracellular bacterial infection. *J Immunol* 181(2):1375-1385.

32. Papillion AM, Kenderes KJ, Yates JL, & Winslow GM (2017) Early derivation of IgM memory cells and bone marrow plasmablasts. *PLoS One* 12(6):e0178853.

33. Yates JL, Racine R, McBride KM, & Winslow GM (2013) T cell-dependent IgM memory B cells generated during bacterial infection are required for IgG responses to antigen challenge. *J Immunol* 191(3):1240-1249.

34. Naradikian MS, *et al.* (2016) Cutting Edge: IL-4, IL-21, and IFN-gamma Interact To Govern T-bet and CD11c Expression in TLR-Activated B Cells. *J Immunol* 197(4):1023-1028.

35. Jones DD, *et al.* (2015) The omentum is a site of protective IgM production during intracellular bacterial infection. *Infect Immun* 83(5):2139-2147.

36. Peng SL, Szabo SJ, & Glimcher LH (2002) T-bet regulates IgG class switching and pathogenic autoantibody production. *Proc Natl Acad Sci U S A* 99(8):5545-5550.

37. Jegerlehner A, *et al.* (2007) TLR9 signaling in B cells determines class switch recombination to IgG2a. *J Immunol* 178(4):2415-2420.

38. Rubtsov AV, *et al.* (2011) Toll-like receptor 7 (TLR7)-driven accumulation of a novel CD11c(+) B-cell population is important for the development of autoimmunity. *Blood* 118(5):1305-1315.

39. Hao Y, O'Neill P, Naradikian MS, Scholz JL, & Cancro MP (2011) A B-cell subset uniquely responsive to innate stimuli accumulates in aged mice. *Blood* 118(5):1294-1304.

40. Rubtsova K, Rubtsov AV, van Dyk LF, Kappler JW, & Marrack P (2013) T-box transcription factor T-bet, a key player in a unique type of B-cell activation essential for effective viral clearance. *Proc Natl Acad Sci U S A* 110(34):E3216-3224.

41. Barnett BE, *et al.* (2016) Cutting Edge: B Cell-Intrinsic T-bet Expression Is Required To Control Chronic Viral Infection. *J Immunol* 197(4):1017-1022.

42. Moir S, *et al.* (2008) Evidence for HIV-associated B cell exhaustion in a dysfunctional memory B cell compartment in HIV-infected viremic individuals. *J Exp Med* 205(8):1797-1805.

43. Winslow GM, Papillion AM, Kenderes KJ, & Levack RC (2017) CD11c+ T-bet+ memory B cells: Immune maintenance during chronic infection and inflammation? *Cell Immunol* 321:8-17.

44. Kenderes KJ, *et al.* (2018) T-Bet(+) IgM Memory Cells Generate Multi-lineage Effector B Cells. *Cell Rep* 24(4):824-837 e823.

45. Chiu C & Openshaw PJ (2015) Antiviral B cell and T cell immunity in the lungs. *Nat Immunol* 16(1):18-26.

46. Onodera T, *et al.* (2012) Memory B cells in the lung participate in protective humoral immune responses to pulmonary influenza virus reinfection. *Proc Natl Acad Sci U S A* 109(7):2485-2490.

47. Murakami J, *et al.* (1999) Functional B-cell response in intrahepatic lymphoid follicles in chronic hepatitis C. *Hepatology* 30(1):143-150.

48. Sansonno D, *et al.* (2004) Intrahepatic B cell clonal expansions and extrahepatic manifestations of chronic HCV infection. *Eur J Immunol* 34(1):126-136.

49. Racanelli V, *et al.* (2001) Molecular characterization of B cell clonal expansions in the liver of chronically hepatitis C virus-infected patients. *J Immunol* 167(1):21-29.

50. Russi S, Dammacco F, Sansonno S, Pavone F, & Sansonno D (2015) Activation-induced cytidine deaminase in B cells of hepatits C virus-related cryoglobulinaemic vasculitis. *Clin Exp Immunol* 182(3):323-331.

51. Tan YG, *et al.* (2018) Clonal characteristics of paired infiltrating and circulating B lymphocyte repertoire in patients with primary biliary cholangitis. *Liver Int* 38(3):542-552.

52. Bemark M, *et al.* (2016) Limited clonal relatedness between gut IgA plasma cells and memory B cells after oral immunization. *Nat Commun* 7:12698.

53. Moro-Sibilot L, *et al.* (2016) Mouse and Human Liver Contain Immunoglobulin A-Secreting Cells Originating From Peyer's Patches and Directed Against Intestinal Antigens. *Gastroenterology* 151(2):311-323.

54. Jacobs W, Bogers J, & Van Marck E (1999) Distinct B-cell populations are present in hepatic and intestinal Schistosoma mansoni granulomas. *Acta Gastroenterol Belg* 62(2):178-181.

55. Fairfax KC, Everts B, Smith AM, & Pearce EJ (2013) Regulation of the development of the hepatic B cell compartment during Schistosoma mansoni infection. *J Immunol* 191(8):4202-4210.

56. Coro ES, Chang WL, & Baumgarth N (2006) Type I IFN receptor signals directly stimulate local B cells early following influenza virus infection. *J Immunol* 176(7):4343-4351.

57. Stephens R, Ndungu FM, & Langhorne J (2009) Germinal centre and marginal zone B cells expand quickly in a second Plasmodium chabaudi malaria infection producing mature plasma cells. *Parasite Immunol* 31(1):20-31.

58. Miura K & Rikihisa Y (2009) Liver transcriptome profiles associated with strain-specific Ehrlichia chaffeensis-induced hepatitis in SCID mice. *Infect Immun* 77(1):245-254.

59. Sonoda E, *et al.* (1997) B cell development under the condition of allelic inclusion. *Immunity* 6(3):225-233.

60. Khalil AM, Cambier JC, & Shlomchik MJ (2012) B cell receptor signal transduction in the GC is short-circuited by high phosphatase activity. *Science* 336(6085):1178-1181.

61. Intlekofer AM, *et al.* (2008) Anomalous type 17 response to viral infection by CD8+ T cells lacking T-bet and eomesodermin. *Science* 321(5887):408-411.

62. Crocquet-Valdes PA, *et al.* (2011) Immunization with Ehrlichia P28 outer membrane proteins confers protection in a mouse model of ehrlichiosis. *Clin Vaccine Immunol* 18(12):2018-2025.

63. Stevenson HL, *et al.* (2006) An intradermal environment promotes a protective type-1 response against lethal systemic monocytotropic ehrlichial infection. *Infect Immun* 74(8):4856-4864.

64. Tsioris K, *et al.* (2015) Neutralizing antibodies against West Nile virus identified directly from human B cells by single-cell analysis and next generation sequencing. *Integr Biol (Camb)* 7(12):1587-1597.

65. Rosenfeld AM, Meng W, Luning Prak ET, & Hershberg U (2018) ImmuneDB, a Novel Tool for the Analysis, Storage, and Dissemination of Immune Repertoire Sequencing Data. *Front Immunol* 9:2107.

66. Sheneman L, Evans J, & Foster JA (2006) Clearcut: a fast implementation of relaxed neighbor joining. *Bioinformatics* 22(22):2823-2824.

67. Huerta-Cepas J, Serra F, & Bork P (2016) ETE 3: Reconstruction, Analysis, and Visualization of Phylogenomic Data. *Mol Biol Evol* 33(6):1635-1638.

68. Dobin A, *et al.* (2013) STAR: ultrafast universal RNA-seq aligner. *Bioinformatics* 29(1):15-21.

69. Liao Y, Smyth GK, & Shi W (2014) featureCounts: an efficient general purpose program for assigning sequence reads to genomic features. *Bioinformatics* 30(7):923-930.

70. Law CW, Chen Y, Shi W, & Smyth GK (2014) voom: Precision weights unlock linear model analysis tools for RNA-seq read counts. *Genome Biol* 15(2):R29.

71. Ritchie ME, *et al.* (2015) limma powers differential expression analyses for RNA-sequencing and microarray studies. *Nucleic Acids Res* 43(7):e47.

72. Thirumalapura NR, Stevenson HL, Walker DH, & Ismail N (2008) Protective heterologous immunity against fatal ehrlichiosis and lack of protection following homologous challenge. *Infect Immun* 76(5):1920-1930.

73. Stone SL, *et al.* (2019) T-bet Transcription Factor Promotes Antibody-Secreting Cell Differentiation by Limiting the Inflammatory Effects of IFN-gamma on B Cells. *Immunity* 50(5):1172-1187 e1177.

74. Rubtsova K, *et al.* (2017) B cells expressing the transcription factor T-bet drive lupus-like autoimmunity. *J Clin Invest* 127(4):1392-1404.

75. Jacob J, Kelsoe G, Rajewsky K, & Weiss U (1991) Intraclonal generation of antibody mutants in germinal centres. *Nature* 354(6352):389-392.

76. William J, Euler C, Christensen S, & Shlomchik MJ (2002) Evolution of autoantibody responses via somatic hypermutation outside of germinal centers. *Science* 297(5589):2066-2070.

77. Jones DD, DeIulio GA, & Winslow GM (2012) Antigen-driven induction of polyreactive IgM during intracellular bacterial infection. *J Immunol* 189(3):1440-1447.

78. Anderson SM, Tomayko MM, Ahuja A, Haberman AM, & Shlomchik MJ (2007) New markers for murine memory B cells that define mutated and unmutated subsets. *J Exp Med* 204(9):2103-2114.

79. Kaji T, *et al.* (2012) Distinct cellular pathways select germline-encoded and somatically mutated antibodies into immunological memory. *J Exp Med* 209(11):2079-2097.

80. Kumar BV, *et al.* (2017) Human Tissue-Resident Memory T Cells Are Defined by Core Transcriptional and Functional Signatures in Lymphoid and Mucosal Sites. *Cell Rep* 20(12):2921-2934.

81. Lavin Y, *et al.* (2014) Tissue-resident macrophage enhancer landscapes are shaped by the local microenvironment. *Cell* 159(6):1312-1326.

82. Moyron-Quiroz JE, *et al.* (2004) Role of inducible bronchus associated lymphoid tissue (iBALT) in respiratory immunity. *Nat Med* 10(9):927-934.

83. Fagarasan S, Kinoshita K, Muramatsu M, Ikuta K, & Honjo T (2001) In situ class switching and differentiation to IgA-producing cells in the gut lamina propria. *Nature* 413(6856):639-643.

84. Fagarasan S, *et al.* (2002) Critical roles of activation-induced cytidine deaminase in the homeostasis of gut flora. *Science* 298(5597):1424-1427.

85. Farci P, *et al.* (2010) B cell gene signature with massive intrahepatic production of antibodies to hepatitis B core antigen in hepatitis B virus-associated acute liver failure. *Proc Natl Acad Sci U S A* 107(19):8766-8771.

86. Dumler JS, Sutker WL, & Walker DH (1993) Persistent infection with Ehrlichia chaffeensis. *Clin Infect Dis* 17(5):903-905.

87. Mueller I, *et al.* (2009) Key gaps in the knowledge of Plasmodium vivax, a neglected human malaria parasite. *Lancet Infect Dis* 9(9):555-566.

88. Meng W, *et al.* (2017) An atlas of B-cell clonal distribution in the human body. *Nat Biotechnol* 35(9):879-884.

89. Magri G, *et al.* (2017) Human Secretory IgM Emerges from Plasma Cells Clonally Related to Gut Memory B Cells and Targets Highly Diverse Commensals. *Immunity* 47(1):118-134 e118.

90. Lindner C, *et al.* (2012) Age, microbiota, and T cells shape diverse individual IgA repertoires in the intestine. *J Exp Med* 209(2):365-377.

91. Takemori T, Kaji T, Takahashi Y, Shimoda M, & Rajewsky K (2014) Generation of memory B cells inside and outside germinal centers. *Eur J Immunol* 44(5):1258-1264.

92. Cattoretti G, *et al.* (2006) Nuclear and cytoplasmic AID in extrafollicular and germinal center B cells. *Blood* 107(10):3967-3975.

93. Marshall JL, *et al.* (2011) Early B blasts acquire a capacity for Ig class switch recombination that is lost as they become plasmablasts. *Eur J Immunol* 41(12):3506-3512.

94. Odegard JM, *et al.* (2008) ICOS-dependent extrafollicular helper T cells elicit IgG production via IL-21 in systemic autoimmunity. *J Exp Med* 205(12):2873-2886.

95. Muller S, *et al.* (2002) Role of an intact splenic microarchitecture in early lymphocytic choriomeningitis virus production. *J Virol* 76(5):2375-2383.

96. Rosche KL, Aljasham AT, Kipfer JN, Piatkowski BT, & Konjufca V (2015) Infection with Salmonella enterica Serovar Typhimurium Leads to Increased Proportions of F4/80+ Red Pulp Macrophages and Decreased Proportions of B and T Lymphocytes in the Spleen. *PLoS One* 10(6):e0130092.

97. Urban BC, *et al.* (2005) Fatal Plasmodium falciparum malaria causes specific patterns of splenic architectural disorganization. *Infect Immun* 73(4):1986-1994.

98. Weller S, *et al.* (2004) Human blood IgM "memory" B cells are circulating splenic marginal zone B cells harboring a prediversified immunoglobulin repertoire. *Blood* 104(12):3647-3654.

99. Luo W, Weisel F, & Shlomchik MJ (2018) B Cell Receptor and CD40 Signaling Are Rewired for Synergistic Induction of the c-Myc Transcription Factor in Germinal Center B Cells. *Immunity* 48(2):313-326 e315.

100. Kurosaki T (1999) Genetic analysis of B cell antigen receptor signaling. *Annu Rev Immunol* 17:555-592.

101. Rowley RB, Burkhardt AL, Chao HG, Matsueda GR, & Bolen JB (1995) Syk protein-tyrosine kinase is regulated by tyrosine-phosphorylated Ig alpha/Ig beta immunoreceptor tyrosine activation motif binding and autophosphorylation. *J Biol Chem* 270(19):11590-11594.

102. Buhl AM & Cambier JC (1999) Phosphorylation of CD19 Y484 and Y515, and linked activation of phosphatidylinositol 3-kinase, are required for B cell antigen receptor-mediated activation of Bruton's tyrosine kinase. *J Immunol* 162(8):4438-4446.

103. Tuveson DA, Carter RH, Soltoff SP, & Fearon DT (1993) CD19 of B cells as a surrogate kinase insert region to bind phosphatidylinositol 3-kinase. *Science* 260(5110):986-989.

104. Saito K, Scharenberg AM, & Kinet JP (2001) Interaction between the Btk PH domain and phosphatidylinositol-3,4,5-trisphosphate directly regulates Btk. *J Biol Chem* 276(19):16201-16206.

105. Astoul E, Watton S, & Cantrell D (1999) The dynamics of protein kinase B regulation during B cell antigen receptor engagement. *J Cell Biol* 145(7):1511-1520.

106. Alessi DR, *et al.* (1997) Characterization of a 3-phosphoinositide-dependent protein kinase which phosphorylates and activates protein kinase Balpha. *Curr Biol* 7(4):261-269.

107. Limon JJ & Fruman DA (2012) Akt and mTOR in B Cell Activation and Differentiation. *Front Immunol* 3:228.

108. Hara K, *et al.* (2002) Raptor, a binding partner of target of rapamycin (TOR), mediates TOR action. *Cell* 110(2):177-189.

109. Nojima H, *et al.* (2003) The mammalian target of rapamycin (mTOR) partner, raptor, binds the mTOR substrates p70 S6 kinase and 4E-BP1 through their TOR signaling (TOS) motif. *J Biol Chem* 278(18):15461-15464.

110. Sarbassov DD, Guertin DA, Ali SM, & Sabatini DM (2005) Phosphorylation and regulation of Akt/PKB by the rictor-mTOR complex. *Science* 307(5712):1098-1101.

111. Yusuf I, Zhu X, Kharas MG, Chen J, & Fruman DA (2004) Optimal B-cell proliferation requires phosphoinositide 3-kinase-dependent inactivation of FOXO transcription factors. *Blood* 104(3):784-787.

112. Fabre S, *et al.* (2005) Stable activation of phosphatidylinositol 3-kinase in the T cell immunological synapse stimulates Akt signaling to FoxO1 nuclear exclusion and cell growth control. *J Immunol* 174(7):4161-4171.

113. Sander S, *et al.* (2015) PI3 Kinase and FOXO1 Transcription Factor Activity Differentially Control B Cells in the Germinal Center Light and Dark Zones. *Immunity* 43(6):1075-1086.

114. Fu C, Turck CW, Kurosaki T, & Chan AC (1998) BLNK: a central linker protein in B cell activation. *Immunity* 9(1):93-103.

115. Wienands J, *et al.* (1998) SLP-65: a new signaling component in B lymphocytes which requires expression of the antigen receptor for phosphorylation. *J Exp Med* 188(4):791-795.

116. Zhang Y, Wienands J, Zurn C, & Reth M (1998) Induction of the antigen receptor expression on B lymphocytes results in rapid competence for signaling of SLP-65 and Syk. *EMBO J* 17(24):7304-7310.

117. DeBell KE, *et al.* (1999) Functional independence and interdependence of the Src homology domains of phospholipase C-gamma1 in B-cell receptor signal transduction. *Mol Cell Biol* 19(11):7388-7398.

118. Trushin SA, Pennington KN, Algeciras-Schimnich A, & Paya CV (1999) Protein kinase C and calcineurin synergize to activate IkappaB kinase and NF-kappaB in T lymphocytes. *J Biol Chem* 274(33):22923-22931.

119. Dolmetsch RE, Lewis RS, Goodnow CC, & Healy JI (1997) Differential activation of transcription factors induced by Ca2+ response amplitude and duration. *Nature* 386(6627):855-858.

120. Healy JI, *et al.* (1997) Different nuclear signals are activated by the B cell receptor during positive versus negative signaling. *Immunity* 6(4):419-428.

121. Hashimoto A, *et al.* (1998) Involvement of guanosine triphosphatases and phospholipase C-gamma2 in extracellular signal-regulated kinase, c-Jun NH2-terminal kinase, and p38 mitogen-activated protein kinase activation by the B cell antigen receptor. *J Exp Med* 188(7):1287-1295.

122. Dal Porto JM, *et al.* (2004) B cell antigen receptor signaling 101. *Mol Immunol* 41(6-7):599-613.

123. Luo W, *et al.* (2019) The AKT kinase signaling network is rewired by PTEN to control proximal BCR signaling in germinal center B cells. *Nat Immunol* 20(6):736-746.

124. He JS, *et al.* (2013) The distinctive germinal center phase of IgE+ B lymphocytes limits their contribution to the classical memory response. *J Exp Med* 210(12):2755-2771.

125. Nowosad CR, Spillane KM, & Tolar P (2016) Germinal center B cells recognize antigen through a specialized immune synapse architecture. *Nat Immunol* 17(7):870-877.

126. Tamir I, Dal Porto JM, & Cambier JC (2000) Cytoplasmic protein tyrosine phosphatases SHP-1 and SHP-2: regulators of B cell signal transduction. *Curr Opin Immunol* 12(3):307-315.

127. Harris SJ, Parry RV, Westwick J, & Ward SG (2008) Phosphoinositide lipid phosphatases: natural regulators of phosphoinositide 3-kinase signaling in T lymphocytes. *J Biol Chem* 283(5):2465-2469.

128. Pauls SD & Marshall AJ (2017) Regulation of immune cell signaling by SHIP1: A phosphatase, scaffold protein, and potential therapeutic target. *Eur J Immunol* 47(6):932-945.

129. Dominguez-Sola D, *et al.* (2015) The FOXO1 Transcription Factor Instructs the Germinal Center Dark Zone Program. *Immunity* 43(6):1064-1074.

130. Setz CS, *et al.* (2019) Pten controls B-cell responsiveness and germinal center reaction by regulating the expression of IgD BCR. *EMBO J* 38(11).

131. Wang J, *et al.* (2018) PTEN-Regulated AID Transcription in Germinal Center B Cells Is Essential for the Class-Switch Recombination and IgG Antibody Responses. *Front Immunol* 9:371.

132. Becker-Herman S, *et al.* (2011) WASp-deficient B cells play a critical, cell-intrinsic role in triggering autoimmunity. *J Exp Med* 208(10):2033-2042.

133. Liu C, *et al.* (2013) N-wasp is essential for the negative regulation of B cell receptor signaling. *PLoS Biol* 11(11):e1001704.

134. Kolhatkar NS, *et al.* (2015) Altered BCR and TLR signals promote enhanced positive selection of autoreactive transitional B cells in Wiskott-Aldrich syndrome. *J Exp Med* 212(10):1663-1677.

135. Kolhatkar NS, *et al.* (2015) B-cell intrinsic TLR7 signals promote depletion of the marginal zone in a murine model of Wiskott-Aldrich syndrome. *Eur J Immunol* 45(10):2773-2779.

136. Recher M, *et al.* (2012) B cell-intrinsic deficiency of the Wiskott-Aldrich syndrome protein (WASp) causes severe abnormalities of the peripheral B-cell compartment in mice. *Blood* 119(12):2819-2828.

137. Meyer-Bahlburg A, *et al.* (2008) Wiskott-Aldrich syndrome protein deficiency in B cells results in impaired peripheral homeostasis. *Blood* 112(10):4158-4169.

138. Tolar P (2017) Cytoskeletal control of B cell responses to antigens. *Nat Rev Immunol* 17(10):621-634.

139. Song W, Liu C, & Upadhyaya A (2014) The pivotal position of the actin cytoskeleton in the initiation and regulation of B cell receptor activation. *Biochim Biophys Acta* 1838(2):569-578.

140. Schwickert TA, *et al.* (2007) In vivo imaging of germinal centres reveals a dynamic open structure. *Nature* 446(7131):83-87.

141. Allen CD, Okada T, Tang HL, & Cyster JG (2007) Imaging of germinal center selection events during affinity maturation. *Science* 315(5811):528-531.

142. Fehon RG, McClatchey AI, & Bretscher A (2010) Organizing the cell cortex: the role of ERM proteins. *Nat Rev Mol Cell Biol* 11(4):276-287.

143. Pore D, *et al.* (2013) Ezrin tunes the magnitude of humoral immunity. *J Immunol* 191(8):4048-4058.

144. Harwood NE & Batista FD (2009) Visualizing the molecular and cellular events underlying the initiation of B-cell activation. *Curr Top Microbiol Immunol* 334:153-177.

145. Treanor B, *et al.* (2010) The membrane skeleton controls diffusion dynamics and signaling through the B cell receptor. *Immunity* 32(2):187-199.

146. Liu W, Meckel T, Tolar P, Sohn HW, & Pierce SK (2010) Antigen affinity discrimination is an intrinsic function of the B cell receptor. *J Exp Med* 207(5):1095-1111.

147. Liu W, Sohn HW, Tolar P, & Pierce SK (2010) It's all about change: the antigen-driven initiation of B-cell receptor signaling. *Cold Spring Harb Perspect Biol* 2(7):a002295.

148. Tolar P, Hanna J, Krueger PD, & Pierce SK (2009) The constant region of the membrane immunoglobulin mediates B cell-receptor clustering and signaling in response to membrane antigens. *Immunity* 30(1):44-55.

149. Mattila PK, *et al.* (2013) The actin and tetraspanin networks organize receptor nanoclusters to regulate B cell receptor-mediated signaling. *Immunity* 38(3):461-474.

150. Harwood NE & Batista FD (2011) The cytoskeleton coordinates the early events of B-cell activation. *Cold Spring Harb Perspect Biol* 3(2).

151. Hao S & August A (2005) Actin depolymerization transduces the strength of B-cell receptor stimulation. *Mol Biol Cell* 16(5):2275-2284.

152. Freeman SA, *et al.* (2011) Cofilin-mediated F-actin severing is regulated by the Rap GTPase and controls the cytoskeletal dynamics that drive lymphocyte spreading and BCR microcluster formation. *J Immunol* 187(11):5887-5900.

153. Treanor B, Depoil D, Bruckbauer A, & Batista FD (2011) Dynamic cortical actin remodeling by ERM proteins controls BCR microcluster organization and integrity. *J Exp Med* 208(5):1055-1068.

154. Yang N, *et al.* (1998) Cofilin phosphorylation by LIM-kinase 1 and its role in Rac-mediated actin reorganization. *Nature* 393(6687):809-812.

155. Liu C, *et al.* (2012) Actin reorganization is required for the formation of polarized B cell receptor signalosomes in response to both soluble and membrane-associated antigens. *J Immunol* 188(7):3237-3246.

156. Parameswaran N, Enyindah-Asonye G, Bagheri N, Shah NB, & Gupta N (2013) Spatial coupling of JNK activation to the B cell antigen receptor by tyrosine-phosphorylated ezrin. *J Immunol* 190(5):2017-2026.

157. Liu C, *et al.* (2011) A balance of Bruton's tyrosine kinase and SHIP activation regulates B cell receptor cluster formation by controlling actin remodeling. *J Immunol* 187(1):230-239.

158. Schreiner GF & Unanue ER (1977) Capping and the lymphocyte: models for membrane reorganization. *J Immunol* 119(5):1549-1551.

159. Cheng PC, Dykstra ML, Mitchell RN, & Pierce SK (1999) A role for lipid rafts in B cell antigen receptor signaling and antigen targeting. *J Exp Med* 190(11):1549-1560.

160. Gupta N, *et al.* (2006) Quantitative proteomic analysis of B cell lipid rafts reveals that ezrin regulates antigen receptor-mediated lipid raft dynamics. *Nat Immunol* 7(6):625-633.

161. Hauser JT & Lindner R (2014) Coalescence of B cell receptor and invariant chain MHC II in a raft-like membrane domain. *J Leukoc Biol* 96(5):843-855.

162. Chaturvedi A, Martz R, Dorward D, Waisberg M, & Pierce SK (2011) Endocytosed BCRs sequentially regulate MAPK and Akt signaling pathways from intracellular compartments. *Nat Immunol* 12(11):1119-1126.

163. Malhotra S, Kovats S, Zhang W, & Coggeshall KM (2009) B cell antigen receptor endocytosis and antigen presentation to T cells require Vav and dynamin. *J Biol Chem* 284(36):24088-24097.

164. Brown BK & Song W (2001) The actin cytoskeleton is required for the trafficking of the B cell antigen receptor to the late endosomes. *Traffic* 2(6):414-427.

165. Onabajo OO, *et al.* (2008) Actin-binding protein 1 regulates B cell receptor-mediated antigen processing and presentation in response to B cell receptor activation. *J Immunol* 180(10):6685-6695.

166. Kwak K, *et al.* (2018) Intrinsic properties of human germinal center B cells set antigen affinity thresholds. *Sci Immunol* 3(29).

167. Murphy DB, *et al.* (1992) Monoclonal antibody detection of a major self peptide. MHC class II complex. *J Immunol* 148(11):3483-3491.

168. Maeda A, *et al.* (1999) Paired immunoglobulin-like receptor B (PIR-B) inhibits BCR-induced activation of Syk and Btk by SHP-1. *Oncogene* 18(14):2291-2297.

169. Dowler S, Currie RA, Downes CP, & Alessi DR (1999) DAPP1: a dual adaptor for phosphotyrosine and 3-phosphoinositides. *Biochem J* 342 ( Pt 1):7-12.

170. Roman-Fernandez A, *et al.* (2018) The phospholipid PI(3,4)P2 is an apical identity determinant. *Nat Commun* 9(1):5041.

171. Marshall AJ, *et al.* (2000) A novel B lymphocyte-associated adaptor protein, Bam32, regulates antigen receptor signaling downstream of phosphatidylinositol 3-kinase. *J Exp Med* 191(8):1319-1332.

172. Jackson LP, *et al.* (2010) A large-scale conformational change couples membrane recruitment to cargo binding in the AP2 clathrin adaptor complex. *Cell* 141(7):1220-1229.

173. Lerner EA, *et al.* (1980) Monoclonal antibody against an Ir gene product? *J Exp Med* 152(4):1085-1101.

174. Le Roux D, *et al.* (2007) Syk-dependent actin dynamics regulate endocytic trafficking and processing of antigens internalized through the B-cell receptor. *Mol Biol Cell* 18(9):3451-3462.

175. Maul RS, *et al.* (2003) EPLIN regulates actin dynamics by cross-linking and stabilizing filaments. *J Cell Biol* 160(3):399-407.

176. Schnoor M, Stradal TE, & Rottner K (2018) Cortactin: Cell Functions of A Multifaceted Actin-Binding Protein. *Trends Cell Biol* 28(2):79-98.

177. Al-Alwan M, Hou S, Zhang TT, Makondo K, & Marshall AJ (2010) Bam32/DAPP1 promotes B cell adhesion and formation of polarized conjugates with T cells. *J Immunol* 184(12):6961-6969.

178. Zhang TT, Al-Alwan M, & Marshall AJ (2010) The pleckstrin homology domain adaptor protein Bam32/DAPP1 is required for germinal center progression. *J Immunol* 184(1):164-172.

179. Southwick FS (2000) Gelsolin and ADF/cofilin enhance the actin dynamics of motile cells. *Proc Natl Acad Sci U S A* 97(13):6936-6938.

180. Hou P, *et al.* (2006) B cell antigen receptor signaling and internalization are mutually exclusive events. *PLoS Biol* 4(7):e200.

181. Veselits M, *et al.* (2017) Igbeta ubiquitination activates PI3K signals required for endosomal sorting. *J Exp Med* 214(12):3775-3790.

182. Franks SE & Cambier JC (2018) Putting on the Brakes: Regulatory Kinases and Phosphatases Maintaining B Cell Anergy. *Front Immunol* 9:665.

183. Davidson D & Veillette A (2001) PTP-PEST, a scaffold protein tyrosine phosphatase, negatively regulates lymphocyte activation by targeting a unique set of substrates. *EMBO J* 20(13):3414-3426.

184. Poe JC, Fujimoto M, Jansen PJ, Miller AS, & Tedder TF (2000) CD22 forms a quaternary complex with SHIP, Grb2, and Shc. A pathway for regulation of B lymphocyte antigen receptor-induced calcium flux. *J Biol Chem* 275(23):17420-17427.

185. Isnardi I, Bruhns P, Bismuth G, Fridman WH, & Daeron M (2006) The SH2 domain-containing inositol 5-phosphatase SHIP1 is recruited to the intracytoplasmic domain of human FcgammaRIIB and is mandatory for negative regulation of B cell activation. *Immunol Lett* 104(1-2):156-165.

186. Ono M, *et al.* (1997) Deletion of SHIP or SHP-1 reveals two distinct pathways for inhibitory signaling. *Cell* 90(2):293-301.

187. Mukherjee O, *et al.* (2012) The SH2-domain of SHIP1 interacts with the SHIP1 C-terminus: impact on SHIP1/Ig-alpha interaction. *Biochim Biophys Acta* 1823(2):206-214.

188. Manno B, *et al.* (2016) The Dok-3/Grb2 adaptor module promotes inducible association of the lipid phosphatase SHIP with the BCR in a coreceptor-independent manner. *Eur J Immunol* 46(11):2520-2530.

189. Pauls SD, *et al.* (2016) FcgammaRIIB-Independent Mechanisms Controlling Membrane Localization of the Inhibitory Phosphatase SHIP in Human B Cells. *J Immunol* 197(5):1587-1596.

190. Saxton TM, van Oostveen I, Bowtell D, Aebersold R, & Gold MR (1994) B cell antigen receptor cross-linking induces phosphorylation of the p21ras oncoprotein activators SHC and mSOS1 as well as assembly of complexes containing SHC, GRB-2, mSOS1, and a 145-kDa tyrosine-phosphorylated protein. *J Immunol* 153(2):623-636.

191. Aman MJ, *et al.* (2000) Essential role for the C-terminal noncatalytic region of SHIP in FcgammaRIIB1-mediated inhibitory signaling. *Mol Cell Biol* 20(10):3576-3589.

192. Ong CJ, *et al.* (2007) Small-molecule agonists of SHIP1 inhibit the phosphoinositide 3-kinase pathway in hematopoietic cells. *Blood* 110(6):1942-1949.

193. Zhang J, Ravichandran KS, & Garrison JC (2010) A key role for the phosphorylation of Ser440 by the cyclic AMP-dependent protein kinase in regulating the activity of the Src homology 2 domain-containing Inositol 5'-phosphatase (SHIP1). *J Biol Chem* 285(45):34839-34849.

194. Zhang J, Walk SF, Ravichandran KS, & Garrison JC (2009) Regulation of the Src homology 2 domain-containing inositol 5'-phosphatase (SHIP1) by the cyclic AMP-dependent protein kinase. *J Biol Chem* 284(30):20070-20078.

195. Park MJ, *et al.* (2016) SH2 Domains Serve as Lipid-Binding Modules for pTyr-Signaling Proteins. *Mol Cell* 62(1):7-20.

196. Li H & Marshall AJ (2015) Phosphatidylinositol (3,4) bisphosphate-specific phosphatases and effector proteins: A distinct branch of PI3K signaling. *Cell Signal* 27(9):1789-1798.

197. Okada H, *et al.* (1998) Role of the inositol phosphatase SHIP in B cell receptor-induced Ca2+ oscillatory response. *J Immunol* 161(10):5129-5132.

198. Tridandapani S, Chacko GW, Van Brocklyn JR, & Coggeshall KM (1997) Negative signaling in B cells causes reduced Ras activity by reducing Shc-Grb2 interactions. *J Immunol* 158(3):1125-1132.

199. Tridandapani S, Kelley T, Cooney D, Pradhan M, & Coggeshall KM (1997) Negative signaling in B cells: SHIP Grbs Shc. *Immunol Today* 18(9):424-427.

200. Tamir I, *et al.* (2000) The RasGAP-binding protein p62dok is a mediator of inhibitory FcgammaRIIB signals in B cells. *Immunity* 12(3):347-358.

201. Lemay S, Davidson D, Latour S, & Veillette A (2000) Dok-3, a novel adapter molecule involved in the negative regulation of immunoreceptor signaling. *Mol Cell Biol* 20(8):2743-2754.

202. Landego I, *et al.* (2012) Interaction of TAPP adapter proteins with phosphatidylinositol (3,4)-bisphosphate regulates B-cell activation and autoantibody production. *Eur J Immunol* 42(10):2760-2770.

203. Wullschleger S, Wasserman DH, Gray A, Sakamoto K, & Alessi DR (2011) Role of TAPP1 and TAPP2 adaptor binding to PtdIns(3,4)P2 in regulating insulin sensitivity defined by knock-in analysis. *Biochem J* 434(2):265-274.

204. Franke TF, Kaplan DR, Cantley LC, & Toker A (1997) Direct regulation of the Akt proto-oncogene product by phosphatidylinositol-3,4-bisphosphate. *Science* 275(5300):665-668.

205. Thomas CC, Deak M, Alessi DR, & van Aalten DM (2002) High-resolution structure of the pleckstrin homology domain of protein kinase b/akt bound to phosphatidylinositol (3,4,5)-trisphosphate. *Curr Biol* 12(14):1256-1262.

206. Salsman S, Felts N, Pye QN, Floyd RA, & Hensley K (2001) Induction of Akt phosphorylation in rat primary astrocytes by H2O2 occurs upstream of

phosphatidylinositol 3-kinase: no evidence for oxidative inhibition of PTEN. *Arch Biochem Biophys* 386(2):275-280.

207. Brooks R, *et al.* (2010) SHIP1 inhibition increases immunoregulatory capacity and triggers apoptosis of hematopoietic cancer cells. *J Immunol* 184(7):3582-3589.

208. Helgason CD, *et al.* (1998) Targeted disruption of SHIP leads to hemopoietic perturbations, lung pathology, and a shortened life span. *Genes Dev* 12(11):1610-1620.

209. Haddon DJ, *et al.* (2009) SHIP1 is a repressor of mast cell hyperplasia, cytokine production, and allergic inflammation in vivo. *J Immunol* 183(1):228-236.

210. Locke NR, *et al.* (2009) SHIP regulates the reciprocal development of T regulatory and Th17 cells. *J Immunol* 183(2):975-983.

211. Tarasenko T, *et al.* (2007) T cell-specific deletion of the inositol phosphatase SHIP reveals its role in regulating Th1/Th2 and cytotoxic responses. *Proc Natl Acad Sci U S A* 104(27):11382-11387.

212. Sly LM, *et al.* (2007) The role of SHIP in macrophages. *Front Biosci* 12:2836-2848.

213. Hadidi S, *et al.* (2012) Myeloid cell-specific expression of Ship1 regulates IL-12 production and immunity to helminth infection. *Mucosal Immunol* 5(5):535-543.

214. Akerlund J, Getahun A, & Cambier JC (2015) B cell expression of the SH2-containing inositol 5-phosphatase (SHIP-1) is required to establish anergy to high affinity, proteinacious autoantigens. *J Autoimmun* 62:45-54.

215. O'Neill SK, *et al.* (2011) Monophosphorylation of CD79a and CD79b ITAM motifs initiates a SHIP-1 phosphatase-mediated inhibitory signaling cascade required for B cell anergy. *Immunity* 35(5):746-756.

216. Chen Y, *et al.* (2017) SHIP-1 Deficiency in AID(+) B Cells Leads to the Impaired Function of B10 Cells with Spontaneous Autoimmunity. *J Immunol* 199(9):3063-3073.

217. Leung WH, *et al.* (2013) Aberrant antibody affinity selection in SHIP-deficient B cells. *Eur J Immunol* 43(2):371-381.

218. Karlsson MC, *et al.* (2003) Macrophages control the retention and trafficking of B lymphocytes in the splenic marginal zone. *J Exp Med* 198(2):333-340.

219. Chambard JC, Lefloch R, Pouyssegur J, & Lenormand P (2007) ERK implication in cell cycle regulation. *Biochim Biophys Acta* 1773(8):1299-1310.

220. Takai T (2005) Paired immunoglobulin-like receptors and their MHC class I recognition. *Immunology* 115(4):433-440.

221. Ho LH, Uehara T, Chen CC, Kubagawa H, & Cooper MD (1999) Constitutive tyrosine phosphorylation of the inhibitory paired Ig-like receptor PIR-B. *Proc Natl Acad Sci U S A* 96(26):15086-15090.

222. Nakamura A, Kobayashi E, & Takai T (2004) Exacerbated graft-versus-host disease in Pirb-/- mice. *Nat Immunol* 5(6):623-629.

223. Munitz A, *et al.* (2010) Paired immunoglobulin-like receptor B (PIR-B) negatively regulates macrophage activation in experimental colitis. *Gastroenterology* 139(2):530-541.

224. Pereira S, Zhang H, Takai T, & Lowell CA (2004) The inhibitory receptor PIR-B negatively regulates neutrophil and macrophage integrin signaling. *J Immunol* 173(9):5757-5765.

225. Zhang H, Meng F, Chu CL, Takai T, & Lowell CA (2005) The Src family kinases Hck and Fgr negatively regulate neutrophil and dendritic cell chemokine signaling via PIR-B. *Immunity* 22(2):235-246.

226. Uehara T, *et al.* (2001) Inhibition of IgE-mediated mast cell activation by the paired Ig-like receptor PIR-B. *J Clin Invest* 108(7):1041-1050.

227. Ujike A, *et al.* (2002) Impaired dendritic cell maturation and increased T(H)2 responses in PIR-B(-/-) mice. *Nat Immunol* 3(6):542-548.

228. O'Keefe TL, Williams GT, Batista FD, & Neuberger MS (1999) Deficiency in CD22, a B cell-specific inhibitory receptor, is sufficient to predispose to development of high affinity autoantibodies. *J Exp Med* 189(8):1307-1313.

229. Kubo T, *et al.* (2009) Augmented TLR9-induced Btk activation in PIR-B-deficient B-1 cells provokes excessive autoantibody production and autoimmunity. *J Exp Med* 206(9):1971-1982.

230. Pelletier S, Gingras S, & Green DR (2015) Mouse genome engineering via CRISPR-Cas9 for study of immune function. *Immunity* 42(1):18-27.